Master's thesis

2023

Daan Koetzier

**NTNU**
Norwegian University of
Science and Technology
Faculty of Engineering
Department of Marine Technology

Master's thesis

Daan Koetzier

# Onsite Blade Exchange on a Tension-Leg Platform Floating Wind Turbine using a Self-Climbing Crane

October 2023

NTNU
Norwegian University of
Science and Technology

NTNU
Norwegian University of
Science and Technology

NTNU
Norwegian University of
Science and Technology

# Onsite Blade Exchange on a Tension-Leg Platform Floating Wind Turbine using a Self-Climbing Crane

Daan Koetzier

MS Wind | European Wind Energy Master (EWEM)
Submission date: October 2023
Supervisor: Zhen Gao
Co-supervisor: Oriol Colomes Gene

Norwegian University of Science and Technology
Department of Marine Technology

# Preface

This thesis is written to complete the master's degree European Wind Energy Master at the Delft University of Technology (TU Delft) and the Norwegian University of Science and Technology (NTNU). This thesis was written in the period of January 2023 until September 2023 in collaboration with TU Delft, NTNU and the supervising company Heerema Engineering Solutions. A collaboration between Heerema Engineering Solutions and the company who own the design of the self-climbing crane, Huisman Equipment BV, was set up in order to carry out this project. Huisman Equipment BV have kindly supplied the design of the crane and provided extra guidance during the project.

During this project, I have had great support from all involved parties. Firstly, I would like to thank everyone at HES for welcoming me into the group. I especially enjoyed the Thursday TED-talks, the company outings and all the good laughs at the lunch table. A lot of you have also given me new ideas and great feedback while writing this thesis and preparing for the defense, which I am very grateful for.

I would like to thank Oriol Colomés Gené from TU Delft for his supervision during this project, and his ability to keep an eye on the more fundamental aspects of my model. You also helped me understand how to work academically, and how to define my research scope into something that could contribute academically. I would also like to thank Zhen Gao for his supervision, even after leaving NTNU and moving to China to further pursue his academic career. I admire your dedication to supervising not only me, but also other students from EWEM, while working and living in a different continent and time zone. You helped me by making me focus on a structured step-by-step assessment of the operational sequence early on in the project.

I want to thank Casper van Lynden from HES for his time and effort in supervising me, and his help with the modeling software I used. I learned a lot from sparring over my models and results with you, and would like to thank you for your help and guidance during the times my models were not working.

I am very grateful for the supervision of Elisa Romero Pascual from HES during the literature review and the thesis itself. You were always able to point me towards the right direction, and keep an eye on the bigger picture and added value of my thesis. I appreciate your solution oriented vision on floating wind, and I enjoyed discussing all the possible maintenance solutions for floating wind with you. I would also like to thank you for setting up the collaboration with Huisman, and trusting me with the responsibility of working at an external company.

From Huisman Equipment BV, I would like to express my thanks to Dieter Wijning. Thank you for enabling the collaboration between HES and Huisman, and I look forward to what is to come from Huisman in the area of floating wind, with you as an innovator. I would also like to thank Wing Lee for his supervision from Huisman's side. Sparring with you about design aspects of the crane and its application to floating wind helped to form my thesis. Your humour was also a great addition to my Fridays at Huisman.

Last but not least, I would like to thank my colleagues from EWEM, with whom I travelled to three different countries, and to all the other friends I made during that time. All the laughs and adventures I had during the EWEM program will stay with me for a long time.

*Daan Koetzier*
*Delft, September 2023*

# Abstract

Floating offshore wind turbines offer a means to access wind resources in waters that are too deep for bottom-fixed offshore wind turbines. To operate a floating wind farm, it must be possible to perform maintenance on the turbines. A critical maintenance aspect is the exchange of a major component such as a blade. It involves a lift of a large component to and from the turbine, which is subject to dynamic excitations from environmental loads. Jack-up vessels are used for major component exchanges on bottom-fixed offshore wind turbines, but due to the increased water depth in floating wind farms these type of vessels cannot extend their legs to the seabed and operate. As an alternative, an onsite blade exchange using a turbine mounted crane is considered in this thesis. The lifting dynamics during the operation are studied, as a knowledge gap is identified in this area.

A 15 MW floating wind turbine on a tension-leg platform (TLP) is considered as a case study. This type of floater is considered the most difficult to disconnect from its mooring and tow to a port for maintenance using a shore-based crane. The Offshore Self-Climbing Crane (OSCC) from Huisman Equipment is considered as maintenance equipment, which consists of a base docked on the TLP and a lattice structure coupled to the turbine tower, on which a crane is mounted. Due to the mass of the OSCC, the tension in the tendons of the TLP is reduced, which lowers its natural frequencies in surge, sway and yaw and shifts them closer to wind excitation frequencies. The roll and pitch natural frequencies of the TLP are lowered due to the top mass of the crane and the coupling between the bending modes of the lattice and the tower, shifting them closer to wave excitation frequencies. Snap loads in the tendons occur for sea states with wave peak periods near the roll and pitch natural periods at significant wave heights of 2.5 meters and above.

Steps of the blade exchange operation are studied. The operability of the installation of the OSCC is found to be limited by vessel motions, while the TLP remains relatively still. Installation of the OSCC is found to be a bottleneck in the blade exchange due to low operability and a limited number of suitable installation vessels.

Free-hanging blade installation is not deemed possible, due to low installation operability and the unconstrained yaw mode. The stiffness in yaw resulting from a line-up tool attached to the blade root or yoke is assessed. The low stiffness of the line-up tool at the yoke results in a large response due to crane tip displacements caused by wind-induced motions of the TLP. Placing a line-up tool at the root of the blade results in the highest operability of the blade lifts. Yoke motions during its attachment to the old blade become limiting instead. The design choices of the top crane mass, lattice stiffness and the type of line-up tool are related to the operability of the blade exchange.

# Contents

# List of Figures

# List of Tables

# Nomenclature

## Abbreviations

| Abbreviation | Definition |
|---|---|
| AHTS | Anchor-Handling Tug Supply (vessel) |
| BEM | Blade Element Method |
| BFOW | Bottom-Fixed Offshore Wind |
| CoB | Center of Buoyancy |
| CoG | Center of Gravity |
| CoM | Center of Mass |
| DP | Dynamic Positioning |
| FOW | Floating Offshore Wind |
| FOWT | Floating Offshore Wind Turbine |
| HLV | Heavy-Lift Vessel |
| MPM | Most Probable Maximum |
| OSCC | Offshore Self-Climbing Crane |
| PSD | Power Spectral Density (plot) |
| RAO | Response Amplitude Operator |
| RNA | Rotor Nacelle Assembly |
| SDA | Significant Double Amplitude |
| SSA | Significant Single Amplitude |
| SDMPM | Significant Double Most Probable Maximum |
| SSMPM | Significant Single Most Probable Maximum |
| TLP | Tension-Leg Platform |
| WTG | Wind Turbine Generator |

## Symbols

| Symbol | Definition |
|---|---|
| $A_{WL}$ | Waterplane area of floating body |
| $\mathbf{A}$ | Added mass matrix |
| $\mathbf{B}$ | Damping matrix |
| $BM$ | Distance from CoB to metacenter |
| $B_{vessel}$ | Vessel breadth |
| $\mathbf{C}$ | Stiffness matrix |
| $d_{yaw}$ | The translational offset the CoM of the blade makes for an angular displacement in yaw |
| $e$ | Euler's number |
| $EA$ | Axial stiffness |
| $EI$ | Bending stiffness |
| $g$ | Gravitational constant |
| $GM$ | Distance from CoG to metacenter |
| $H_{max}$ | Maximum wave height |
| $H_s$ | Significant wave height |
| $i$ | Imaginary number, $\sqrt{-1}$ |
| $I$ | Moment of inertia |
| $k$ | Stiffness |

| Symbol | Definition |
|---|---|
| $k_{yaw}$ | Stiffness in the degree of freedom yaw |
| $KB$ | Distance from keel to CoB |
| $KG$ | Distance from keel to CoG |
| $\delta l$ | Tendon deformation |
| $l_{hoist}$ | Length of the hoist wire |
| $L$ | Tendon length |
| $L_{vessel}$ | Vessel length |
| $l_0$ | Unstretched tendon length |
| $m$ | Mass |
| $M$ | Mass |
| $\mathbf{M}$ | Mass matrix |
| $M_{rest}$ | Restoring moment |
| $\underline{q}$ | Vector containing system's degrees of freedom |
| $r_{hoist}$ | Distance between line-up tool attachment and hoist wire |
| $r_p$ | Pontoon radius of TLP |
| $r_{xx}$ | Radius of gyration around the X-axis |
| $r_{yy}$ | Radius of gyration around the Y-axis |
| $r_{zz}$ | Radius of gyration around the Z-axis |
| $S(\omega)$ | Spectrum |
| $T$ | Tension |
| $T_{nat}$ | Natural period |
| $\alpha_{\text{tendon}}$ | Tendon inclination angle |
| $\Phi$ | Velocity potential |
| $\phi_{hoist}$ | The angle of the hoist wire with respect to a vertical plane |
| $\nabla$ | Displacement |
| $\omega$ | Frequency |
| $\psi_{yaw}$ | Angular displacement in yaw |
| $\zeta$ | Wave amplitude |
| $\rho$ | Density of medium |
| $N_{cycles}$ | Number of cycles in a reference period |

# 1

# Problem statement and report outline

## 1.1. Introduction

Offshore wind is expanding globally, and developers are aiming to exploit wind resources in deeper water. To make the foundation of a wind turbine commercially and technically feasible at greater water depths, the foundations must be floating structures. This new approach to wind turbine foundations brings along a new set of challenges, one of which is maintenance of major components of the wind turbine such as blades or a gearbox.

The replacement of a major component on a wind turbine involves a lift to remove the old component, and a lift to install the new component. Methodologies that are currently used to exchange or install components on wind turbines usually involve jack-up vessels, which are able to extend their legs down to the seabed to provide a stable platform from which a lift of a component to the wind turbine can be executed. This method is not feasible for floating wind turbines, as they will be placed in deeper waters.

As a solution to this problem, methodologies have been proposed where the floating turbine is towed away from its deep water location to a harbor or sheltered location where it can be serviced by a land based crane. However, not all floater types are suitable for this. Furthermore, the disconnection of the mooring lines and towing of the floating turbine can take up a significant amount of time, resulting in unwanted downtime of the turbine. Towing operations for maintenance are expected to become a complex logistical challenge at the scale of a complete wind farm.

Onsite maintenance on floating wind turbines provides several advantages as opposed to offsite maintenance. There is no need to displace and disconnect the turbine, which could significantly decrease its downtime. Additionally, the vessel used for the operation could remain at the wind farm and service multiple turbines in one operation.

The challenge of onsite maintenance lies in the dynamics of the lift of the components. The floating turbines will experience larger motions than their bottom-fixed counterparts, as there is no rigid connection to the seabed. Using a floating vessel to perform the lift will result in large relative motions between the vessel's crane and the turbine, as the two could have different motion characteristics and phase. To minimize relative motions between the crane used in the maintenance operation and the floating wind turbine, a turbine-mounted crane could provide a solution.

In this thesis, a blade exchange using a turbine-mounted solution is therefore investigated. A blade exchange is considered challenging due to the tight tolerances during installation and its susceptibility to wind excitation. A floating wind turbine based on a Tension-Leg Platform (TLP) is chosen as a case study for the onsite maintenance operation, as this type of floater cannot easily be displaced for maintenance due to its dependence on its mooring lines for stability, and its maintenance is therefore limited to onsite operations.

Motions of the floater will cause displacements of the turbine mounted crane, which will induce motions of the lifted blade. Furthermore, the blade is subject to aerodynamic loads, which will also excite the motions of the blade. These motions will result in operating limits of the component exchange. A low operating limit for a component exchange could result in unwanted downtime of the turbine in case of a component failure, driving up the cost for maintenance of the floating wind turbine. Although the operating limit is an important factor in determining the feasibility of a component exchange using a turbine mounted crane, it is still poorly understood.

## 1.2. Thesis objective

The aim of this thesis is to give insight into the feasibility of an onsite component exchange by assessing the dynamics of the lifted components during the blade exchange and installation of the turbine-mounted crane, and evaluate design choices on an existing turbine-mounted crane concept. The Offshore Self-Climbing Crane (OSCC) from Huisman Equipment BV is taken as maintenance equipment in this thesis. A collaboration is set up with Huisman, who has provided the detailed design of the crane, which is shown in figure 1.1. The contribution of this thesis will be twofold:

- Contributing towards understanding the dynamics of a component lifted with a turbine-mounted crane from a floating wind turbine. Doing so will help in gaining knowledge on the operability and weather windows for this type of maintenance solution, which will help developers of floating wind farms in choosing a suitable solution for a major component exchange.
- Evaluating design choices of the OSCC, with operability as a performance measure. This will contribute towards improving its weather window, which will make the OSCC a more competitive maintenance solution. Increasing the weather windows for a major component exchange will also ultimately lower the cost of floating wind maintenance.

**Figure 1.1:** The Offshore Self-Climbing Crane that will be used as a case study in this thesis

In order to define the scope of this thesis, a set of research questions is drawn up. To assess the feasibility of a blade exchange using the OSCC, the following aspects will be covered in this thesis:

1. What are the constraints and requirements for a support vessel, and how does the support vessel influence the operation?
2. What is the influence of the OSCC on the static and dynamic behaviour of a Tension-Leg Platform?
    a) *What influence does the OSCC have on the tension in the tendons of a TLP?*
    b) *How are the natural frequencies of a TLP affected by the OSCC?*
    c) *Can snap loads occur in the tendons under sea states in which the OSCC can operate?*
3. What is the operability of a blade exchange using the OSCC, based on the identified critical factors?
    a) *Is it necessary to control the blade's motions during lifting, how can this best be done and how does this influence the operability?*
    b) *What are the variables during the blade exchange that are governing for the operability?*
    c) *What means can be used to improve the operability?*

## 1.3. Report outline

The report is split up in a summary of the literature review that preceded this thesis, a description of the model that was built to describe the dynamics of the operation, and the subsequent research that was done.

In the summary of the literature review, an overview is given of possible floating wind maintenance methodologies and their advantages and disadvantages, and a knowledge gap is discussed. Blade lifting technology and installation limits are discussed.

In the model description, the operational sequence of a blade exchange using the OSCC is presented, and critical aspects are discussed. Based on this, the scenarios that are modeled are chosen. The underlying modeling theory and its assumptions and limitations are then discussed. A description is then given of the model that is built of the turbine, the tension-leg platform and the support vessel.

In the research part, the influence of the OSCC on the statics and dynamics of the TLP is addressed. The response of critical parameters during the blade exchange is then discussed, to understand which aspects and dynamic modes influence the response. Based on an operability assessment, two line-up tools are judged. The research is concluded by answering the research questions, and recommendations for future research are shared.

# Part I

# Summary of the literature review

# 2

# Floating wind maintenance

## 2.1. Floating foundations

Areas like the North Sea have become important hubs for offshore wind because of their favourable bathymetry and geotechnical conditions [31]. The soft soils and shallow waters allow for relatively cheap and simple bottom-fixed wind turbine foundations. However, with the most favourable wind farm locations already occupied, and the potential for even greater wind resources further out at sea, wind farm developers are looking towards locations in deeper waters at greater distances from shore for potential new wind farm sites. It is estimated that 80% of Europe's wind resource is found at locations with a water depth over 50 meters, with more constant and stronger wind blowing further offshore [44]. Furthermore, new markets are opening up in areas like the Mediterranean, Norway, the US and Japan, which do not have the advantages of the relatively shallow North Sea. Deeper waters quickly drive up the cost of bottom-fixed foundations. The increased water depth causes a larger moment arm for the wave and wind loads on the structure, which requires the structure to be more stiff. The increased foundation stiffness leads to more material usage and drives up the price. Bottom-fixed foundations therefore reach a point in water depth where they become economically unattractive. This turning point is currently around 50-60 meters [44].

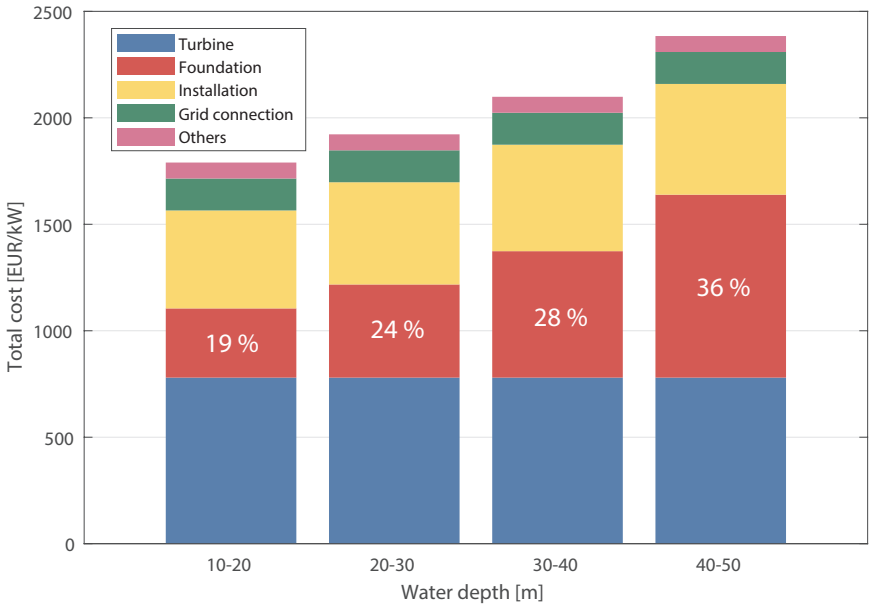


**Figure 2.1:** The increase of subsystem cost with water depth, with foundation cost depicted as fraction of the total cost [44]

For deep waters, floating wind turbine foundations offer a better perspective than bottom-fixed foundations. The floating foundations, so-called floaters, are only in contact to the seafloor through mooring lines, which means they can be installed in very deep waters. Depths up to 300 meters are considered at the moment, while deeper waters are not unthinkable either [53]. The floaters are stabilized through a restoring moment that is dominated by either their waterplane area, ballast or mooring lines. At the moment, the three floater types that receive the most interest are the spar-buoy, the semi-submersible and the tension-leg platform (TLP). A spar-buoy floater is a long cylinder with a center of mass deep below the waterline, which means it is ballasted at the bottom. Displacement of the turbine causes a restoring moment because of the spar-buoys low center of mass, which balances the system. A semi-submersible floater has a large waterplane area that is located at a distance from the center of the turbine, which causes a restoring moment. A spar-buoy and a semi-submersible both have catenary mooring, which also contribute to the platforms' stability. The tension-leg platform is a buoyant platform which is not stable by itself, but is pulled down by tendons to create stability. It is therefore mooring stabilized and has taut mooring lines. There is no consensus yet on which floater type will become dominant. Each floater type is still in an early phase of development, with cost reduction of the floating platform being the most important design driver, as the cost of floating wind is still higher than bottom-fixed wind and other energy sources [44]. What is certain is that these floaters will house very large turbines to make optimal use of the available wind resources, in order to drive the cost of floating wind down, as it has done with bottom-fixed wind [38].

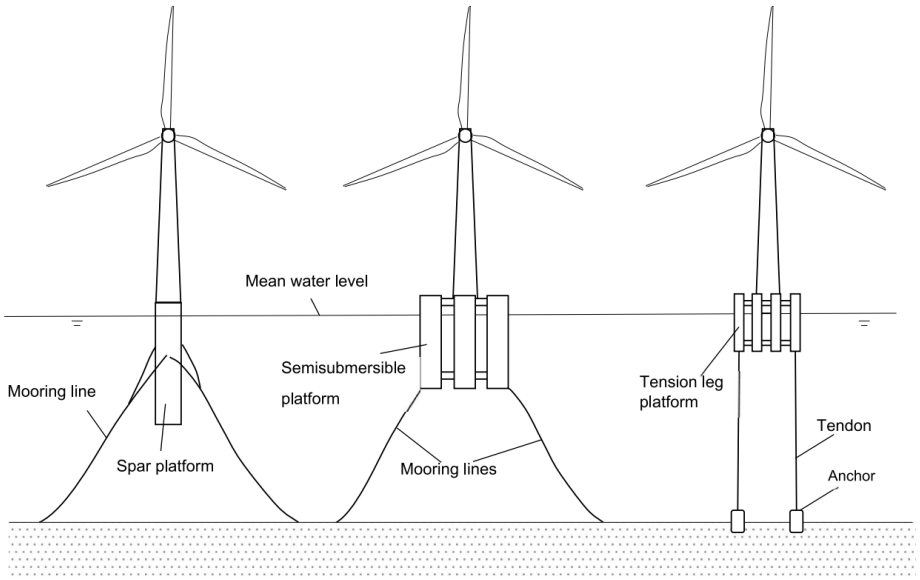


**Figure 2.2:** Different floater types, a spar-buoy, semi-submersible and TLP from left to right [21]

## 2.2. Operational challenges in floating wind

Floating offshore wind (FOW) technology is currently in the process of scaling up. The industry is still in its infancy, with only 73 MW currently installed, but this could increase to up to 70 GW by 2040 [45]. There are still major hurdles to overcome before the technology can reach this mature status. A great deal of research is going on into the different aspects of FOW, such as floater design, mooring design, large-scale manufacturing and operations [44] [11]. The main motivation behind this research is driving down the cost of FOW, to make it competitive with other sources of energy. If FOW can achieve a similar cost reduction as bottom-fixed offshore wind, estimates are that the levelised cost of energy of FOW can reach roughly the same order of magnitude as bottom-fixed offshore wind [44]. Most of the research on FOW cost reduction is focused on reducing the capital, upfront expenditure (CapEx). Since the industry has mainly been active in demonstration projects and testing campaigns, the operational expenditure (OpEx) has received less attention. However, if large-scale FOW farms are to be installed, the OpEx becomes more and more important. Efficient operation and maintenance (O&M) strategies are critical to having a low OpEx.

O&M is a broad term. It covers all actions that are necessary to keep an asset available and working accordingly. As the term implies, it is divided partly in operations and partly in maintenance, and both are closely related. Operations include condition monitoring, weather and maintenance forecasting, logistic planning, the sourcing of parts and more. Maintenance covers the repair and replacement of components, whether it is preventative or corrective. The category of maintenance also covers all actions surrounding the maintenance action. This involves the vessels and offshore technicians that are required for the operation, which can differ a lot for the type of maintenance. Maintenance on large components can also involve a lifting operation. Personnel, vessels, the lifting operation and the replacement components therefore all fall under the category of maintenance [35] [12]. Of the two categories, maintenance costs contribute to a large part of the total O&M costs [35].

This will especially be true for floating wind, compared to bottom-fixed wind. The logistical challenge of bringing components and vessels further offshore is costly. Floating wind farms could also be placed in more remote areas where servicing ports could be far away, resulting in more downtime of the turbines due to increased travel time to the wind farm. Moreover, the fact that the floating turbine is placed in an area with better wind resources also means that it will encounter a harsher environment, which could lead to faster degradation of the asset and a smaller weather window for maintenance. Floating wind turbines will also experience larger motions than their bottom-fixed counterparts, since the floating platform does not have a fixed connection with the sea floor. These induced motions increase the chance of mechanical defects in components sensitive to turbine motions and accelerations, like the gearbox. It also contributes to higher fatigue damage due to increased vibrations in components like the blades. This suggests that the maintenance of floating offshore wind turbines (FOWTs) could be an important aspect in the LCOE of FOW [30].

## 2.3. Methodologies for major maintenance in floating wind

In case a major component on a FOWT fails, it must be possible to replace it in order to keep the FOWT operational. The replacement of a major component on a FOWT requires a different approach than the same operation would on a bottom-fixed offshore wind turbine. When a blade or another major component is exchanged on a BFOW turbine, a similar method is followed as the installation of the component. The broken component is removed by a crane vessel in the reverse manner of its installation, and the replacement component is lifted up to the turbine and installed. The crane vessels used for these operations are called jack-up vessels. They have four or more legs, which they can extend to the sea floor, after which they can lift (jack up) their hull above sea level. Jack-ups are used to service BFOW turbines as their legs extend the reach of the crane, and their legs offer the required stability for a precise lift such as the installation of a blade. Most jack-ups used for the installation or maintenance of BFOW turbines have a maximum jacking depth of around 60 meters. As floating wind farms will be placed in deeper waters, the use of jack-ups for maintenance is not an option, and alternative methodologies must be investigated.

**Figure 2.3:** Installation or maintenance on a bottom-fixed wind turbine using a jack-up vessel

In literature, several methodologies have thus far been discussed as a solution for major component exchange on FOWTs. A distinction can be made in onsite maintenance, where the turbine is serviced in the same location as it is operated, and offsite maintenance, where the turbine is relocated. As the turbines are floating, they can be relocated without the dismantling of their substructure. In the next subsections the proposed methodologies are discussed.

### 2.3.1. Offsite maintenance

One of the problems of major component maintenance in FOW is the inability of traditional maintenance equipment to work in locations with deep water. In order to make the FOWTs accessible for maintenance equipment, several solutions have been suggested where the FOWT's mooring system and power cable are disconnected, and the turbine is towed to a more accessible location by tugboats. To service the turbine, it can be towed to a port, where a land-based crane is able to access it. The advantage is that there is no need for a crane vessel because of the onshore crane, since a lift by an offshore vessel can be up to ten times more expensive than a lift by an equivalent onshore crane [35].

In order for the FOWT to be towed, its stability during towing is of importance. Since the mooring lines of the floater will be disconnected, its hydrostatic stability is the dominant factor. A semi-submersible and SPAR floater have good hydrostatic stability for towing, but a TLP is unstable when its tendons are disconnected. As a TLP has no ballasting system, it is not possible to tow it, unless it is externally stabilized or ballasted. It is noteworthy that a SPAR-type floater would not be ideally suitable for a tow-to-port maintenance scenario. Because of its large draft, a SPAR would not be able to enter any port where it could be serviced. The only possible location for maintenance for a SPAR would be a fjord in for example Norway, where it would be in reach of a land-based crane in deep waters. However, such infrastructure there is scarce [46]. A potential solution would be to use a Heavy-Lift Vessel (HLV) such as the Saipem 7000, which has been used in the installation of five SPAR-type floating wind turbines in a fjord in Norway [36] as shown in figure 2.4. However, HLVs are among the offshore industry's most expensive vessels, and lack hook height for performing maintenance at the hub heights of next generation's wind turbines [46].

| ***Floater type*** | ***Suitability for towing for maintenance*** |
|---|---|
| Semi-submersible | Good, inherently stable |
| SPAR | Moderate, limited locations and HLV necessary |
| Tension-Leg Platform | Bad, unstable without tendons |


**Figure 2.4:** Construction work on a SPAR-type FOWT using the HLV Saipem 7000 in the Hardangerfjorden at Stord, Norway [36]

A towing for maintenance operation has already been performed on a semi-submersible FOWT from the floating offshore wind farm Kincardine, where a semi-submersible floater type FOWT was towed from Scotland to the Netherlands using anchor-handling tug supply (AHTS) vessels [50]. Maintenance was performed on the turbine in the port of Rotterdam, after which it was towed back to the wind farm and the AHTS reinstalled the mooring lines.

**Figure 2.5:** A semi-submersible floater being towed from Kincardine to Rotterdam

Although this solution is technically feasible, there are a few drawbacks that challenge the operational feasibility of so-called tow-backs for entire floating wind farms. Ports suitable for facilitating FOW structures are scarce, and with the expected growth of FOW might not always be available due to ongoing construction and installation of FOWTs. Quayside load bearing capacities are also important to be able to facilitate large wind turbine components and are not always up to the required level, and the availability of onshore cranes capable of operating at the hub height of next generation wind turbines is also an issue [46]. With few ports then available for maintenance, the distance that needs to be covered during the towing operation increases. This increases the downtime of the turbine, and adds to the cost of the vessels that are used in the towing operation. For the tow-back maintenance operation on a FOWT from the Kincardine floating wind farm, three AHTS were involved for a total of almost a hundred vessel days during a three-months operation [41].

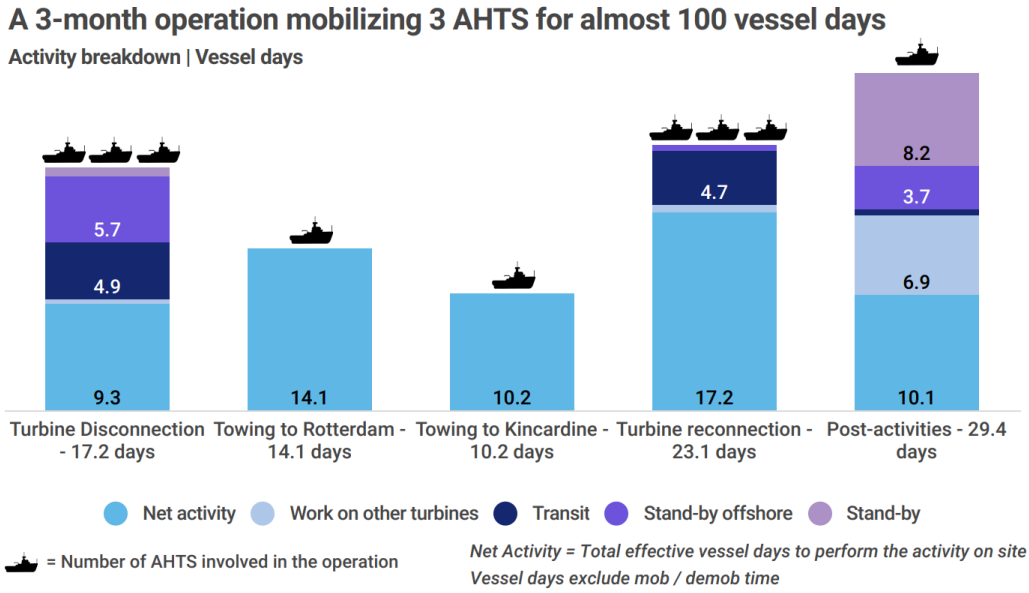


**Figure 2.6:** AHTS requirement for maintenance of a single FOWT in a tow-to-port scenario [41] (Figure courtesy of Spinergie)

Extrapolating this data to the case of an entire FOW farm, would mean a high amount of downtime when multiple FOWTs need maintenance and would lead to a large demand for AHTS for major maintenance on the FOWTs. This greatly increases the complexity of the operation of a FOW farm and adds significant emissions to the environmental footprint of the wind farm.

### 2.3.2. Onsite maintenance

As an alternative to offsite maintenance where the turbine has to be towed to the location where it will be serviced, several maintenance solutions have been presented where the turbine is serviced at its location within the FOW farm. Because the floater does not need to be displaced, and its mooring does not need to be disconnected, onsite maintenance can potentially reduce the complexity and duration of a maintenance operation. This reduces risk and turbine downtime. In the Floating Wind Joint Industry Project Phase 3, multiple concepts for onsite maintenance for FOWTs are introduced, and their cost-effectiveness is compared to a tow-to-port scenario [46]. The methodologies for onsite maintenance are presented below.

#### Heavy-lift vessels

Firstly, HLVs are presented as an option to service FOWTs for maintenance onsite. The old component would be lifted down from the turbine and a replacement component would be installed on the turbine by the cranes of the HLV, similar to how a jack-up vessel would do on a bottom-fixed turbine. As presented in the Joint Industry Project, the biggest challenge when performing a lift from a floating vessel to a floating structure is the relative motion between the lifted object and the floating structure. As the HLV will not be connected to the FOWT, the HLV and FOWT will have significantly different motion characteristics. The lifted component will see oscillations caused by wave loads on the HLV. Even though HLVs are relatively stable vessels, the vessel motions will be amplified at the lifting height required to install the component. Furthermore, displacements of the FOWT will lead to motions relative to the lifted component, and these motions are also amplified at the hub height of the FOWT.

To perform a major component exchange on a FOWT, the HLV should be able to lift to the hub height of the turbine. Floating turbines are expected to have a hub height of at least 150 meters such as the IEA 15 MW reference turbine [51]. The hook height of most HLVs is not high enough for this, and currently only the HLV Sleipnir would be able to lift components to this height [9]. Other downsides of using an HLV are the high vessel costs, and the availability of HLVs. An HLV must be mobilized and sail to the wind farm, which can lead to even higher vessel costs for unscheduled maintenance, where the vessel is not booked beforehand and marine spread can lead to unavailability of the vessel.

#### Turbine mounted cranes

Other solutions for onsite maintenance are also presented, which mitigate the challenge of relative motions between the crane and FOWT. Turbine mounted temporary cranes are introduced as an alternative to using a crane vessel. As the crane is mounted on the turbine, the crane tip will follow the motions of the turbine, which will reduce the relative motions between the lifted component and the FOWT. Another advantage is that a smaller and thus cheaper crane can be used. Different concepts exist for turbine mounted cranes. The concepts originate from the onshore wind sector, where heavy lifts with land-based cranes are a big cost driver. Self-hoisting cranes, which lift themselves up through their own hoisting cables using an attachment point at the nacelle of the turbine, are presented as one solution. An example of a self-hoisting crane solution is shown in figure 2.7. Self-hoisting cranes require a structural modification of the nacelle, which should be able to host the crane and to carry the loads from the crane. The hoisting of the crane requires a tensioned cable to the ground, which for offshore operations would be to a vessel. This could lead to large dynamic oscillations of the crane during the hoisting process, as the vessel will be subject to hydrodynamic loads and will transfer its motion to the tensioned cable.


**(a)** Hoisting of the crane

**(b)** Component exchange

**Figure 2.7:** A component exchange using a self-hoisting crane [28]

Another solution for using a turbine-mounted crane is a crane that is installed at the bottom of the turbine by a crane vessel, and erects itself or climbs up by itself along the tower of the turbine. The advantage is that no structural modifications of the nacelle are required, and the hoisting procedure is avoided altogether. Different concepts exist for climbing cranes, of which some are already applied in the onshore wind sector. Two examples of self-climbing cranes are shown in figure 2.8, one from Lagerwey and one from Huisman. Lagerwey builds climbing cranes which are specifically built for certain wind turbines, as they use the tower to climb [25]. Although the crane offers many advantages to a traditional onshore crane, such as a smaller construction area around the turbine and the fact that it is more easy to transport, it is not used widely due to the need of a specific tower design. The tower has strong points and attachment points for the crane, which it uses to climb upwards. The climbing crane is not used on wind turbine towers that are not designed specifically to host the climbing crane. Industry experience tells that wind turbine manufacturers are very hesitant about loads applied to their tower that they are not designed for. As towers are generally designed on the limit and have a thickness of only a few centimeters, manufacturers do not want to take the risk of applying loads to the tower that do not come directly from the rotor and nacelle. The added cost of tower modifications necessary for hosting a climbing crane is also something that wind turbine manufacturers are not keen on. These aspects hold back the large-scale development of this maintenance and installation solution, which makes it unlikely that this type of solution will be applied on a large scale in floating wind.

This is where the idea of the Huisman climbing crane comes from. The crane is installed in a single lift and fastened onto the floater, that has small outliers to which the crane can attach. The crane then climbs up by extending its lattice structure. The crane only holds the tower for horizontal stability, and the vertical load is transferred to the floater. The idea is that the structural design constraints are less stringent on the floater, and it will be better suited to carry a load.

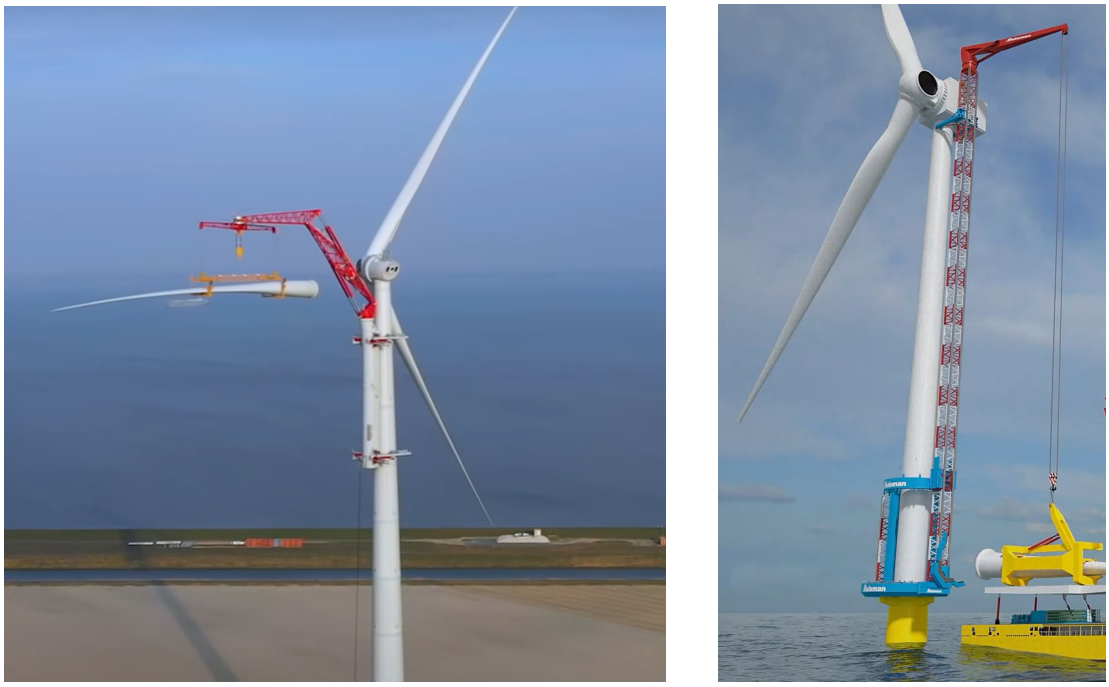

**(a)** Lagerwey climbing crane

**(b)** Huisman climbing crane

**Figure 2.8:** Self-climbing crane concepts

Figure 2.9 shows a concept from WindSpider, which features a turbine mounted crane that consists of a series of truss sections that are based on a modified platform attached above the landing platform of the turbine [52]. The base platform is installed first, after which the truss sections are loaded onto the platform and installed. The stiff truss sections are able to carry a heavier crane than the other turbine mounted cranes. The crane is mounted on the turbine through multiple lifts. An advantage of this concept is that the complete nacelle can be removed, so it is more accessible for maintenance, although this will require multiple lifts as the blades must first be removed. However, this concept is estimated to be heavier than the other concepts, which will have adverse effects on the structural requirements on the FOWT and will negatively impact its static stability and dynamic behaviour. Furthermore, this concept will take more time to be constructed on the FOWT due to its large size and the requirement for multiple lifts to the FOWT, which will lead to more downtime and higher vessel costs.

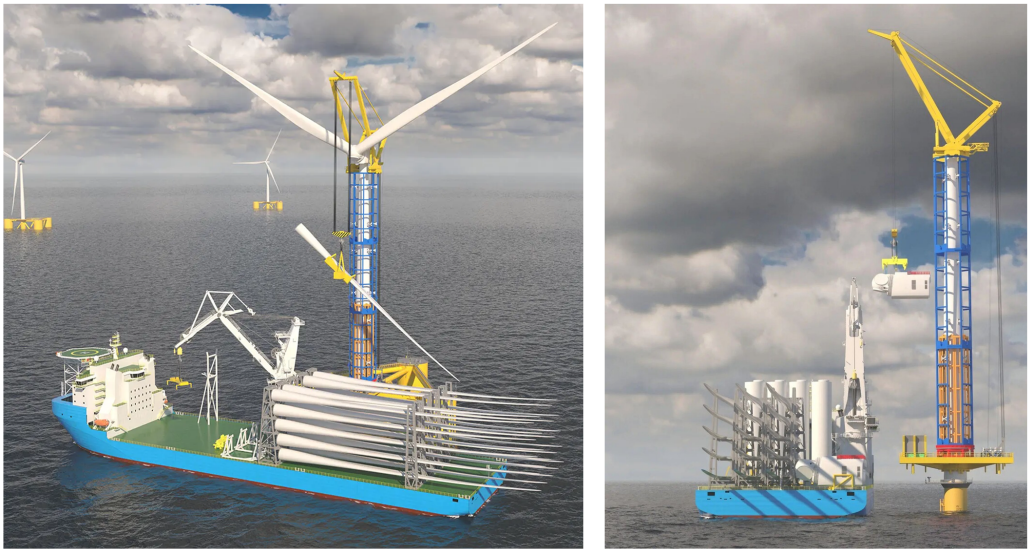

**Figure 2.9:** The WindSpider turbine mounted crane [52]

An installation and maintenance solution has been demonstrated by SenseWind that can remove the rotor and nacelle assembly using a turbine mounted crane [37], which is shown in figure 2.10. Lifting a nacelle vertically would require redesign of certain components in the nacelle, as they are only designed to be in a horizontal position. Furthermore, this solution would require significant modifications to the tower of the FOWT, as the crane must be able to travel along the length of the tower loaded with the rotor and nacelle.

Once removed, the rotor and nacelle assembly would need to be lifted from the FOWT to a vessel, as the nacelle can no longer be accessed from the FOWT itself. This lift must be done by a floating vessel and could result in oscillations of the rotor and nacelle assembly when lifted. Due to the complex geometry of the rotor and nacelle assembly, this lift could be limiting due to clashing of the assembly with other components involved in the operation. Lifting the nacelle back to the FOWT could also be a challenging operation due to the component dynamics.


**(a)** Lifting of the rotor and nacelle **(b)** Installation of the rotor and nacelle

**Figure 2.10:** The SenseWind turbine mounted crane that can remove the rotor and nacelle assembly [37]

### Motion compensated solutions

The last methodology for onsite maintenance that is presented, is the use of motion compensated systems to access the turbine. To eliminate the problem of vessel and floater motions that occur during floating to floating operations, several solutions have been suggested that make use of motion compensation. Motion compensation is already widely distributed in the marine industry, with motion compensated hexapods, barges and grippers as prominent examples. Using a motion compensated crane can eliminate the vessels contribution to the relative motions, leaving only the turbine motions. However, a heavy duty motion compensation system must be used, that can handle the load of the lifted component. The motion compensation requirements in this case are less driven by heave compensation, and more driven by the need to compensate the motions at the crane tip resulting from pitch and roll of the vessel and the turbine [46]. This is because these motions are amplified by the large crane height, resulting in large horizontal motions from the lifted component. Using a heavy-duty motion compensation system that is able to compensate angular motions has not been done yet, and might be very costly.

Several solutions have also been suggested that make use of a frame that grips the wind turbine tower, and allows for a guided blade installation. The gripper frame is attached to a vessel and has motion compensation at its footing to avoid large loads from either the ship's or turbine's motions. It is a telescopic frame, which means it can be less bulky and heavy than a traditional crane, and therefore fitted to a smaller vessel. The advantage of using a frame for installation is that the relative motions between the blade and nacelle are cancelled. This also makes it suitable for the maintenance of FOW. The blade is guided in its approach to the hub, which makes installation more easy. An improvement to the design shown in figure 2.11 could be to have an attachment point at the bottom of the tower, reducing the structural requirements for the attachment.

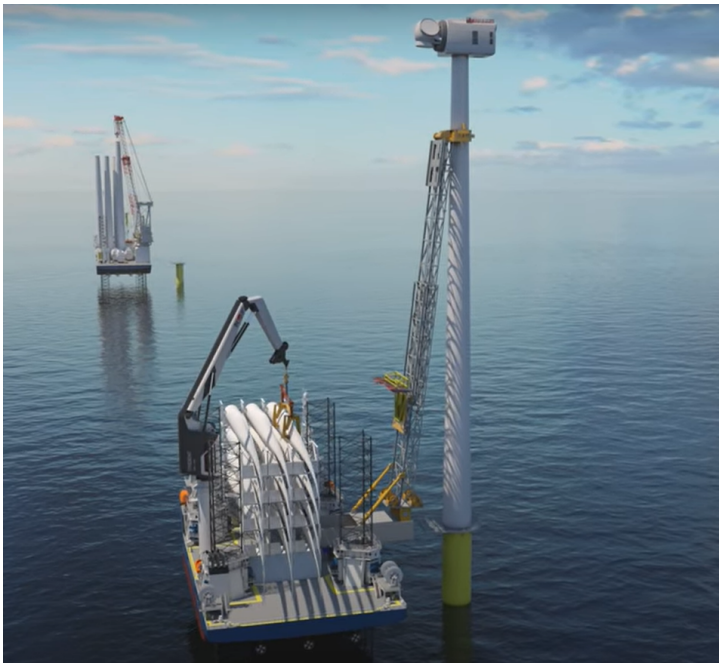

**Figure 2.11:** A gripper frame for blade installation, with a supporting crane and a transferable yoke (Image courtesy of NOV)

### 2.3.3. Comparison of methodologies

In the Floating Wind Joint Industry Project Phase 3, a preliminary economic assessment is made of the methodologies presented in section 2.3 [46]. The methodologies are assumed to be technically feasible, with a suitable weather window in place. The methodologies considered are an HLV with sufficient hook height, a turbine mounted crane that has a long installation duration (crane A), a turbine mounted crane that has a short installation duration (crane B), a motion compensated vessel mounted crane and a tow to port scenario. Several assumptions are made in order to perform the analysis. Distance to port, turbine size and environmental parameters are assumed. Two case studies are examined: a single blade replacement, and a 50 blades replacement campaign. The cost of a blade replacement is calculated, taking into account the mobilization time of each asset, the duration of the blade replacement, the resulting downtime of the turbine, and the crane and vessel charter cost. The result is shown in figure 2.12. It becomes clear that onsite maintenance can be more competitive than offsite maintenance, as turbine downtime is a driving factor. Turbine mounted cranes that have quick deployment are seen as one of the most competitive methodologies, together with motion compensated solutions. It should be noted that the weather window for onsite maintenance is a remaining knowledge gap, which could have a large influence on the results presented in the Joint Industry Project.

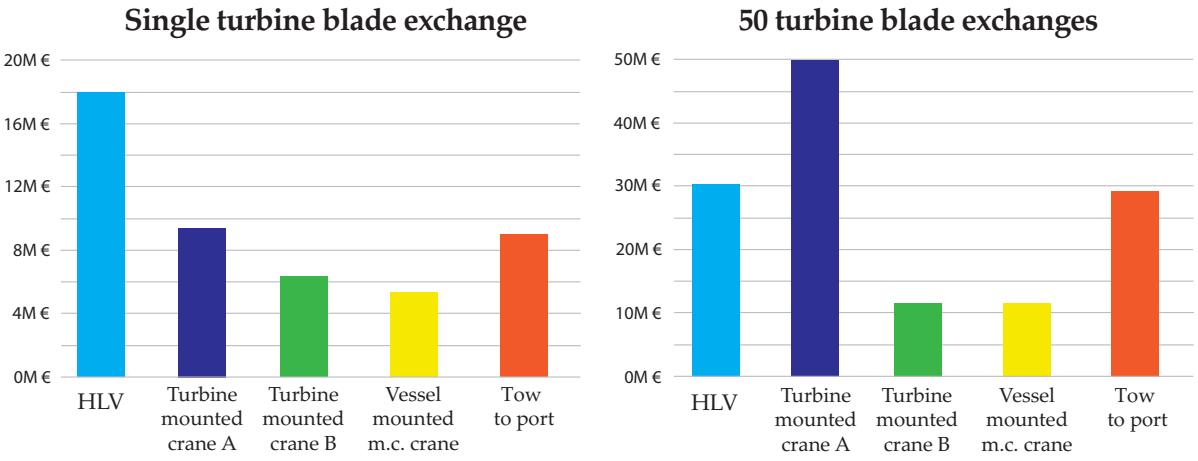


**Figure 2.12:** A comparison of the cost of replacing blades on FOWTs with different proposed maintenance methodologies [46]

### 2.3.4. Judgement

As becomes clear from subsection 2.3.3, the business case for using either a turbine mounted crane or a motion compensated solution is the best. A gripper frame as shown in figure 2.11 that is able to attach at the bottom of the FOWT, and features a motion compensated base is expected to be a feasible maintenance solution. Having a motion compensated crane is expected to be more costly than this type of solution.

All turbine mounted solutions require modifications of either the floater or turbine. It is clear that these type of maintenance solutions should therefore be considered in the design phase of FOWTs. Modifying the floater or turbine will increase costs for the manufacturer. It is therefore desirable to have the least possible amount of modifications, at the least critical parts of the design.

Self-hoisting cranes require an attachment point in the nacelle with enough structural resistance to cope with loads from the crane and lifted component. This will add top mass to the FOWT, which will negatively impact its dynamics. This has consequences for the fatigue seen in the FOWT, and mitigating this results in extra costs for the manufacturer. Furthermore, the potential for dynamic oscillations during the hoisting procedure might limit the weather window of a self-hoisting crane.

The SenseWind and Lagerwey turbine mounted solutions require redesign of the tower. As the Lagerwey onshore climbing crane is not widely used due to this constraint, it is expected that both of these solutions will be difficult to implement on a large scale in FOW. Furthermore, the SenseWind solution will require the rotor and nacelle assembly to be lifted to a vessel, which is expected to be a complicated lifting procedure and therefore could limit weather windows.

The WindSpider turbine mounted solution and Huisman climbing crane require a structural modification of the floater, and have tower supports. The design constraints on the floater are considered to be less stringent than on the tower, which is why it is expected that these type of designs will have a competitive advantage. The WindSpider concept is expected to be the heaviest of the two, which will negatively impact the dynamics of the FOWT which will translate into larger motions of the lifted components during the maintenance operation. Furthermore, the WindSpider concept will have a longer construction duration, which negatively impact sthe cost of a blade exchange as has been shown in figure 2.12. Therefore, the Huisman climbing crane is expected to be the most competitive solution of the two.

## 2.4. Knowlegde gap

As a turbine mounted solution provides a competitive business case for maintenance on a FOWT, it is worthwhile to investigate this type of maintenance solution further. A knowledge gap can be identified in the behaviour of the FOWT when the crane is mounted to the turbine, and the dynamics of the components during lifting. As the FOWT is a moving structure, its motions will cause oscillations of the lifted components that could constrain allowable weather windows due to limits on the motions of components during installation. Assessing these will provide input to the preliminary financial assessment presented by the Floating Wind Joint Industry Project and could provide more insights into what type of major component maintenance solution is most suitable for FOWTs.

# 3

# Single blade installation and exchange

To replace a blade on a wind turbine generator (WTG), an old blade must be removed and a new blade installed. Blades are installed by lifting them up to hub height and installing them in the hub of the turbine. Blades can be lifted in different configurations, ranging from a lift of the complete hub and three rotor blades to a single blade. For this thesis, a lift to replace a single blade is considered. Within this category, different installation methodologies can still be differentiated. Most blades are installed horizontally, although there are some installation methodologies where blades are installed at an inclination or completely vertical. For horizontal blade installation, it depends on the WTG manufacturer whether a blade must be installed at a 9 o'clock configuration such as in figure 3.1, or at a 3 o'clock configuration.

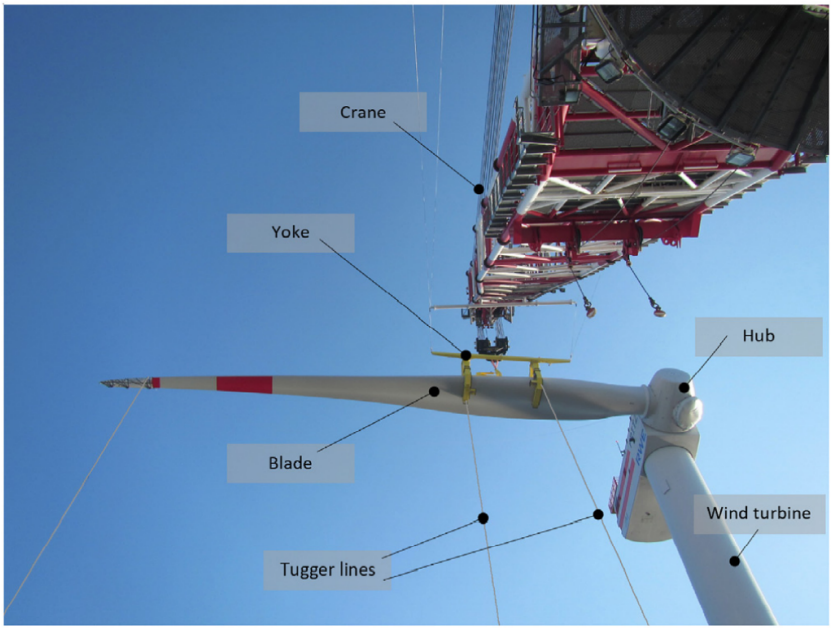


**Figure 3.1:** Horizontal installation of a single blade

## 3.1. Lifting equipment

To install a blade on an offshore WTG, blades are transported in blade racks on an installation vessel. As blades are long and slender components, substantial effort must be taken to fit them appropriately to the deck of a vessel, and in many cases blades are protruding the vessel's edges.

**Figure 3.2:** Blades stacked in a blade rack on an installation vessel

Since blades are relatively fragile structures made of fiberglass and their shape is optimized for aerodynamic performance, it is not possible to make lifting points on a blade. Blades are therefore lifted using a specialized handling tool, called a yoke. It is clamped to the blade at two points along the blade's length, in order to balance the blade. The blade is clamped in high friction rubber mats, which prevent the blade from moving in the yoke during the lift and mitigate any material damage on the blade. Most yokes have remotely controlled functions, and can clamp on to a blade without the presence of a technician.

**Figure 3.3:** A yoke is used to grab and lift a blade

To limit the motions of a lifted blade, tugger lines are used, as can be seen in figure 3.1. As a yoke is lifted with a single hoisting cable, the yawing mode of the blade is unconstrained, and tugger lines are used to compensate for this motion. Tugger lines damp out the oscillations of the blade while it is being lifted, as they provide a force which is proportional to the velocity of the blade. The tugger lines are usually attached to the crane that is lifting the blade, and can travel along the crane in order to guide the blade along the length of the crane boom.

## 3.2. Blade removal

There is not much publicly available information on the removal of blades on modern offshore wind turbines. The public information on blade removal comes mostly from video's from maintenance campaigns. When a blade is removed, a yoke is lifted up to the blade, where it is attached. From public sources, the available information shows a yoke that features belts that go around the blade. At the hub, technicians wrap a second belt around the blade. Because the blade could be damaged, its center of mass is unknown and it is floated in its bearing to test if the yoke is placed correctly. Then, the bolts are undone and the blade is removed from the hub. Although it has not been done yet, a remotely controlled yoke could also be attached to a blade in order to remove it. Extra care should then be taken to ensure that the center of mass of the blade is still at the center of the yoke. When the blade is lifted down, it is either placed directly in a blade rack or on the deck of the vessel.

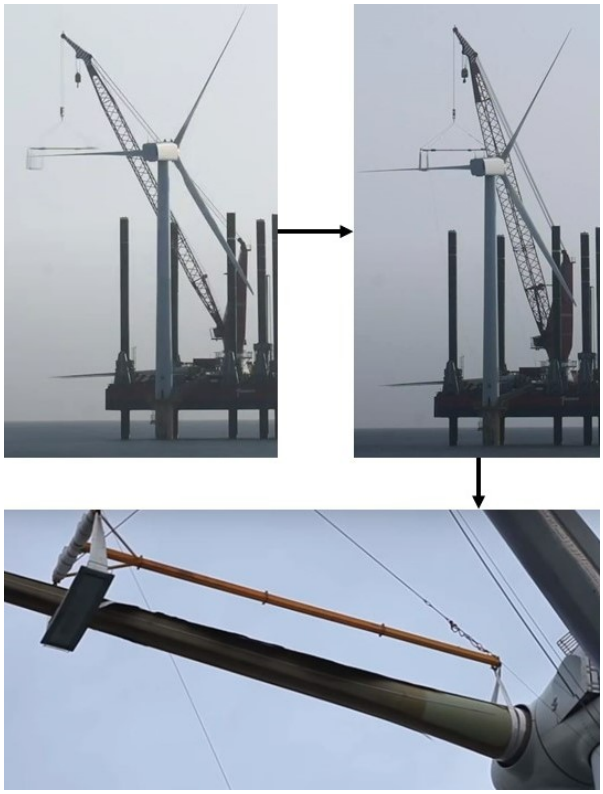

**Figure 3.4:** Yoke with belts attachment sequence [15] [49]

## 3.3. Blade installation

When a blade is installed, a yoke is attached to it and it is lifted directly from a blade rack up to hub height. A blade is installed in feathered position, which means the aerodynamic loads are as low as possible, but there is still potential for oscillations due to aerodynamic loading. The installation of a blade is a precise process, as the bolts in the blade need to be matched with the corresponding holes in the bearing. This procedure is called the mating process. This is done by first matching a long guide pin in a specific flange hole, after which the blade is set in its position and is installed further. A technician is present in the hub, who is able to make final adjustments on the position of the blade while it is brought towards the hub during the mating process.

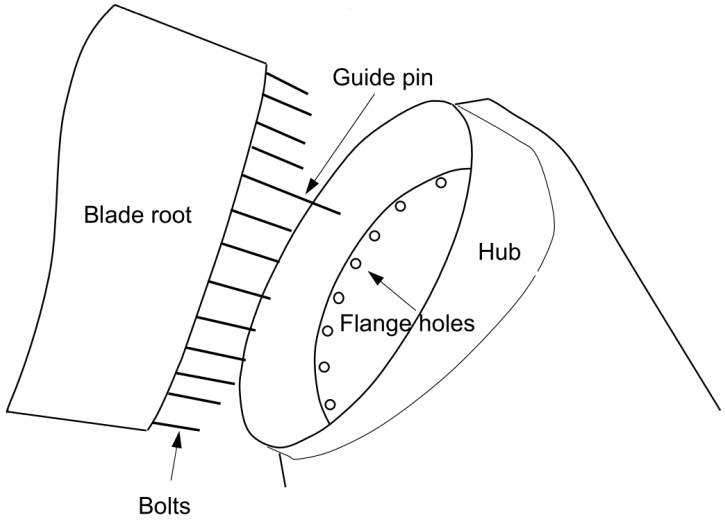


**Figure 3.5:** Sketch of the components that are mated during blade installation [21]

A blade cannot be installed properly if its motions relative to the hub are too large. If this is the case, there is a risk of damaging the guiding pins, which after being damaged are not easily replaced [48]. In order to perform an operational analysis, it is therefore of importance to have a criterion on which the operability of a blade installation can be assessed. This is provided by *K. de Leeuw* [27]: *In the alignment phase the distance between the hub centre and blade root centre should not exceed the safe boundary. Together with a lifting supervisor the safe boundary is determined at 0.2 m.* This distance refers to the in-plane excursions between the hub and the blade root, as shown in figure 3.6. This distance can be exceeded once per minute, which means the maximum relative motion between the blade root and hub is 0.2 meters for one minute.

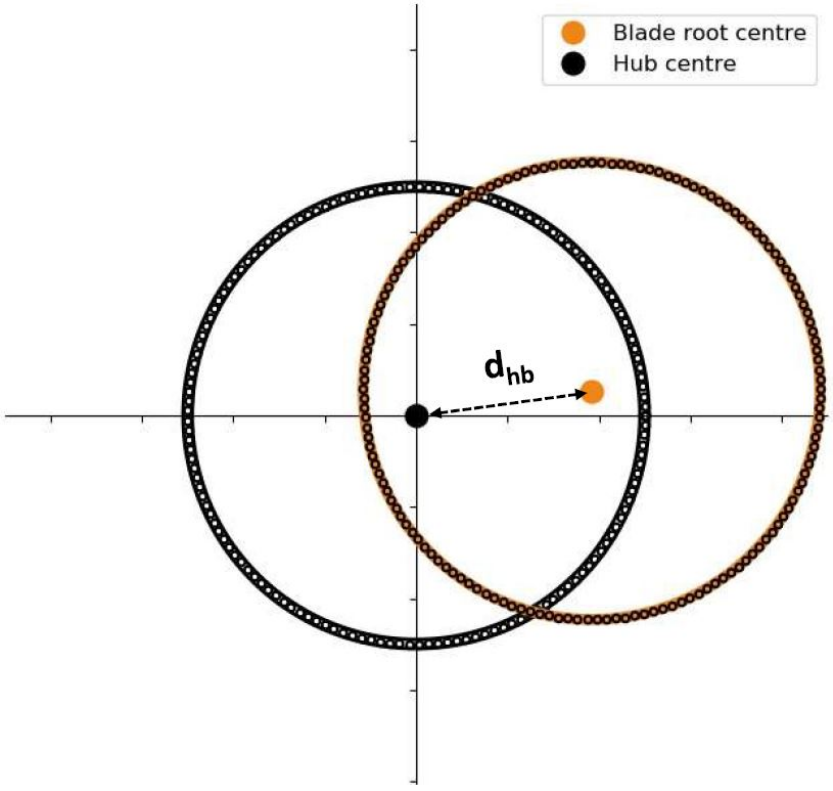


**Figure 3.6:** Alignment definition of blade root relative to hub [27]

Rotations of the blade will also cause misalignment issues. A yawing or pitching motion of the blade will displace the guide pin with respect to its flange hole, which will hinder the mating process. A rolling motion of the blade will misalign all bolts with respect to their flange holes. Therefore, an operational limit is set on the rotation of the blade. It is estimated that the amplitude of the yaw and pitch motion of the blade should stay within 1.5 degree during its installation, due to the alignment of the guide pin. The limit on roll motion amplitude is estimated to be 3 degrees for the bolts to be aligned.

# Part II

# Research scope and model definition

# 4

# Self-climbing crane design and operational procedure

In this section, a compact technical description of the design of the Offshore Self-Climbing Crane is given. The operational procedure of a blade exchange using the OSCC is then discussed. In this overview, the most critical aspects of the design and operation will be outlined. Based on this, a research scope is defined.

## 4.1. Design overview

The OSCC consists of a base, an extendable lattice and a crane, and has a total mass of 1021.1 mT. Two operational modes can be distinguished, the compressed and the extended mode. In the compressed mode, the lattice is not extended and the OSCC can be transported or lifted. In the extended mode, the lattice is fully erected and the crane can operate. The lattice segments are stored in between half-rings in the crane base in the compressed mode, and are slid to the side of the base and erected in the extended mode.

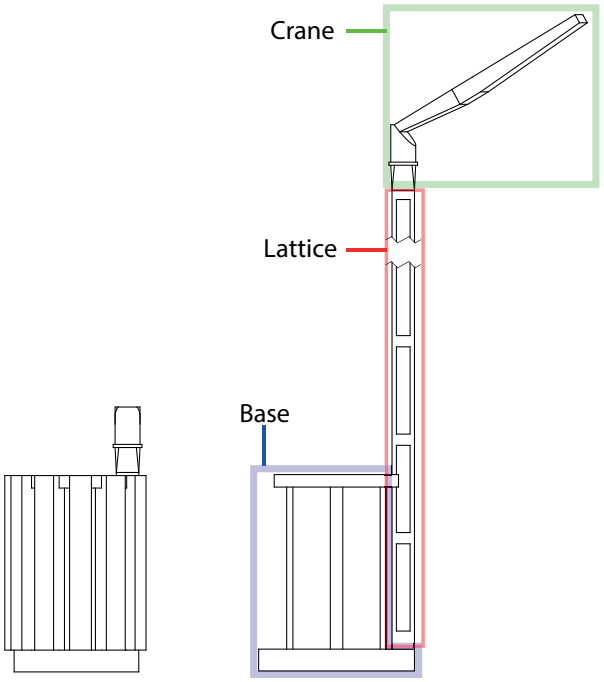


**Figure 4.1:** The compressed mode of the OSCC (left) in which it is lifted and docked and the extended mode of the OSCC (right) in which it operates

### 4.1.1. Climbing sequence

All components of the OSCC are carried by the base, and the OSCC can therefore be transferred in one piece. The lattice structure that houses the crane is divided into multiple segments. In its compressed mode, the lattice segments are carried by the base of the crane in a circular half ring. One of the lattice segments is longer than the others, and has the crane permanently mounted on it. This end segment is located on the right of the base. It is slotted into a guide, which features a motor that can jack the lattice segment upward. The other lattice segments can slide along the ring to where they can be slotted into this motor and connected to the lattice segment above. The crane 'climbs' by sliding new lattice segments into this motor, which jacks up the lattice.

**Figure 4.2:** The climbing sequence of the OSCC, in which it can jack itself up starting from its compressed mode, to its extended mode

### 4.1.2. Connection points

To prevent deformation of the lattice structure, caused by the overturning moment on the structure from tilt of the floater and the mass of the lifted component, there are connections to the tower along the lattice. The tower connections can travel along a rails on the tower side of the lattice, which enables the lattice to slide upwards during the climbing process while the lattice is also connected to the tower. This reduces the reaction loads in the motor while the OSCC is climbing.

#### Tower connections

The tower connections consist of steel cylinders that reach out to the tower. A pretensioned wire is wrapped around the tower at each connection point, which forms the connection between the cylinders and the tower. Because the wire is pretensioned, the stiffness of the connection comes from the cylinders. The stiffness of the tower connections is assumed to be unidirectional, and rotations are assumed to be fixed.

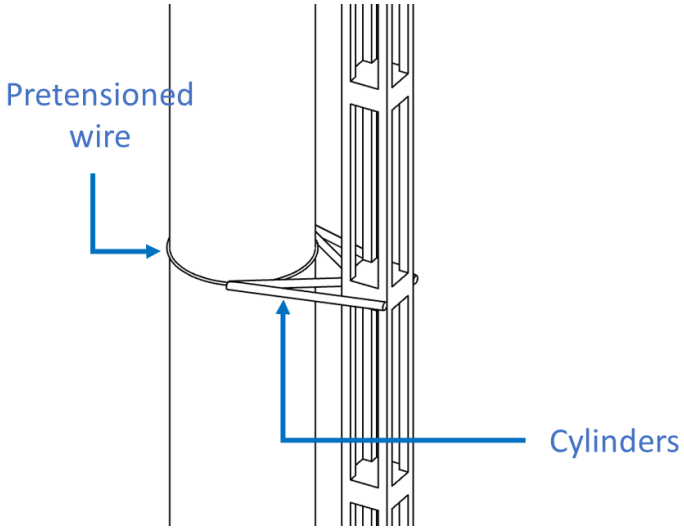


**Figure 4.3:** Close-up view of a tower connection

### Floater connection

The base of the OSCC is docked onto the floater. To make this possible, a connection point should be present on the floater. This connection point must carry the vertical load of the crane and the overturning moment that is not transferred to the tower connections. Strengthened protrusions onto which the crane can be docked are suggested by Huisman. This needs to be taken into account during the design of the floater, and it implies the floater design takes into account a maintenance scenario. Careful communication and planning with the manufacturer of the floater is therefore required, and agreements must be made before the floater is manufactured. This poses a constraint on the use of the OSCC which must be taken into account early in the design process of a floating wind turbine.

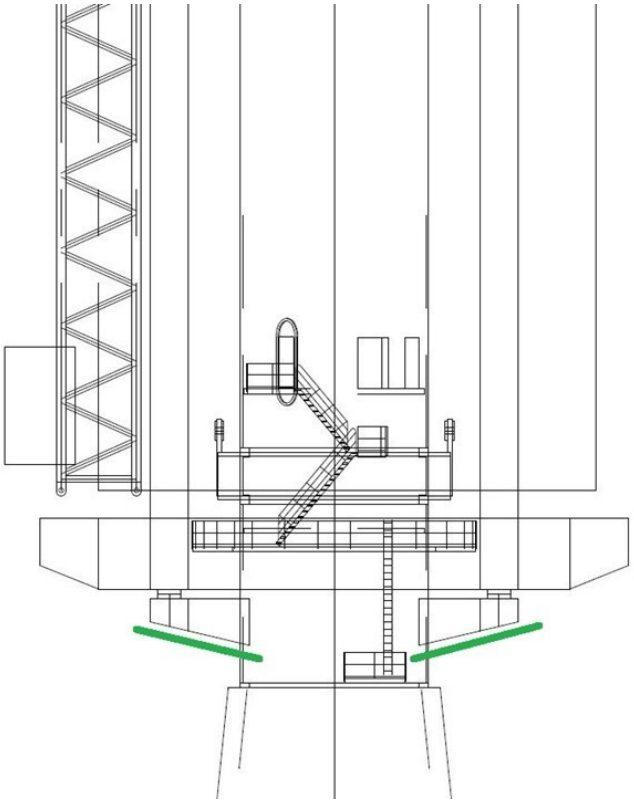

**Figure 4.4:** The protrusions that will carry the crane underlined in green

### 4.1.3. Line-up tool

To control blade motions while lifting, a line-up tool is included in the design of the OSCC. The line-up tool is used to control the yawing motion of the blade while it is being lifted. The line-up tool can move along the lattice over a rails, and is attached to the blade along the length of the lattice. This means it can be used during pickup or setdown of the blade, and during installation.

Two possible configurations of the line-up tool are studied in this thesis. Firstly, a line-up tool that attaches to the root of the blade. A gripper holds the blade, with slip mats on the inside in order to prevent damage to the blade. Secondly, a line-up tool that attaches to the yoke is studied, which requires a specialized yoke to which it can be attached.

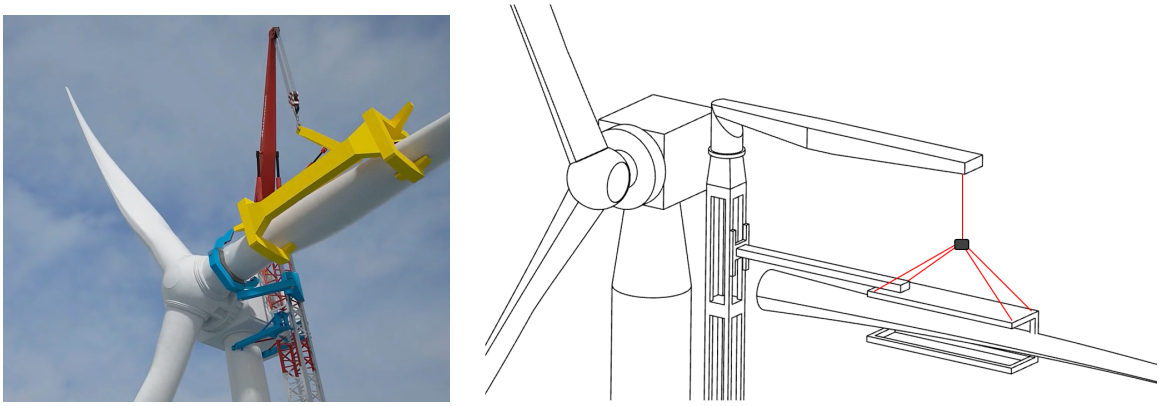

**(a)** Line-up tool at the blade root

**(b)** Line-up tool at the yoke

**Figure 4.5:** Possible line-up tool configurations

The line-up tool mitigates translational motions at its point of attachment. It is therefore modeled by constraining translational motion. In both configurations, the tool is not built for constraining a moment, so rotational motion at the point of attachment is still possible. A schematic of the modeling of either of the two configurations of the line-up tool is shown in figure 4.6. The red translational degrees of freedom are constrained motions, and the green rotational degrees of freedom are free.

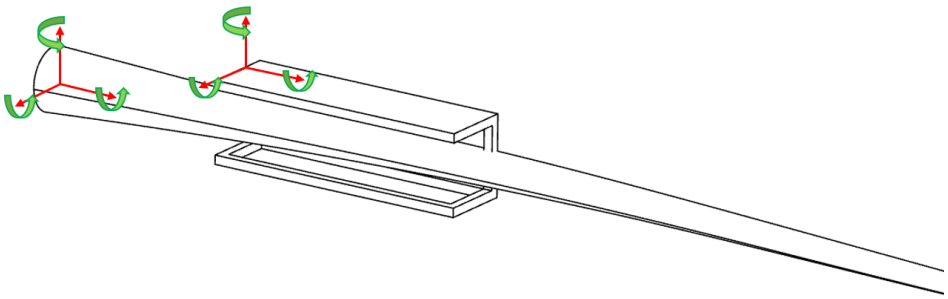

**Figure 4.6:** Modeling of either of the constraints the line-up tool imposes on the blade motion

It is expected that constraining the full motion of the blade by fixing the rotations in the connection point of the line-up tool, will lead to large loads in the line-up tool. In this case, the line-up tool must also be able to constrain moments in its connection point. These moments will be caused by aerodynamic loads on the blade and changes in the hoist cable tension due to crane tip displacements. It is expected a large amount of equipment material is required to give the line-up tool enough structural resistance to withstand these loads, which is expensive and unfavourable from a design point of view. Therefore, the line-up tools are modeled without a constraint in rotation. By using both line-up tools together, the motions of the blade will also be fully constrained, and large loads are also expected. Therefore, only one of the line-up tools can be used.

## 4.2. Support vessel

A support vessel must be used that is able to install the OSCC onto the turbine. Ideally, the vessel should have enough deck space for the OSCC and the replacement components of the wind turbine. If this is not the case, a separate supply vessel or barge must be used, which complicates the operation. Since a precise lift must be performed to bring the crane to the turbine, the support vessel should have a dynamic positioning (DP) system. A DP system controls the low-frequent station keeping of the vessel by actuating the thrusters of the vessel in such a way that it can remain in the same position and heading under wave, wind and current loads.

To lift the OSCC to the turbine, the vessel should feature a construction crane. In the following subsections, the possibility of having a single and a dual crane support vessel is discussed.

### 4.2.1. Single crane lift

The center of gravity of the OSCC in its compressed mode lies roughly in the midpoint of the half-ring crane base. When the OSCC is lifted with a single crane, its static equilibrium will be such that its center of gravity is beneath the crane tip. However, its center of gravity coincides with the turbine tower in its installed position, and this would mean the crane tip would clash with the tower. This means the OSCC can not be lifted with the lifting point above its center of gravity. Instead, it must be lifted so that the crane tip does not collide with the WTG, so the crane must go alongside the tower. The center of gravity of the OSCC will therefore not be underneath the rigging, and it will tilt with its base towards the vessel.

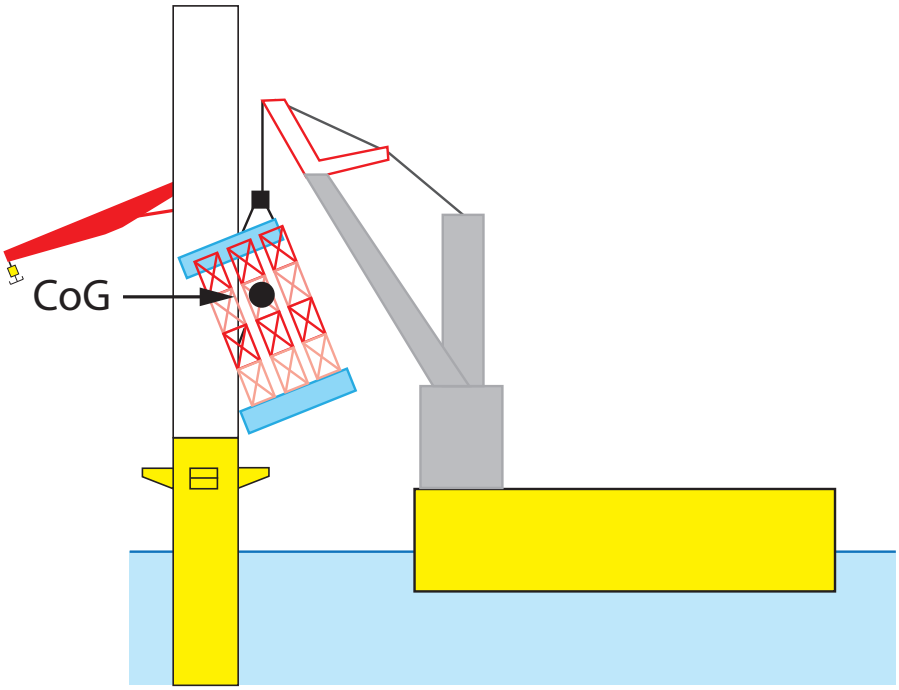


**Figure 4.7:** Static equilibrium of the tilted OSCC when lifted with a single crane

Because the base tilts towards the vessel, it is not possible to mitigate the tilt of the OSCC with lines, as they only work in tension. A pushing mechanism is sketched in figure 4.8 that could mitigate the tilt of the OSCC and aid in the installation of the base. It can be seen that for this type of lifting arrangement, the clearance of the crane boom to the WTG tower becomes critical.

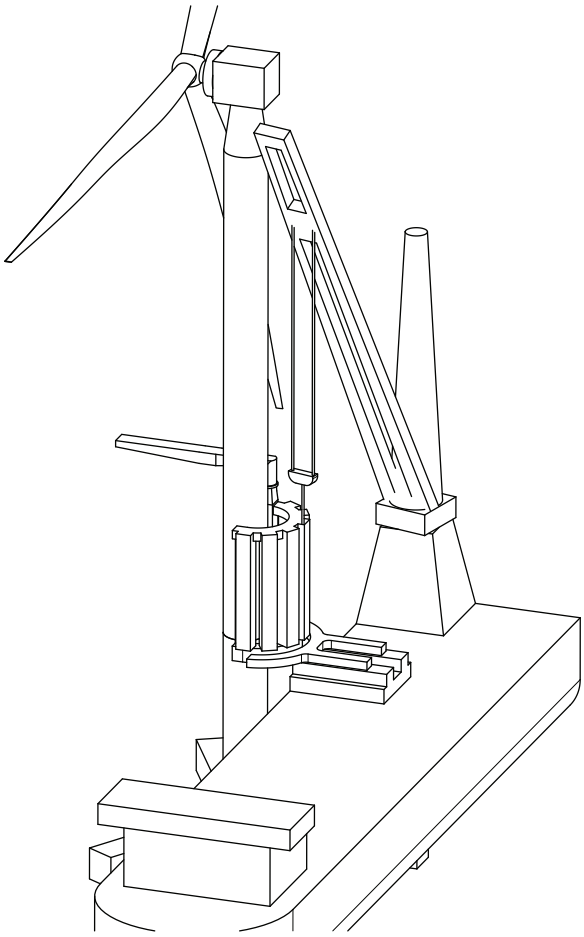

**Figure 4.8:** Sketch of single-crane installation of the OSCC

### 4.2.2. Dual crane lift

When a dual-crane vessel is used, the OSCC can be lifted such that its center of mass lies in between the lift points. Furthermore, the cranes can go around the turbine tower which makes it possible to install the OSCC with this lifting configuration. This crane configuration is shown in figure 4.9.

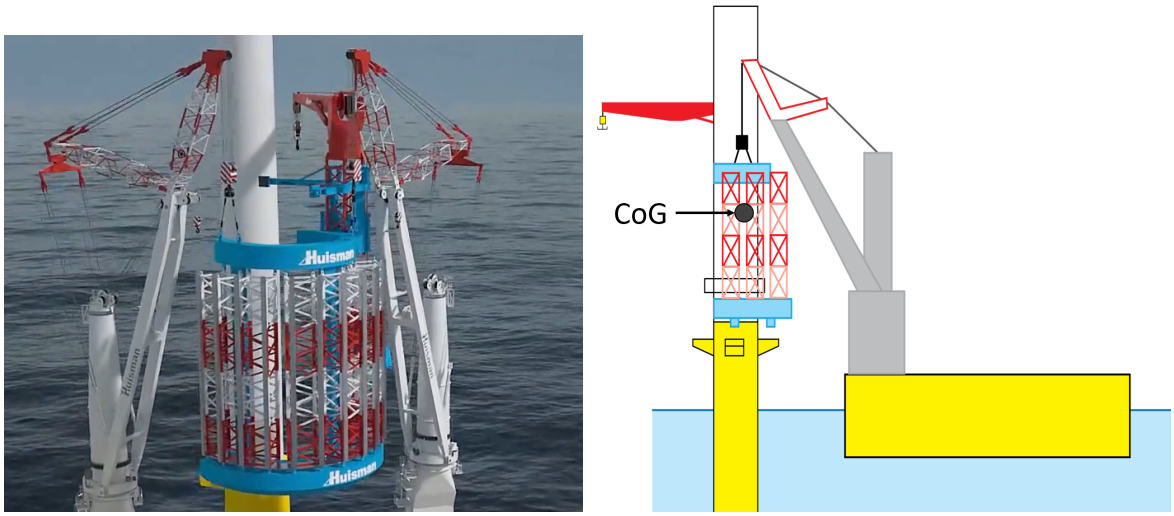


**(a)** The dual crane lift of the OSCC

**(b)** Center of gravity with respect to the rigging of the vessel's cranes

**Figure 4.9:** The dual-crane lift of the OSCC and the position of its center of gravity

To limit the vessel charter cost, which is an important driver in the total maintenance cost, a small support vessel is preferred. Concretely, this rules out large SSCVs with two cranes as potential vessels for the operation. This and the previously mentioned requirements leave several vessels as suitable candidates for a dual crane support vessel.

The market for dual crane vessels with a large deck space comes mostly from the shipping industry, with vessel owners Jumbo, BigLift, SAL and Spliethoff as examples. However, since these vessels are mainly used to ship large components and are not frequently used in offshore construction, many of these vessels lack a DP system. Only a few of these type of vessels have been used for offshore construction, and therefore feature a DP system. The vessels that meet the requirements are listed in table 4.1.

**Table 4.1:** Suitable vessel candidates for the support vessel of the operation

| ***Owner*** | ***Vessel Name*** | ***Length (m)*** | ***Breadth (m)*** | ***Draft (m)*** | ***DP*** | ***Cranes (mT)*** |
|---|---|---|---|---|---|---|
| Jumbo | Fairplayer | 144.1 | 26.7 | 8.1 | DP2 | 2x 900 |
| Jumbo | Javelin | 144.1 | 26.7 | 8.1 | DP2 | 2x 900 |
| Jumbo/SAL | Lone | 160.6 | 27.91 | 9.01 | DP2 | 2x 1000 |
| Jumbo/SAL | Svenja | 160.6 | 27.91 | 9.01 | DP1 | 2x 1000 |

Only four dual-crane vessels meet the constraints for a support vessel. The low number of suitable vessels could potentially be an operational bottleneck due to vessel unavailability and marine spread. This risk is lower for the case of single crane installation. A list of suitable single crane vessels is given in appendix A, which consists of 15 vessels. However, the crane tip clearance with the turbine tower and the need for additional installation equipment when using a single crane vessel is deemed more of an operational challenge than the low number of suitable dual crane vessels. Therefore, a dual crane vessel is chosen as a support vessel.

The suitable dual crane vessels have similar specifications, with similar deck space and crane capacity. Because the information found on the Jumbo Fairplayer is the most thorough, this vessel is used as the support vessel for the scope of this thesis. It features two 900 mT mast cranes, that are able to mount a flyjib for added lifting height and range. Adding the flyjib reduces the capacity of each crane to 700 mT, which is still sufficient for the OSCC. The Jumbo Fairplayer is shown in figure 4.10.

**Figure 4.10:** The Jumbo Fairplayer

## 4.3. Operational sequence and limiting factors

To understand how the OSCC works, and find which aspects of the operation might influence its working limits, an operational sequence is described in this section. A high-level overview of the component exchange operation is given in figure 4.11. The sequence includes the transport of the OSCC to site, its installation on the turbine, the exchange of a component and the required steps for safe decommissioning and return.

Crew transfer is also included in the sequence, as crew must be present on the turbine to detach the rigging of the OSCC after it is installed, assist the removal and installation of the blade at hub height, and attach the hooks of the vessel cranes to the OSCC before it can be decommissioned. There must be a connection between the turbine and the support vessel all times that the crew is on board the turbine. As the vessel needs to reposition during the operation, either a walkway must be used that is able to rotate and keep a connection to the turbine, or a separate crew transfer vessel is required.

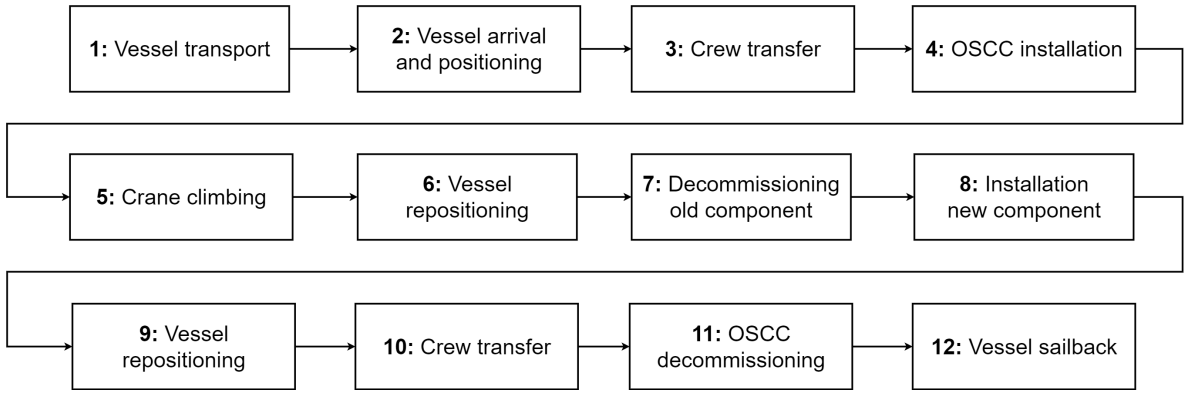


**Figure 4.11:** Overview of all required steps in a component exchange with the OSCC

### 4.3.1. Response limits

During the lifting or installation of components, certain critical responses determine whether the operation is feasible or safe. Limits can be assigned to these responses, which in turn determine under which environmental conditions the operation can be performed. Limits can be determined in the form of clearances between objects, installation tolerances and maximum allowable relative motions between components with regards to safe operation. The limits of the critical responses are given in subsection 4.3.2 for each lifting scenario. The limits will be given as an SSMPM, a statistical unit that will be explained in detail in section 5.8. A number of cycles is also given, which corresponds to how many oscillation periods are used to calculate the statistical maximum of a response variable. 1500 cycles corresponds to a 3 hour window of operation, and 250 cycles to a 30 minute window.

Limits are given to the following component motions:

- **OSCC motions when it is installed**

  The installation limits for the horizontal motions between the TLP and the OSCC are determined from dimensional drawings of the connection point between the two. A conical docking and attachment hole with a diameter of 1.5 meter is present on the floater. It is estimated that if the SSA of the horizontal motions is equal to the radius of the docking point, the docking will be successful. The SSA is a statistical unit that will be explained in detail in section 5.8. In practice, this means that for 86.5 % of the time, the OSCC is within the boundary of the conical docking point, in which it can be installed. A further limit is set to rotational motion of 3 degrees SSMPM and vertical motion of 1.5 meter SSMPM, as this could also influence installation of the OSCC.
- **Blade motions during its installation**

  In chapter 3, an installation limit on the in-plane motions of the blade was given, together with an indicative limit on rotational motions. In appendix B, these are converted to an SSMPM.

- **Yoke motions when it is attached to a blade**

  A limit is assigned to horizontal and rotational motions of the yoke relative to the blade, when it is attached to a blade. Overly large motions of the yoke during its attachment are expected to cause difficulties in making a connection between the yoke and blade. An SSMPM of 0.75 meters in horizontal motions is assumed, and 1 meters for vertical motions. Furthermore, an SSMPM of 5 degrees is given to roll motion, and an SSMPM of 3 degrees to pitch and yaw motion. This difference is due to the geometry of the yoke, as yaw and pitch motions will cause a clash with the blade more quickly than roll motions.
- **Blade motions when it is set down on the vessel**

  To ensure docking of the blade is possible, and ensure safe operation on the vessel, a limit is set on the motions of the blade when it is set down on the vessel. As the blade is a long object, yaw and pitch motions can cause large displacements at its tip. Therefore, an SSMPM of 1 degree is given to yaw and pitch motion of the blade. A larger limit of 3 degrees SSMPM is given to roll motion of the blade. A limit of 0.75 meters SSMPM is also assigned to horizontal motions of the blade with respect to its docking point on the vessel.

Furthermore, a seasickness criterion for technicians on the WTG is taken from literature and converted into an SSMPM in appendix B. Clearances are also taken into account. A maximum clearance between objects is taken to be 3.5 meters.

### 4.3.2. Detailed sequence

A detailed description of the operational sequence for a blade exchange is given in the following enumeration, with critical elements and their limits given for each step that involves a dynamic lift scenario.

1. **Vessel transport**

   The OSCC and replacement blades are transported on the Jumbo Fairplayer or a similar vessel. A possible deck layout is given in figure 4.12. A set of blades is transported in a blade rack, and the OSCC is placed in between the cranes, seafastened to deck. Making an exact deck layout is deemed out of the scope of this thesis, as the design of the OSCC is in a preliminary phase and there are too many unknowns about the support vessel.

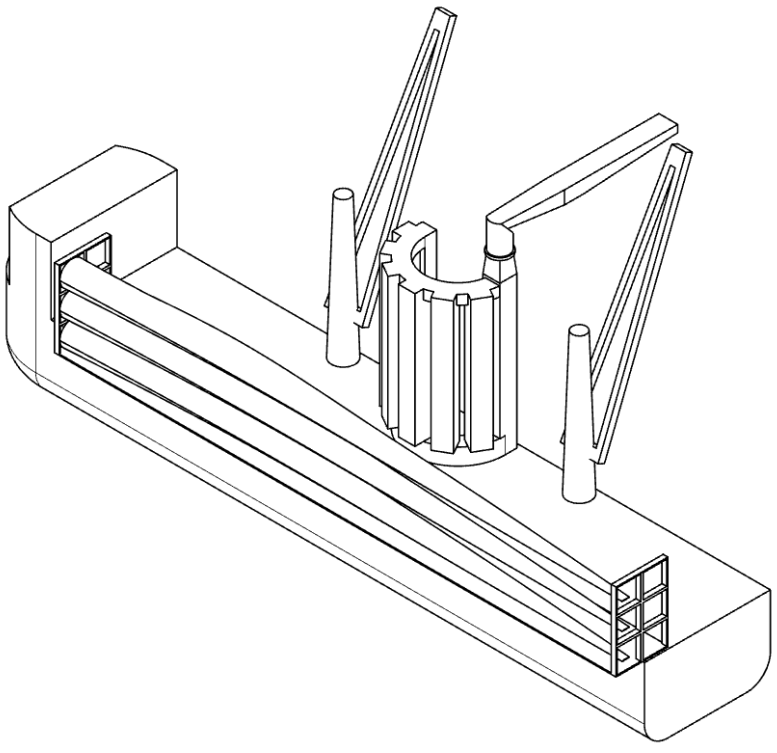

**Figure 4.12:** Possible deck layout of the support vessel, with a blade rack and the OSCC

2. **Vessel arrival and positioning**

   When the vessel arrives at the WTG, its DP system is turned on to keep it in place. In order to be able lift the OSCC onto the WTG, it is positioned close to the WTG. To ensure that there is no risk of collision between the WTG and the vessel, a clearance of 15 meters between the WTG and vessel is set.

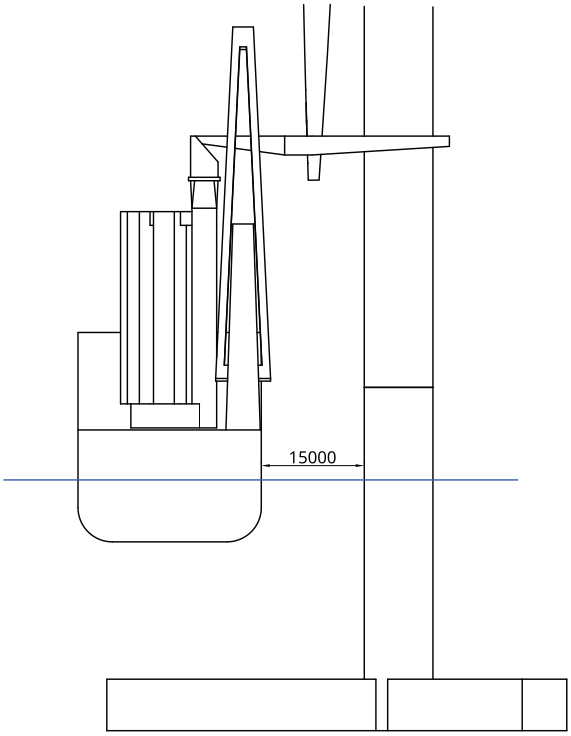


**Figure 4.13:** Clearance between the WTG and vessel

3. **Crew transfer**

   Crew must be present on the FOWT to assist the installation of the OSCC and detach its rigging from the crane hooks. In offshore operations that involve high relative motions between the assets that crew needs to be transferred to and from, motion compensated walkways are used. There is no publicly available information on the exact motions that can be compensated, but limits on wave height are generally given, albeit to transfer to bottom-fixed structures. As walkways exist that can compensate sea states with wave heights of 4.5 meters [1], the motion compensation requirements of existing walkways are deemed sufficient in order for motions during crew transfer not to become limiting.

   The seasickness requirement for the technicians is assessed at the RNA and at the interface height of the TLP. The seasickness requirement is applied when the OSCC is docked on the TLP and operational.

**Table 4.2:** Seasickness criterion

| Body of interest | Property | Response Parameter | Allowable Limit | $N_{cycles}$ |
|---|---|---|---|---|
| RNA and TLP | Motions and accelerations w.r.t. seasickness technician | Horizontal acc. | 0.15*g m/s$^2$ | 1500 |
| | | Vertical acc. | 0.19*g m/s$^2$ | 1500 |
| | | Rotational displacement | 9.5 deg | 1500 |

4. **OSCC installation**

   The OSCC must be lifted with enough clearance to the crane booms, while the vessel remains at a safe distance from the WTG. The vessel's position is therefore determined by its crane curve and the geometry of the WTG and OSCC. From the center-to-center distance of the cranes and the lift points, taking into account the clearance between the vessel and the WTG, it is determined that the working radius of the cranes is 25 meters at an angle of approximately 50 degrees to the vessel.

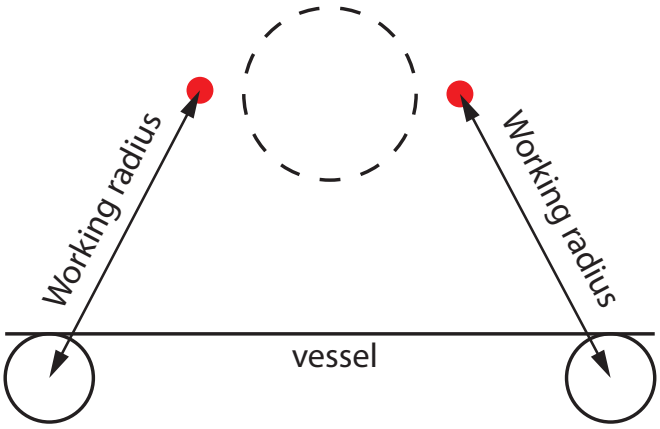


**Figure 4.14:** Working radius of the cranes from the vessel to the lift points of the OSCC

The crane curve of the Jumbo Fairplayer is shown in figure 4.15. At a working radius of 25 meters, the crane capacity is sufficient to lift the OSCC. When the OSCC is docked, its lift points will be at a height of 45 meters, determined by the height of the docking point and the crane base. From the crane curve, it can be derived that there is 15 meters between the lift points and the crane tip. The lift point of the OSCC is plotted in the crane curve below. It is assumed that 5 meters in height of rigging are necessary between the OSCC and the crane hook, which leaves 10 meters of hoist cable length.

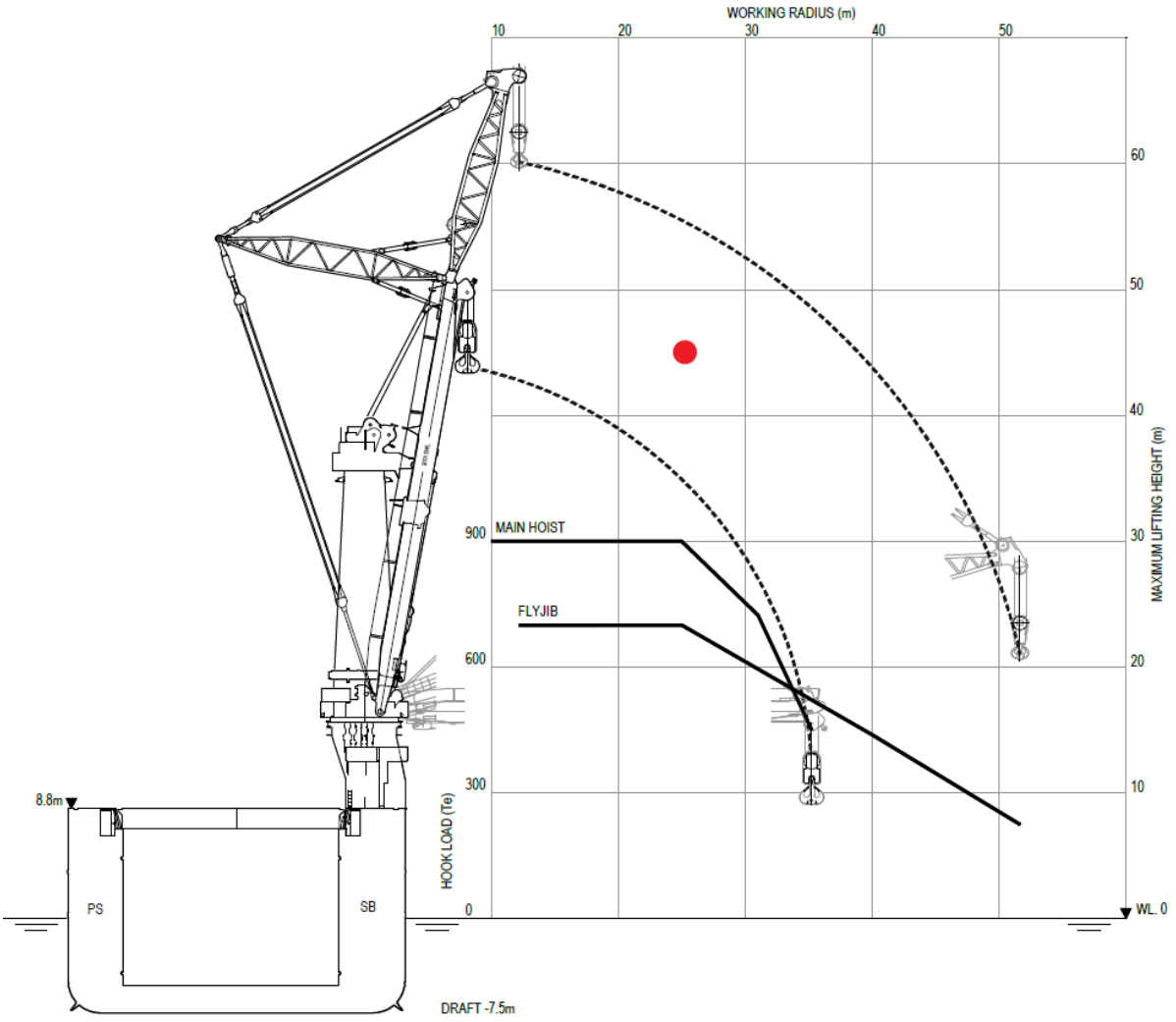


**Figure 4.15:** The crane curve of the Jumbo Fairplayer, with the lifting point marked in red

From dimensional drawings of the OSCC installation steps, it is determined that the clearance between the crane booms and the OSCC is 5 meters at its minimum, and the clearance between the crane tips and the tower is 6 meters. This is at the hovering phase at the docking point of the OSCC on the TLP. As this phase is also the most interesting for analyzing the relative motions during docking, it is chosen to model this phase. All phases of the lifting of the OSCC are given in figure 4.16.

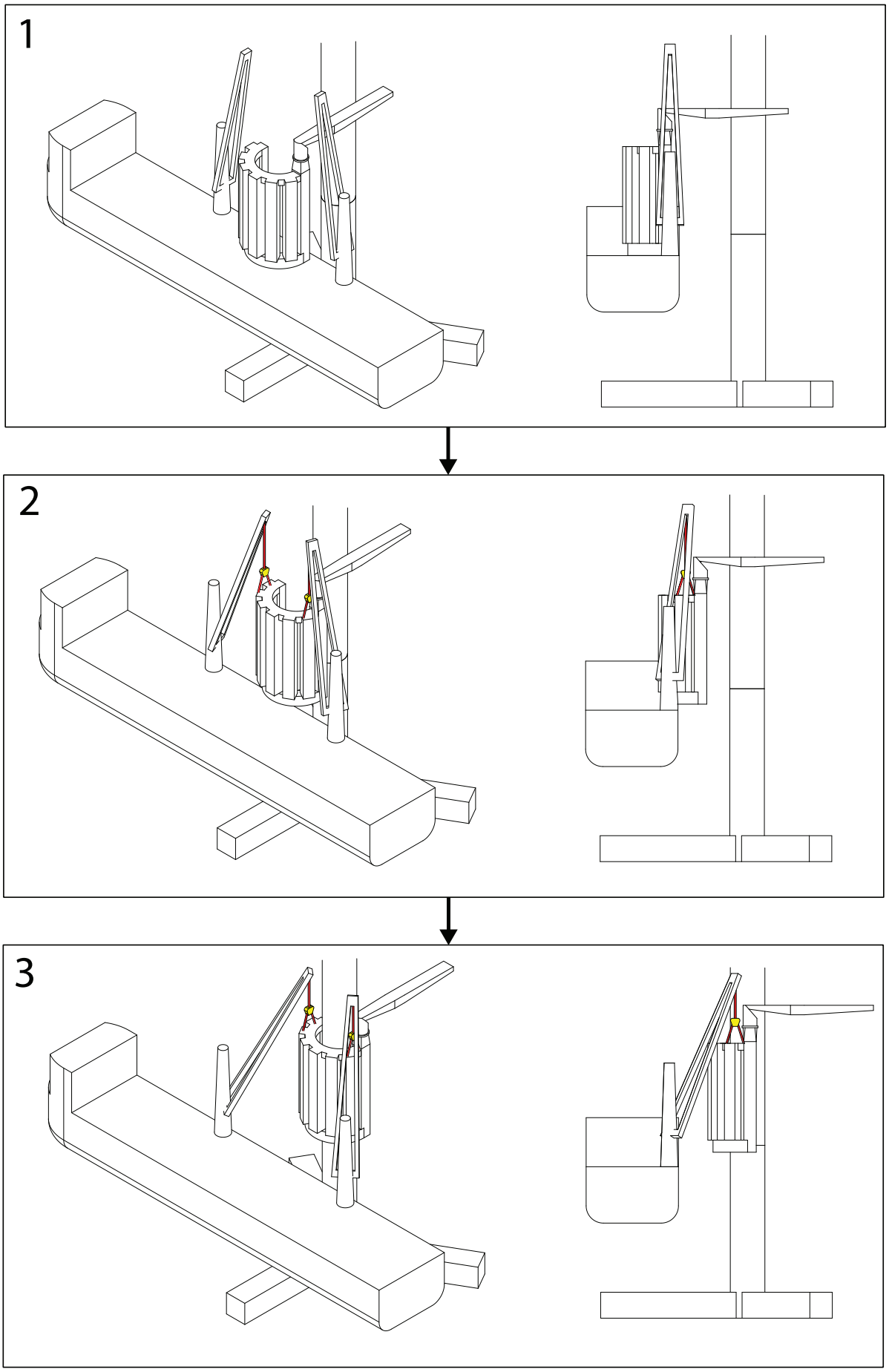


**Figure 4.16:** The lifting sequence of the OSCC to the WTG

Phase 3, the hovering of the OSCC at the TLP before it is docked, will be modeled. It is expected that the motions during this phase will be the most critical, with regards to the installation constraints and crane clearances. The limiting factors are identified as the clearance between the vessel cranes and the OSCC, the relative motions between the docking point at the TLP and the OSCC, and the clearance between the vessel cranes and the WTG. It is estimated that the final hovering phase of the OSCC will last around 30 minutes. The relative motions are computed at the centerlines of the OSCC and the TLP. The complete lifting procedure will take more time, due to the fact that the vessel needs to reballast to compensate for the overturning moment of the OSCC. Therefore, the limit regarding a clash of the OSCC and the vessel cranes is regarded to be in place for three hours. The installation limits given in subsection 4.3.1 are translated to an SSMPM through the number of cycles and presented in table 4.3.

**Table 4.3:** Indicative limiting factors during OSCC installation

| Body of interest | Property | Response Parameter | Allowable Limit | $N_{cycles}$ |
|---|---|---|---|---|
| Vessel | Clearance | Distance vessel crane - OSCC | 1.5 m | 1500 |
| OSCC | | | | |
| TLP | Relative motion | Rotational motions | 3.0 deg | 250 |
| OSCC | | Horizontal motions | 1.25 m | 250 |
| | | Heave | 1.5 m | 250 |
| Vessel | Clearance | Distance vessel crane tip - Tower | 2.5 m | 1500 |
| WTG | | | | |

5. **Crane climbing**

   As the crane climbs, the loads in the jacking system should be kept within safe boundaries. The moment in the jacking system that results from the weight of the crane will be an important parameter, which is why a connection with the tower during the climbing phase is important.

6. **Vessel repositioning**

   The vessel repositions itself for component transfer. To unload a blade from the OSCC's crane, it is positioned alongside the WTG. In this configuration, a blade can be docked in the length of the vessel, while a line-up tool is able to clamp on to the blade root or the yoke.

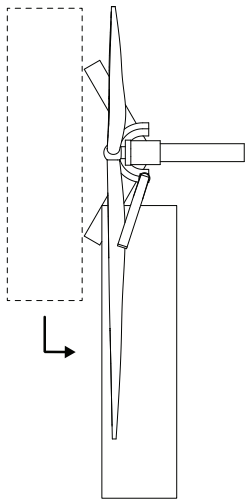

**Figure 4.17:** Repositioning of the vessel to the side of the WTG

7. **Decommissioning old component**

There are several steps to decommissioning the blade that is to be replaced. A yoke must be lifted up to the blade by the OSCC crane, in which the blade is clamped. The blade must be lifted down, and set on the vessel. When a line-up tool is used, it must either be clamped on to the blade during its removal, or attached to the yoke. When a line-up tool at the yoke is used, it is ideally attached to the yoke at the vessel, in order to limit the motions of the yoke while being lifted.

7.1 *Yoke pickup and lift*

A yoke is picked up from the support vessel, and lifted to hub height. If a line-up tool attached to the yoke is used, it is attached at deck level.

7.2 *Yoke attachment*

At hub height, the yoke is brought to the blade. It is held at close proximity to the blade in order for the blade to be clamped in the yoke. Because this is a dynamic lift scenario, it will be modeled and its operability will be assessed. Depending on the choice of the line-up tool, it is either attached to the yoke or not used in this phase.

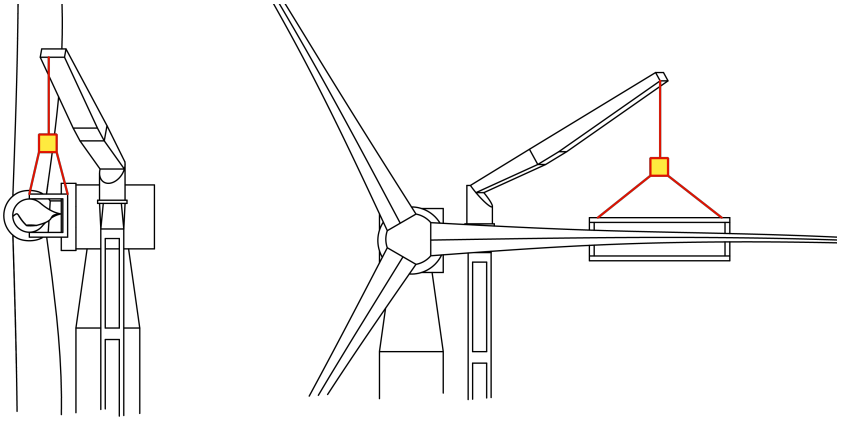

**Figure 4.18:** Schematic of yoke attachment to the old blade

The motions between the blade and yoke determine whether or not the operation is possible. The limiting factors of the final attachment phase are given in table 4.4. The final attachment phase is assumed to be performed in 30 minutes.

**Table 4.4:** Indicative limiting factors during yoke attachment

| Body of interest | Property | Response Parameter | Allowable Limit | $N_{cycles}$ |
|---|---|---|---|---|
| Yoke | Relative motion Yoke - Blade | Horizontal motions | 0.5 m | 250 |
| WTG | | Roll | 5 deg | 250 |
| | | Pitch/Yaw | 3 deg | 250 |
| | | Heave | 1 m | 250 |

The roll and pitch coordinates of the blade and yoke are defined in figure 4.19. The limit in roll is lower than the limit in pitch and yaw because of the geometry of the yoke. If the yoke rotates around its center of gravity in pitch or yaw with respect to the blade, the misalignment will be larger and therefore the limit in pitch has been set lower.

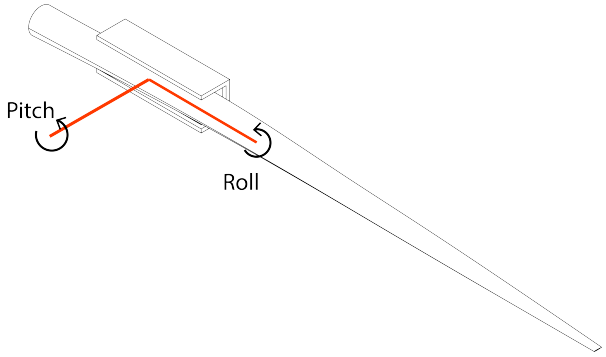


**Figure 4.19:** Axes convention for the blade and yoke

7.3 *Line-up tool attachment*

The line-up tool attaches to the root of the blade, in order to control its motion while it is removed. Alternatively, the line-up tool has already been attached at deck level.

There will be relative motions between the line-up tool and the yoke when it is attached at deck level. As will be explained in section 4.4, the focus of this thesis is on the component dynamics during the lifting processes. Therefore, the attachment phase is not modeled and assumed possible.

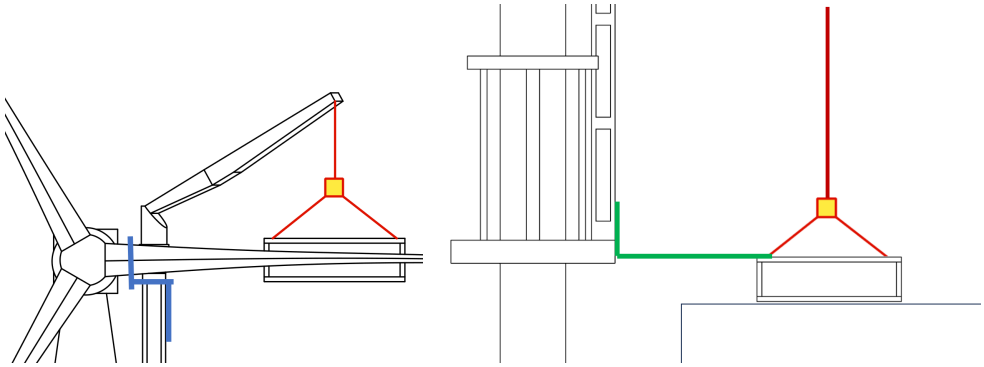

**(a)** Attachment at hub height to blade root **(b)** Attachment at deck level to yoke

**Figure 4.20:** Possible line-up tool attachment phases

7.4 *Blade removal*

In order to remove the old blade, a technician must unscrew the bolts that connect the blade to the hub. The blade is lifted slightly by the OSCC's crane, which makes it float in its bearing. As a consequence, the tension in the bolts releases and they can be unscrewed. The blade is then lifted out of the hub.

An offset in heel or trim of the FOWT due to the presence of the climbing crane could potentially complicate the removal of the blade. If the FOWT heels, the blade is no longer in a horizontal position and there will be tension in the bolts due to its mass. It is not possible to undo the bolts while they are tensioned, and floating the blade in its bearing might not be enough to untension the bolts.

7.5 *Blade lift down*

After the blade is removed from the hub, the blade is lifted down. The blade is lifted along the lattice of the OSCC to the support vessel. The motion of the blade is controlled through the line-up tool. As the motions of the blade are expected to be more critical during docking, this phase is not modeled.

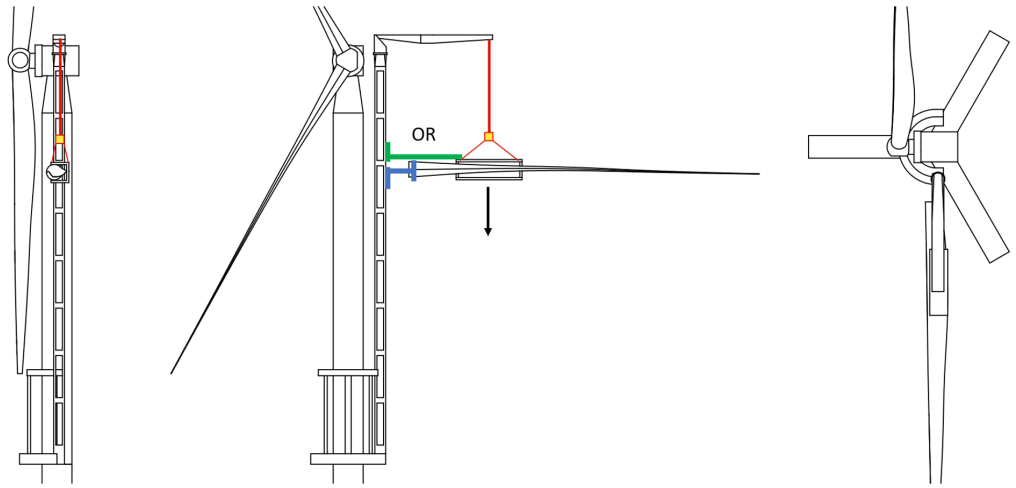


**Figure 4.21:** Schematic of the lowering of the old blade

7.6 *Blade docking*

When the blade is at the deck level of the vessel, it is docked onto the vessel or into a blade rack. The blade will be docked at the back of the vessel, as shown in figure 4.22, which will influence the dynamics coming from the vessel. As this is a dynamic lift scenario, it will be modeled and its operability will be assessed.

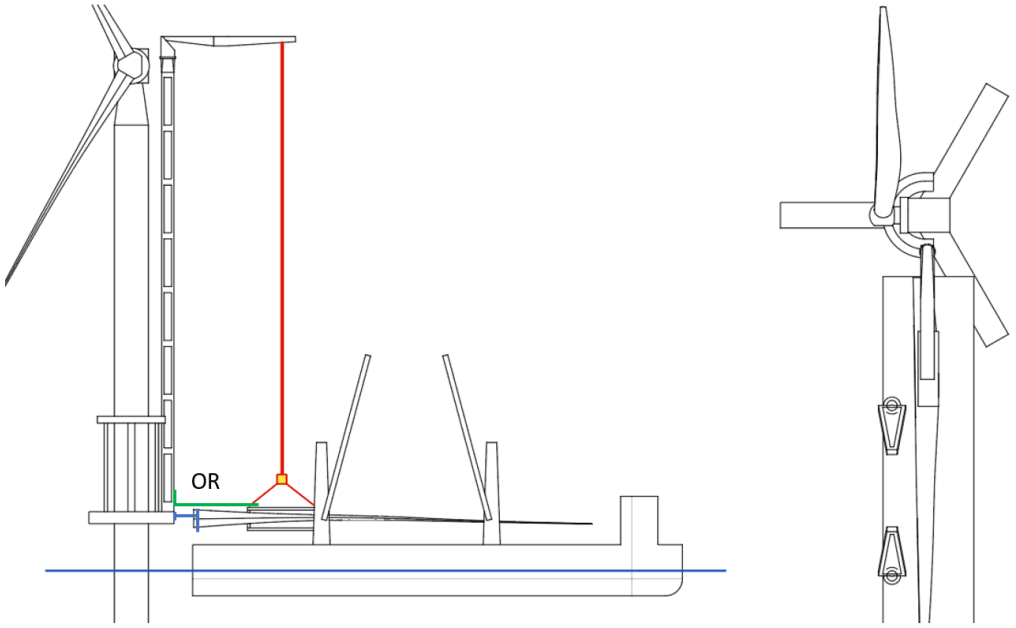


**Figure 4.22:** Schematic of the docking of the old blade

In order for the blade to be safely docked onto the vessel, its motion relative to the vessel should be limited. In the docking process of the blade, it will be hovered above the blade rack before it is finally docked. This is the phase that will be modeled, and the limits are stated in table 4.5. A low limit is given on pitch and yaw of the blade, because an angular displacement in these modes could lead to large motions at the tip of the blade due to its length. This could be a safety concern at the deck level of the vessel.

**Table 4.5:** Indicative limiting factors during blade docking

| Body of interest | Property | Response Parameter | Allowable Limit | $N_{cycles}$ |
|---|---|---|---|---|
| Blade | Relative motions | Horizontal motions | 1 m | 250 |
| Vessel | | Heave | 1.5 m | 250 |
| | | Roll | 3 deg | 250 |
| | | Pitch/yaw | 1 deg | 250 |

8. **Installation of new component**

To install the new blade, it must be lifted from the vessel and up to hub height. There, it is installed in the hub and fastened. The different steps taken in this sequence are described in more detail below.

8.1 *Yoke attachment*

In order for the new blade to be lifted, it should be attached to the yoke. The motions of the yoke should be limited so it can clamp on to the replacement blade safely. This is a dynamic lift scenario, but it is not modeled since the docking of the old blade is deemed a very similar and more critical scenario, due to the aerodynamic loads on the blade that are present during its docking. The motions of the yoke at the vessel deck can also be mitigated using taglines attached to the yoke.

8.2 *Line-up tool attachment*

When a line-up tool at the blade root is used, the line-up tool is now attached. If the line-up tool configuration that attaches to the yoke is used, the line-up tool stays attached to the yoke during the entire operation.

8.3 *Blade lift up*

The blade is lifted up from the vessel deck up to hub height.

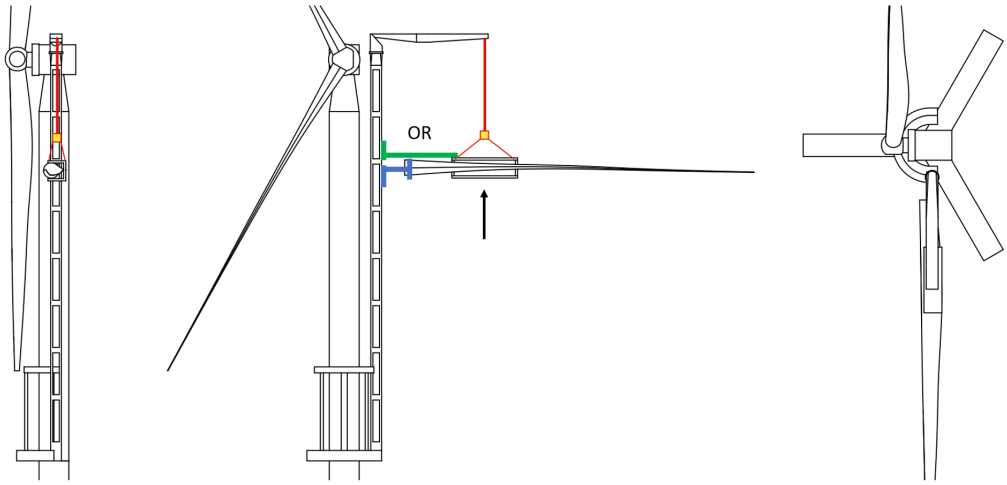


**Figure 4.23:** Schematic of the lifting of the new blade

8.4 *Mating of the blade and hub*

After the blade is lifted to hub height, it is mated with the hub. First, the blade is hovered at hub height. The blade root is then slid into the hub, and the guide pins on the blade root enter their corresponding holes. A technician installs and fastens the nuts on the bolts of the blade root, and the blade is installed. As the mating phase of the blade and hub is a dynamic lift scenario, it will be modeled and its operability will be assessed.

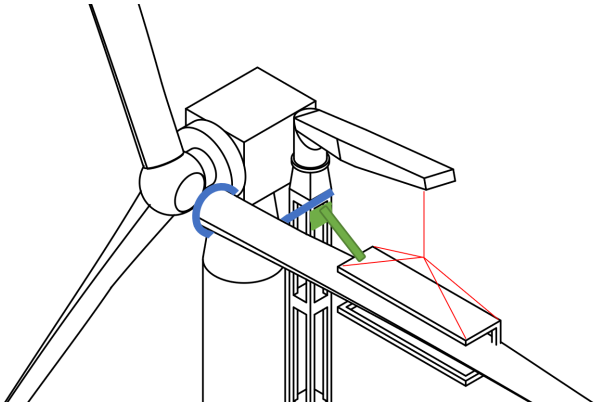

**Figure 4.24:** Schematic of the installation of the new blade

The alignment criterion mentioned in chapter 3.3 must be satisfied in order for the blade to be properly mated to the hub. This is taken at the blade root, with respect to the hub. Furthermore, an indicative alignment criterion is added in the rotations of the blade. A limit is set on the relative rotation between the hub and blade root, because a large offset in roll and pitch could lead to alignment issues.

**Table 4.6:** Limiting factors during blade installation

| Body of interest | Property | Response Parameter | Allowable Limit | $N_{cycles}$ |
|---|---|---|---|---|
| Blade | Relative motions | In-plane excursion | 0.223 m | 150 |
| Hub | | | | |
| Blade | Alignment | Roll | 3 deg | 150 |
| Hub | | Pitch/Yaw | 1.5 deg | |

9. **Vessel repositioning**

   As the new component is now installed, the yoke can be brought to deck and the vessel can reposition itself again. The vessel repositions itself back to where the vessel cranes can lift the OSCC.

10. **Crew transfer**

    The last step for which technicians are required, is to attach the rigging to the OSCC after it has climbed down, so it can be lifted from the TLP. Afterwards, crew is transferred back.

11. **OSCC decommissioning**

    The OSCC can be decommissioned and brought back to the vessel. When the OSCC is lifted off its connection point on the TLP, impact with the TLP and WTG should be avoided. As this is also the case for its installation, the operability of decommissioning the OSCC is deemed equal to installation, and therefore this step is not assessed further.

12. **Vessel sailback**

## 4.4. Research scope

From the previous section, it becomes clear that there are several scenarios in which there are limits on the maximum allowable motions that can be seen in the operation. As these motions can limit the operation, it is reasoned that the feasibility of a blade exchange with the OSCC and can be studied by assessing these motions.

To limit the scope of this thesis, the choice is made to only assess and model the scenarios in which components are lifted. This means that the phase of the line-up tool attachment is not included, although there are still motions in this phase that could be limiting for the operation. Thus, this phase is given lower priority to the dynamics of the lifted components. The motions during the attachment of the line-up tool can be mitigated by choosing a larger and more stable support vessel, or using a motion compensated platform to support the blade or yoke while the line-up tool is attached. The motions of the blade while lifting are more difficult to mitigate, and therefore it is reasoned that studying the motions of the blade while lifting gives a more fundamental understanding of the feasibility of turbine mounted solutions. Studying these motions also allows for a quantitative measure in assessing design choices on the OSCC.

To study the motions at the critical scenarios, a dynamic model is made of a TLP and a WTG. The OSCC is modeled and placed onto the TLP. A support vessel is also included in the model, to assess the installation of the OSCC on the TLP. A schematic overview of the modeling scope of this thesis is given in figure 4.25. A theoretical background to all aspects of the models is given in chapter 5

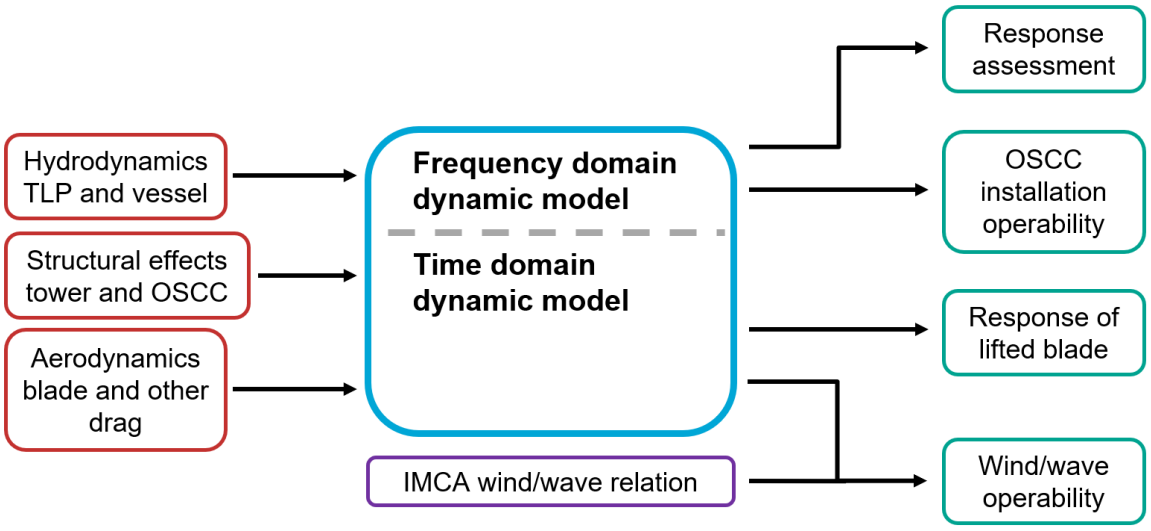


**Figure 4.25:** Modeling scope for the dynamic analyses

# 5

# Theoretical background for modeling the blade exchange

The modeling of the blade exchange requires understanding of the physical principles that influence the operation, and the limitations of the theoretical formulations that are used. Modeling the operation of a component exchange requires understanding of multi-body dynamics to model the dynamic interaction between all the components in the operation, understanding of hydromechanics to describe the behaviour of the floater and vessel, understanding of response statistics, understanding of aerodynamics to model wind loads on the lifted blade and finite-element theory to model the flexibility of the tower and lattice of the OSCC. Offshore construction practicalities such as working limits for technicians should also be understood and accounted for. In this chapter, all underlying theory that is used in the model of the operation is presented.

## 5.1. Multi-body dynamics

The model of a component exchange on the tension-leg platform features many components, such as the floater and wind turbine assembly, the crane, the replacement component and the support vessel. The dynamics of one component influence the dynamics of another component. For example, wave induced motions of the floater influence the crane tip motion of the turbine mounted crane, which in turn induce motions on the lifted component. To understand the dynamic response of the complete system, all the bodies or components that influence the operation should be included in the model. This is done by modeling the connections between bodies as either rigid or flexible, and including the mass properties and weight distribution of the modeled bodies.

### 5.1.1. Equations of motion

The movement of a body can be described by degrees of freedom in a coordinate system. A degree of freedom is a direction or angle a body can translate or rotate in. To describe the motion of a rigid body in three dimensional space, six degrees of freedom are necessary, of which three are translational and three are rotational. This is illustrated in figure 5.1.

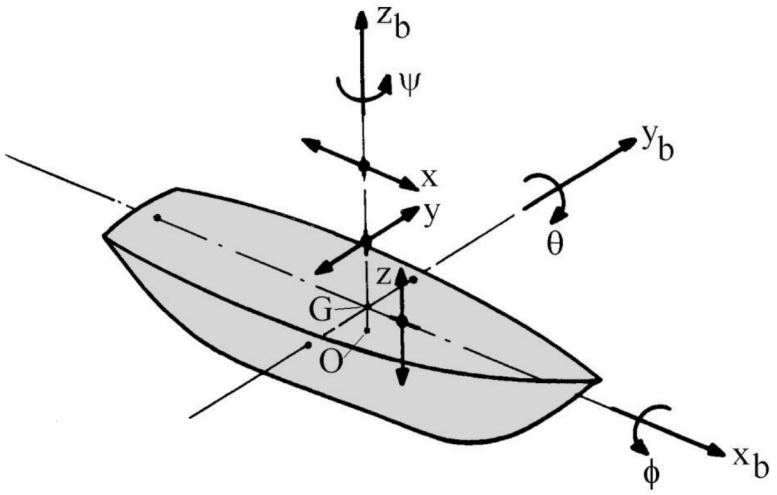


**Figure 5.1:** The degrees of freedom of a floating structure [23]

The degrees of freedom can be written in a vector format and the resulting coefficients from the equations of motion in a matrix format, which results in the systems equations of motion:

$$\mathbf{M}\underline{\ddot{q}} + \mathbf{B}\underline{\dot{q}} + \mathbf{C}\underline{q} = \mathbf{F}(t) \tag{5.1}$$

With

$$\underline{q} = \begin{pmatrix} x \\ y \\ z \\ \varphi \\ \theta \\ \psi \end{pmatrix} \tag{5.2}$$

The system properties are contained in the **M**, **B** and **C** matrices. They are determined by the mass, damping and stiffness properties of the system, respectively. When more bodies are included in the model, their degrees of freedom are appended to the system vectors and matrices in the equations of motion. In order to determine the equations of motion of a multi-body system, the Lagrangian of the system can be drawn up. The Lagrangian is defined as the kinetic energy of the system, $T$, minus the potential energy of the system $U$,

$$L = T - U \tag{5.3}$$

The kinetic and potential energy of the system can be written for each degree of freedom. As the energy contained in the system should remain constant, the derivative of the Lagrangian in each degree of freedom should always be equal to zero. The equations of motion can be derived with this theorem in each degree of freedom $q$, resulting in equation 5.4 [47].

$$\frac{d}{dt}\frac{\partial L}{\partial \dot{q}_j} - \frac{\partial L}{\partial q_j} = 0 \tag{5.4}$$

## 5.2. Dynamic analysis

The dynamics of a system can be computed by solving the equations of motion. The equations of motion can be solved in frequency domain, in which a harmonic excitation of the system is assumed, and in time domain, where the equations of motion are numerically integrated over time.

### 5.2.1. Frequency domain

Solving the response of a system in the frequency domain is a quick method of determining the systems response based on the frequency of the load. This method of solving is linear and assumes a harmonic load. Therefore, non-linearities or a time varying load are not captured by this method. However, a fast initial analysis can be done which can provide valuable information about the system, such as its natural frequencies and its mode shapes. A harmonic load written as a complex function is applied:

$$\mathbf{M}\underline{\ddot{q}} + \mathbf{B}\underline{\dot{q}} + \mathbf{C}\underline{q} = \underline{\tilde{X}}e^{i\omega t} \tag{5.5}$$

Here the load frequency is denoted by $\omega$ and the complex load magnitude by $\underline{\tilde{X}}$. This could be a harmonic regular wave. As the load is harmonic, the response will be of the same frequency $\omega$ but a different magnitude $\underline{\tilde{x}}$:

$$\underline{q} = \underline{\tilde{x}}e^{i\omega t} \tag{5.6}$$

Therefore the equation of motion can be rewritten as:

$$\left[-\omega^2\mathbf{M} + i\omega\mathbf{B} + \mathbf{C}\right]\underline{\tilde{x}} = \underline{\tilde{X}} \tag{5.7}$$

The relation between the response and load can therefore be written as

$$\underline{\tilde{x}} = \left[-\omega^2\mathbf{M} + i\omega\mathbf{B} + \mathbf{C}\right]^{-1}\underline{\tilde{X}} \tag{5.8}$$

If the inverse system matrix is seen as a transfer function $\mathbf{H}(\omega)$, the equation becomes

$$\underline{\tilde{x}}(\omega) = \mathbf{H}(\omega)\underline{\tilde{X}}(\omega) \tag{5.9}$$

To find the actual response magnitude, the real part of the transfer function is taken. Because this function relates the load amplitude to the response amplitude for different frequencies, it is called a response amplitude operator (RAO):

$$|\mathbf{H}(\omega)| = \left|\frac{\underline{\tilde{x}}(\omega)}{\underline{\tilde{X}}(\omega)}\right| \tag{5.10}$$

The RAO of a system gives a linear relation between the response of a system at a certain frequency and a magnitude of the load at the same frequency. The RAO can also be computed at different locations on the structure through a transformation matrix. For floating bodies, it is computed such that it directly relates the response amplitude of a degree of freedom $q_{j_a}$ to the wave height amplitude $\zeta_a$:

$$\mathbf{RAO}_j(\omega) = \left|\frac{q_{j_a}(\omega)}{\zeta_a(\omega)}\right| \tag{5.11}$$

This equation also highlights the linearity of frequency domain. There is a linear relationship between the wave amplitude and response amplitude, meaning that if the wave amplitude doubles, the response amplitude doubles as well.

#### Spectral response through frequency domain

The RAO of a floating body computes the response from a harmonic wave over a range of wave frequencies. The RAO can be used to compute the response of a system for a spectrum of irregular waves. Following *Journee and Massie*, the wave energy spectrum can be expressed as a function of the corresponding wave amplitudes $\zeta_{a_n}$ for a range of frequencies $\omega$ [23]:

$$S_\zeta(\omega_n) \cdot d\omega = \frac{1}{2}\zeta_a^2 \tag{5.12}$$

Correspondingly, the response spectrum in a degree of freedom $j$ can be expressed similarly, as equation 5.11 shows that the system's response is linearly related to the wave amplitude:

$$S_{q_j}(\omega_n) \cdot d\omega = \frac{1}{2}q_{j_a}^2 \tag{5.13}$$

This can be rewritten to show that the response of a degree of freedom can be expressed by its RAO:

$$S_{q_j}(\omega)d\omega = \frac{1}{2}q_{j_a}^2(\omega) = \frac{1}{2}\frac{q_{j_a}^2}{\zeta_a^2}(\omega)\cdot\zeta_a^2(\omega) = S_\zeta(\omega)d\omega\cdot\left|\frac{q_{j_a}}{\zeta_a}\right|^2(\omega) \tag{5.14}$$

The response spectrum can therefore be written as a function of the wave spectrum and the RAO by combining equations 5.11 and 5.12:

$$S_{q_j}(\omega) = S_\zeta(\omega)\cdot\mathbf{RAO}_j^2(\omega) \tag{5.15}$$

The response spectrum will show the energy contained in the response at each response frequency, and correspondingly shows at which frequencies the system is excited most. Furthermore, certain motion properties of the response can be extracted from the spectrum. Following *Journee and Massie*, it can be found that *the significant amplitude can be calculated from the spectral density function of a response* [23]. This is done by finding the zero-th order spectral moment $m_0$:

$$m_{0q_j} = \int_0^\infty \omega^0\cdot S_{q_j}(\omega)\cdot d\omega \tag{5.16}$$

The significant double amplitude of the response can then be expressed as:

$$\mathbf{SDA}_{q_j} = 4m_{0q_j} \tag{5.17}$$

### 5.2.2. Time domain

As can be seen in equation 5.1, the equations of motion are differential equations, that can be solved iteratively in the time domain. This is done by a step-by-step numerical integration of the equations of motion. This results in a discretized signal of the system's response. Time domain integration methods can be implicit or explicit, meaning that the equations of motion are solved at the beginning or end of a timestep, respectively. Implicit methods are usually faster and therefore used more often in practice. Time domain simulations can take into account the full non-linearity of the system loads acting on it. It is possible to apply any resulting load from a non-linear process at a certain timestep, since the differential equations of motion can be solved numerically. Wind is an important environmental load in modeling the component exchange, and can only be included in time domain because aerodynamic loads are non-linear.

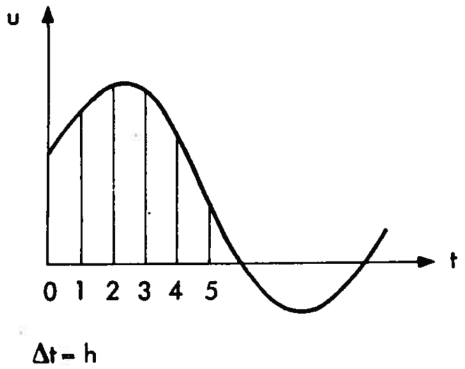


**Figure 5.2:** Discretization of the response through a time-domain analysis

### 5.2.3. Software for dynamics

In order to perform the dynamic analysis, software is used. Two software programs are used in order to perform dynamic analyses: LiftDyn, the internal frequency-domain software from Heerema Engineering Solutions, and OrcaFlex, a commercial software package for time-domain simulations. Both software packages compute the equations of motion of a system of bodies. The system matrices for the equations of motion of the bodies are computed through a Lagrangian approach, taking into account their interaction, hydrostatic and -dynamic properties and any possible constraints. This is then used as a starting point for the dynamic analysis.

LiftDyn
LiftDyn works in frequency domain, and computes the spectral response as described in subsection 5.2.1. All mode shapes of the system of bodies are computed, and are used to determine the total spectral response. Through this spectral response, motion properties of the system are calculated and used to calculate operability, which will be described in further detail in section 5.8. LiftDyn assumes all bodies are rigid bodies. Damping is added artificially in all degrees of freedom, by adding 1.5 % of critical damping.

OrcaFlex
OrcaFlex numerically solves the equations of motion implicitly in time-domain through the generalized-$\alpha$ method [8]. A time-signal of the loads on the system is computed, which is applied to the equations of motion. A time-history of all responses of the system is computed and can be analyzed. OrcaFlex can compute structural response and beam elements through a finite-element method. It is also possible to perform a modal analysis in OrcaFlex, which gives the natural frequencies and mode shapes of the system.

## 5.3. Hydrostatics

The static interaction of a floating body with a body of water is described by hydrostatic theory. When a floating body is displaced in heave, roll or pitch, there will be a restoring force or moment exerted on the body by the surrounding water. This is called hydrostatic stiffness, and it is included in the stiffness matrix in the equations of motion of a floating body. In order to compute this stiffness, the metacentric height of a body must be computed. The metacenter the point in which the lines of the vertical buoyant forces for a displacement of the floating body intersect. The distance from the center of buoyancy $B$ to the metacenter $M$ can be calculated through the displacement volume $\nabla$ and the second moment of area of the water plane, $I$:

$$BM = \frac{I}{\nabla} \tag{5.18}$$

The stability lever arm of the restoring buoyant force of the body is equal to the distance between its center of gravity $G$ and its metacenter $M$. Following *Journee and Massie*, this can be calculated as follows [23],

$$GM = KB + BM - KG \tag{5.19}$$

where $KB$ is the distance of the keel of the body $K$ to its center of buoyancy $B$, and $KG$ is the distance of the keel of the body $K$ to its center of gravity $G$. The restoring coefficient in roll can be calculated with the stability arm $GM$. The same can be done for pitch, but the second moment of area is then taken in longitudal direction of the floating body, which leads to a longitudinal $GM_L$. The hydrostatic restoring coefficients are [23]:

$$\begin{aligned} \text{heave} &: \quad \mathbf{C}_{3,3} = \rho g A_{WL} \\ \text{roll} &: \quad \mathbf{C}_{4,4} = \rho g \nabla \cdot GM \\ \text{pitch} &: \quad \mathbf{C}_{5,5} = \rho g \nabla \cdot GM_L \end{aligned} \tag{5.20}$$

These coefficients are calculated by the modeling software through the hydrostatic properties of the floating bodies, and applied in the static and dynamic solution.

### 5.3.1. Static solvers

In order to construct the multi-body models of the FOWT and the OSCC, software is used in order to obtain a static equilibrium of all the bodies in the model. The influence of gravity, hydrostatics and connections between bodies is accounted for. The in-house multi-body static solver AGES from Heerema Engineering Solutions is used. A static equilibrium of all bodies is found by displacing them in their degrees of freedom, and computing a force balance. The software converges towards an equilibrium by displacing each body such that the resulting forces on them become smaller, until a threshold is met. The results are exported to both LiftDyn and OrcaFlex.

## 5.4. Environmental loads

Any offshore activity is subject to a number of parameters that induce loads on structures, such as wind, waves and current, which together form the environmental conditions. Some of these parameters can be seen as constant as they vary slowly over time, such as the current velocity or the tide. Other parameters are time varying throughout the duration of interest, such as waves and wind speed, and must be modeled as such. Not all environmental conditions influence the operation equally. Effects such as icing or soil mechanics are not governing for a component exchange on a floating wind turbine, which means they can be left out of the analysis. Tidal variations and current are not considered in this thesis. The loads that are taken into account are waves and wind, as they are expected to have the biggest influence on the dynamics of the system during the component exchange.

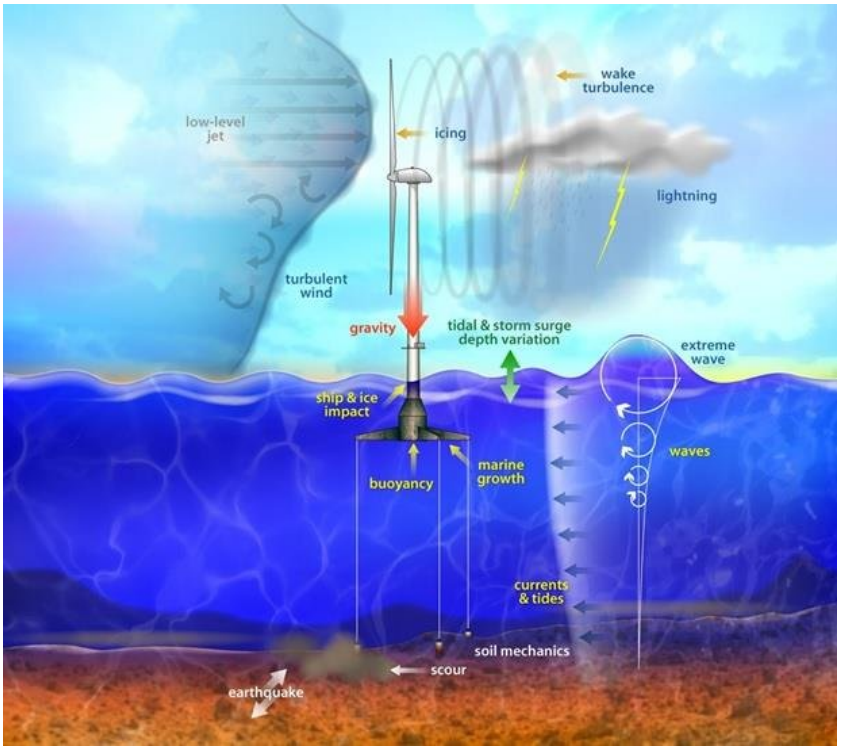


**Figure 5.3:** Environmental conditions for a FOWT [22]

### 5.4.1. Waves

Waves can be described based on their height $H$, period $T$, speed $c$ and length $\lambda$. When a wave is propagating through deep water, its shape can be described by a harmonic function. The deep water criterion relates to the fraction of the wave length and water depth. As the FOWT will be placed in relatively deep water, this principle is applied in the model. The water depth for which the operation is modeled is 150 meters. It can be calculated through the dispersion relation that waves with a period longer than 7 seconds, the assumption of deep water waves and thus harmonic waves is no longer valid. Therefore, intermediate water depth wave equations are used.

$$\begin{aligned} \frac{d}{\lambda} &< 0,05 : \text{Shallow water} \\ 0,05 < \frac{d}{\lambda} &< 0,5 : \text{Intermediate water} \\ \frac{d}{\lambda} &> 0,5 : \text{Deep water} \end{aligned} \tag{5.21}$$

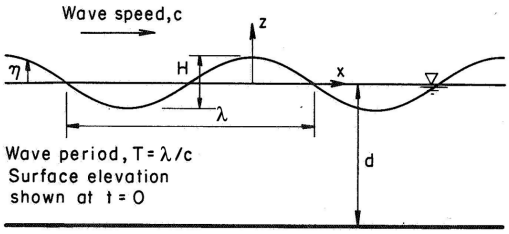


**Figure 5.4:** The description of a regular wave [23]

As previously mentioned, waves can be described by a harmonic function. The surface elevation $\eta$ that is caused by a regular wave can be described as:

$$\eta = \frac{H}{2}\cos(\omega t - kx) \tag{5.22}$$

Where $\omega$ is the wave frequency and $k$ the wave number, which is found through the dispersion relation. A wave generates forward and backward velocities and accelerations of the water particles it passes by. These velocities and accelerations are what causes wave loads on a structure. A convenient way to describe a flow field is through its velocity potential. The velocity potential of a wave can be written as:

$$\phi = -\frac{\omega H}{2k}\frac{\cosh k(z+h)}{\sinh kh}\sin(\omega t + \theta) \tag{5.23}$$

Where $z$ is the (negative) water depth, $k$ the wave number obtained through the dispersion relation, $h$ the water depth and $\theta$ the phase of the wave. Waves characterized by a single frequency or period are known as regular waves. However, a sea state can best be described as a set of irregular waves, a wave field that consists of waves of many frequencies. A sea state can be described in the frequency domain by a wave spectrum. A wave spectrum shows the amount of energy that is contained within a wave frequency. A typical description of sea states in the North Sea is given by the JONSWAP-spectrum, which features a peak enhancement factor to account for North Sea conditions. It accounts for the limited fetch seen in the North Sea, which is the area over which waves are created by wind. As the North Sea is stormy but relatively sheltered, there is less influence by swell waves generated over longer distances in the open ocean. The JONSWAP-spectrum will therefore be used in the model. The spectrum is defined by a significant wave height $H_s$ and peak period $T_P$. The significant wave height relates to the mean of the highest third of all waves, and the peak period specifies the wave frequency which contains the most energy. The JONSWAP-spectrum can be described by the following formulation [23]:

$$S_\zeta(\omega) = \frac{320 \cdot H_s^2}{T_p^4} \cdot \omega^{-5} \cdot \exp\left\{\frac{-1950}{T_p^4} \cdot \omega^{-4}\right\} \cdot \gamma^A \tag{5.24}$$

with

$$\begin{aligned}
&\gamma = 3.3 \quad \text{(peak enhancement factor)}\\
&A = \exp\left\{-\left(\frac{\frac{\omega}{\omega_p} - 1}{\sigma\sqrt{2}}\right)^2\right\}\\
&\omega_p = \frac{2\pi}{T_p} \quad \text{(circular frequency at spectral peak)}\\
&\sigma = \text{ a step function of } \omega \text{ : if } \omega < \omega_p \text{ then: } \sigma = 0.07\\
&\text{if } \omega > \omega_p \text{ then: } \sigma = 0.09
\end{aligned} \tag{5.25}$$

A JONSWAP-spectrum with a peak enhancement factor of 3.3 is used as input to the frequency domain dynamic analysis. In time-domain, a sea state can be described as a superposition of a set of regular waves with different amplitude and frequency that are found through the frequency domain

spectrum of the sea state. The waves that are superimposed have a set of random phases is given to the waves through a uniform distribution. The surface elevation and particle dynamics associated with the regular waves are summed to form the final product. In the time-domain simulations, the wave particle velocities and accelerations obtained through this superposition are used to compute the forces on the submerged bodies.

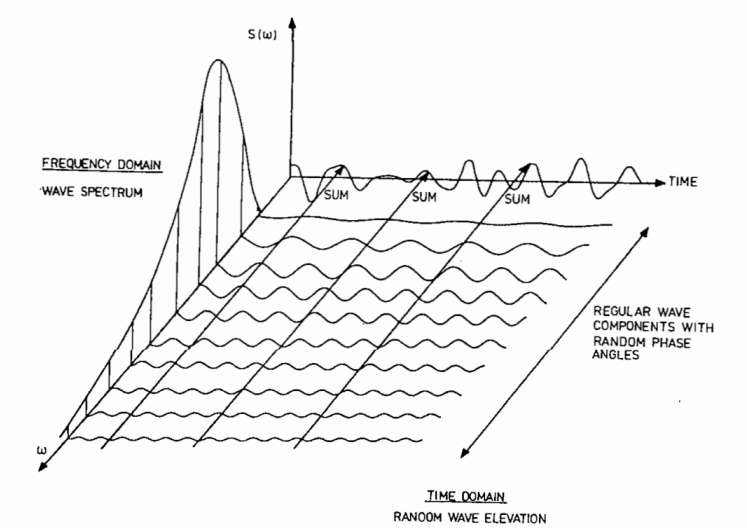


**Figure 5.5:** Superposition of regular waves to form a time series of irregular waves [23]

Occurrence of combinations of wave height and wind speed

A correlation exists between the significant wave height of a sea state, and the most probable corresponding mean wind speed that is encountered. A correlation between the two is described by IMCA, and it is used in the time-domain analyses to consequently relate the sea state with the wind environment. This reduces the number of required time domain simulations, which saves computational effort. The wind-wave relation is used to generate the systems response through which the wind and wave influenced operability is assessed. It should be noted that this wind-wave relation is calibrated for fully developed seas. Areas like the North Sea are fetch-limited, and the corresponding wind speed for wave heights in these kind of areas might be an underestimation of the reality.

**Table 5.1:** Relationship between significant wave height and mean wind speed, as presented by IMCA [19]

| Sig. Wave Height $Hs(m)$ | Mean Wind Speed $Vw(m/s)$ |
|---|---|
| 1.28 | 2.5 |
| 1.78 | 5.0 |
| 2.44 | 7.5 |
| 3.21 | 10.0 |

### 5.4.2. Wind

In order to incorporate the wind induced loads in the model of the operation, a formulation of the wind speed must be used. Similar to waves, wind can be described in the frequency domain and time domain. As the wind speed is not constant with time, the variations in wind speed can be denoted by the energy contained in them as a function of their frequency in the frequency domain. Although a wind spectrum can be described in the frequency domain, it is not possible to include it in the frequency domain dynamic analyses, since the assumption that the response is linear to the load is not valid, as aerodynamic forces are quadratic. A time series of the wind speed must therefore be generated in the same manner as waves. This is done in OrcaFlex.

Different formulations for the wind spectrum exist, which are based on different sets of measurement. Two commonly used spectra which are available in OrcaFlex are the NPD spectrum and the API spectrum [42] [10]. Both spectra are computed for an elevation of 10 meters, and an elevation of 150 meters in figure 5.6. It can be seen that at the presented frequencies and elevations, the API spectrum yields the highest energy. At higher elevations, more energy is placed at lower frequencies, due to the fact that there is less turbulence. In general, the NPD spectrum places more energy in very low frequencies [40], but these frequencies are less relevant for the dynamics of the modeled operation and therefore not presented in the plot. For the most relevant frequencies, the API spectrum yields the highest wind speed, and to be conservative this spectrum is applied in the model.

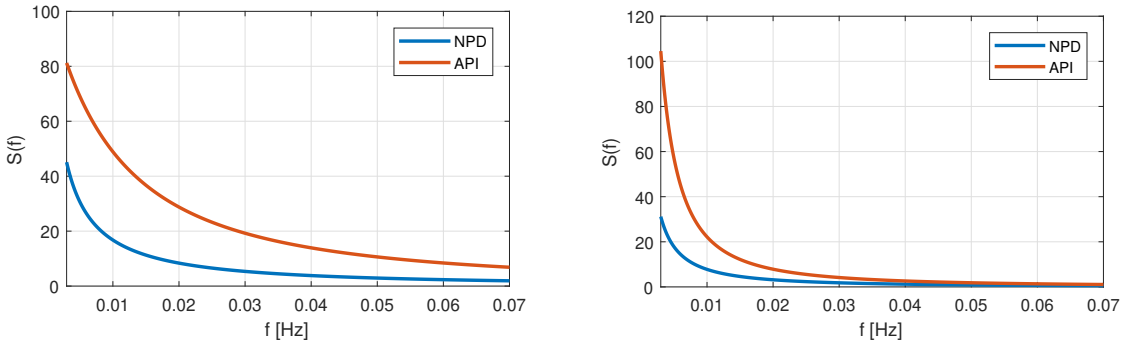


**(a)** NPD and API spectra at 10 meters elevation

**(b)** NPD and API spectra at 150 meters elevation

**Figure 5.6:** Energy density spectra of the NPD and API norm at different elevations

For consistency in the results, the wind spectrum elevation is taken at the hub height of the turbine that will be used in the models, for each modeled stage. As can be seen in the above figure, this yields to an underestimation of the excitation at frequencies from 0.05 Hz and above, which should be kept in mind when drawing conclusions.

It should be noted that the flow field of the wind obtained in OrcaFlex is horizontal and parallel. Turbulence can result in a vertical and tangential velocity component of the wind, but this is not taken into account. This is a non-conservative assumption, since aerodynamic loads on wind turbine blades vary greatly with the angle of inflow. However, as a simplification it is chosen not to model the flow field of the wind in three dimensions.

## 5.5. Hydrodynamics

To understand the dynamic behaviour of a submerged body, its hydrodynamics must be modeled. The hydrodynamic behaviour of a submerged body can be described by a variety of theories, ranging in complexity and required computational time. The choice of theory depends on the geometry of the body that is modeled, the expected frequency range of the motions of the body, and the flow field around it.

The most commonly used theories in hydrodynamics for offshore structures are potential theory, and approximations of viscous effects by semi-empirical theories. More high-fidelity theories such as Computational Fluid Dynamics (CFD) are also used to for example include viscosity in the model, but to a lesser extent because of their computationally demanding nature. Potential theory describes the interaction of a body with a fluid based on Bernoulli's equation, with the assumption that the fluid is incompressible, irrotational, that there are no viscous effects and that there is no surface tension [23]. First order potential theory describes the interaction of the body with a wave of a single frequency, and higher order potential theory takes the interaction between waves into account. The assumption of neglecting viscosity is not always valid, and for some applications viscosity is modeled with semi-empirical formulations such as Morison's equation, which features a drag coefficient that accounts for the viscous drag around the structure.

For large volume structures, potential flow theory can provide an accurate hydrodynamic model. The hydrodynamics are then inertia-dominated, which refers to the inertia of the displaced water under the body's movement, as opposed to drag-dominated. The dimension of the body relative to the wave height determines whether the hydrodynamic interaction is drag or inertia dominated, as can be seen in figure 5.7. When the natural frequencies of the submerged body are either very low or near twice the wave frequency, second-order potential flow theory becomes important. Potential theory of higher orders can also be relevant for floating structures, depending on the expected motions [13].

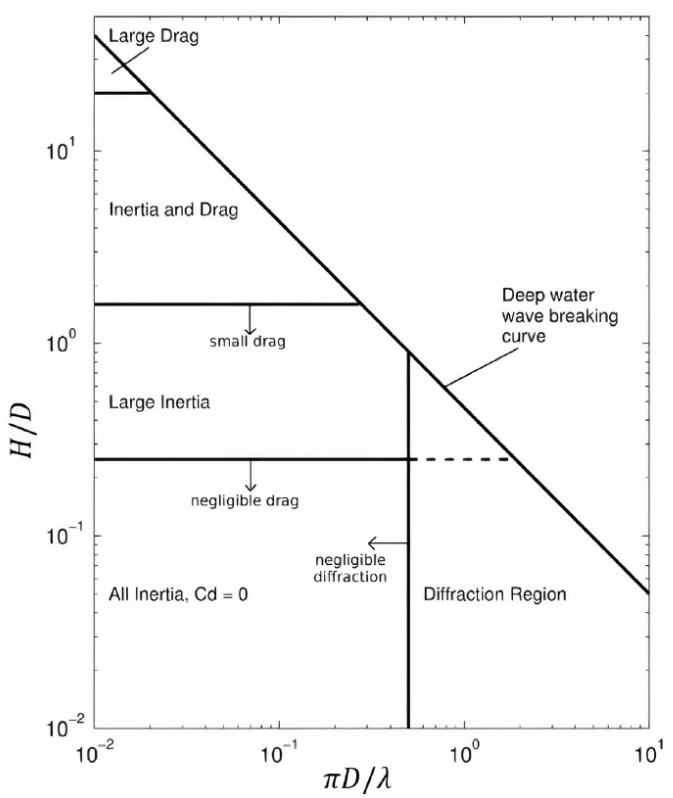


**Figure 5.7:** Classification of the applicability of hydrodynamic principles [7]

### 5.5.1. Potential theory

Hydrodynamic interaction between a body and water can be described by linear potential theory. Linear potential theory assumes that the fluid that the body interacts with is incompressible, irrotational, that there are no viscous effects and that there is no surface tension, and neglects second and higher order terms in its equations [23]. In order to compute the equations of motion of a body with hydrodynamic interaction, the potential flow coefficients can be computed. This is a method which finds the forcing due to hydrodynamic interaction, and the added mass and damping coefficients due to movements of the body.

A linear fluid velocity potential can be superimposed from its two components: its radiation potential $\Phi_r$, which results from the oscillatory motion of the body in still water, and its diffraction potential $\Phi_D$, which is composed of the incident undisturbed wave potential $\Phi_w$, and the diffraction scattering potential $\Phi_s$ of the waves about the restrained body:

$$\Phi(x, y, z; t) = \Phi_R + \Phi_D = \Phi_R + \Phi_w + \Phi_s \tag{5.26}$$

Considering the force on an oscillating body in waves, the force can therefore be described by the superposition of the forces coming from the oscillation of the body, the radiation forces, and the wave forces acting on the restrained body, the diffraction forces. To compute the hydrodynamic interaction of a body, a radiation problem and a diffraction problem can be solved, which are then superimposed.

This analysis is done in the frequency domain, assuming a regular incident wave. To account for a range of frequencies, incident waves of many frequencies are assessed. Through the formulation of boundary conditions on the fluid and on the body, the radiation and diffraction potentials can be found normal to the body shape. For the exact formulation of the boundary conditions of the potential flow problem, the reader is referred to *Journee and Massie* [23].

### Radiation problem

The radiation problem is solved by assuming an oscillatory motion of the body in still water, and solving the velocity potential $\Phi_R$ for the waves propagating from the body. The result of the radiation problem will be the potential coefficients of the body. The potential coefficients are frequency dependent terms that describe the hydrodynamic forces on a body through its own oscillations, proportional to the body's acceleration and velocity in the corresponding degree of freedom. The coefficients proportional to acceleration are known as a body's added mass, and the coefficients proportional to velocity are known as a body's radiation damping coefficients. They are included in the equation of motion of a floating body,

$$(\mathbf{M} + \mathbf{A}(\omega))\ddot{\underline{q}} + \mathbf{B}(\omega)\dot{\underline{q}} + \mathbf{C}\underline{q} = \mathbf{F}(t) \tag{5.27}$$

where $\mathbf{A}(\omega)$ is the added mass matrix and $\mathbf{B}(\omega)$ is the radiation damping matrix, in which the coefficients for each degree of freedom are stored. The radiation potential is written in terms of a velocity potential $\Phi_j$ for each degree of freedom $j$. The radiation potential can be written as a superposition of all the oscillation modes of the body:

$$\Phi_r(x, y, z, t) = \sum_{j=1}^{6} \Phi_j(x, y, z, t) \tag{5.28}$$

In order to find the hydrodynamic forces on the body through the velocity potential, Bernoulli's equation is used. Since the time derivative of the velocity potential is equal to the velocity, the linearized Bernoulli's equation can be written as follows:

$$\frac{\partial \Phi}{\partial t} + \frac{p}{\rho} = 0 \tag{5.29}$$

The radiation forcing on the body can be written as an integral of the pressure over its body. By combining the velocity potential with Bernoulli's equation to find the hydrodynamic pressure, the forcing can be written as,

$$\vec{F_r} = \rho \iint_S (\frac{\partial}{\partial t} \sum_{j=1}^{6} \Phi_j)\vec{n} \cdot dS \tag{5.30}$$

where $S$ is the body surface and $n$ are the normal vectors to the body. An oscillatory motion in each degree of freedom of the body with a frequency $\omega$ can be defined, and the resulting velocity potential can be computed. The forces resulting from this are split in terms proportional to acceleration and velocity of the body, and finally the added mass and damping matrices can be computed for each matrix entry (j, k):

$$\mathbf{A}_{jk} = -\Re e \left\{ \rho \iint_S \phi_k \frac{\partial \phi_j}{\partial n} \cdot dS \right\} \quad \text{and} \quad \mathbf{B}_{jk} = -\Im m \left\{ \rho\omega \iint_S \phi_k \frac{\partial \phi_j}{\partial n} \cdot dS \right\} \tag{5.31}$$

### Diffraction problem

To solve the diffraction problem, forces form the incoming waves and their scattering from the body must be found. Again, the linearized Bernoulli equation can be used in order to compute a surface integral over the body to relate the diffraction velocity potential to the forces acting on it:

$$\tilde{X}_i(\omega) = -i\omega\rho \iint_{S_b} n_i \Phi_D dS \tag{5.32}$$

After solving this equation, the wave forcing becomes a term that is equal to a complex quantity which is directly scaled by the wave height, since the velocity potential depends linearly on the wave

height, as can be seen in equation 5.23. This can be conveniently implemented in the frequency domain solution, as only the complex quantity $\tilde{X}_\omega$, the transfer function $\mathbf{H}(\omega)$ and the wave height are necessary to compute the response of the system.

WAMIT
In order to numerically solve the radiation and diffraction problem, the software program WAMIT is used. WAMIT solves the potential flow problem by setting boundary conditions to the velocity potential, and computing the relevant velocity potentials using the boundary element method. The boundary conditions that are used include the radiation condition, the free surface condition and the body surface boundary condition. The boundary condition on the body is solved by subdividing the body into a finite number of panels. Each panel is a source, from which fluid flows out uniformly in all directions. The boundary condition is solved using the integral equation method. The outward velocity potential of each source is computed using a Green's function, and the interaction between panels is found by the integration of the Green's functions over the panels. The potential coefficients and forcing can be found using the velocity potentials that are obtained on the panels. The solution is dependent on the number of panels used, as this determines how well the interaction between panels is computed and how well the geometry of the body is modeled. For a full explanation, the reader is referred to the WAMIT theory manual [26].

### 5.5.2. Viscous effects
As potential theory is used, viscous loads are neglected. In order to account for quadratic viscous damping, which is important for TLPs [3], Morison elements are used in order to compute drag. The drag term of Morison's equation is used in order to model the load that corresponds with the wave particle velocity $v$ squared. A drag diameter $D$ and element length $L$ are used, in combination with an empirical drag coefficient $C_D$. As the drag load is non-linear, it is only included in the time-domain model in OrcaFlex.

$$F_d = \frac{1}{2}\rho D L C_D v|v| \tag{5.33}$$

## 5.6. Aerodynamics
In order to accurately model the loads on the lifted blade, an aerodynamic formulation of the wind load on the blade is required. In order to do this, a Blade Element Method (BEM) is used. The BEM numerically subdivides the blade into sections, which consist of airfoils. The corresponding airfoil profile is used to compute the lift and drag on the section, and the results are integrated over the length of the blade in order to find the aerodynamic load acting on it. This methodology is implemented in the OrcaFlex simulations.

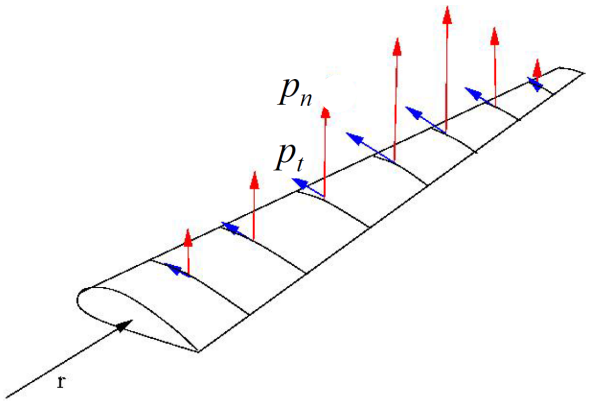


**Figure 5.8:** Subdivision of the blade in airfoils

The angle of attack $\alpha$ of each airfoil along the blade is calculated through its rotation relative to the incoming wind. With the angle of attack known, the airfoil data is then assessed to find a lift and drag coefficient, $C_l$ and $C_d$. These lift and drag coefficients are defined relative to the chord of the airfoil.

The lift and drag loads can then be calculated, and are normal to the chord of the airfoil. The lift and drag load are proportional to the chord length $c$.

$$\begin{aligned} \text{lift} &= \frac{1}{2}\rho_{air} c v_{wind} |v_{wind}| C_l(\alpha) \\ \text{drag} &= \frac{1}{2}\rho_{air} c v_{wind} |v_{wind}| C_d(\alpha) \end{aligned} \tag{5.34}$$

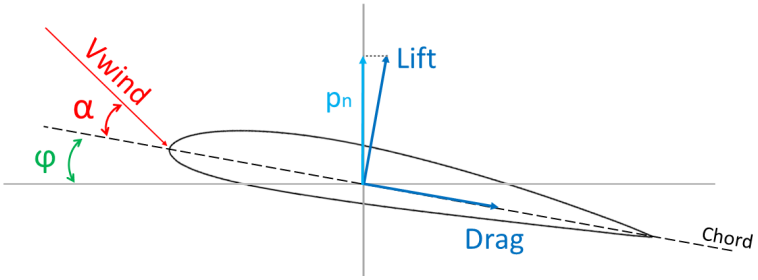


**Figure 5.9:** Decomposition of the aerodynamic forces on the airfoils of the blade

The loads are then translated to the local axis system of the blade through the vector decomposition of the lift and drag, using the airfoils pitch $\phi$. The total load on a blade is then found by the integration of the normal and tangential loads, $p_n$ and $p_t$, along the length of the blade $r$.

$$\begin{aligned} P_n &= \int p_n dr \\ P_t &= \int p_t dr \end{aligned} \tag{5.35}$$

A limitation of the BEM methodology is that the lift and drag forces from the airfoils are calculated only for wind flowing parallel to the chord of the airfoil. Flow along the length of the blade is therefore neglected.

## 5.7. Modeling of flexible beams

In order to account for the flexibility of the tower of the FOWT and the lattice of the turbine mounted crane, they are modeled as flexible beams. The flexibility of these elements is only accounted for in OrcaFlex, as LiftDyn can only work with rigid bodies. The stiffness of the tower and lattice are determined through their bending stiffness $EI$, axial stiffness $EA$ and torsional stiffness $GJ$. OrcaFlex then uses the finite-element method to compute the deflections of the beams. The beams are discretized into elements, that are connected by directional springs whose stiffness is determined by the corresponding beam properties. The mass of each segment is lumped at the connection node between elements. The tower and lattice are dubdivided into elements of 5 meters each, which results in 25 elements in the tower, and 28 elements in the lattice.

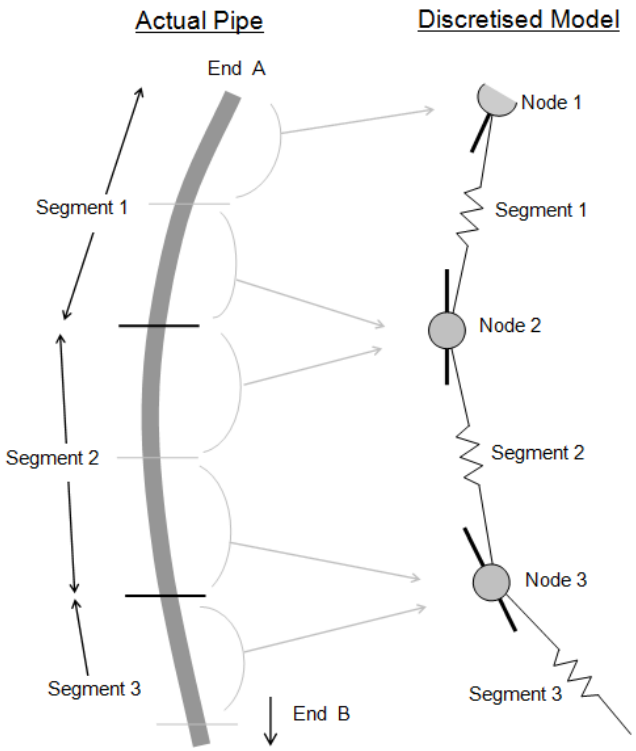


**Figure 5.10:** Discretization of a beam trough the finite-element method using lumped masses and springs [33]

### 5.7.1. Structural damping

In order to avoid resonant behaviour of the tower and lattice, structural damping is included in the form of Rayleigh damping. Rayleigh damping is included in each line node, and is computed as a fraction of the mass and stiffness in a node. A coefficient is given to the damping in axial, bending and torsional deformation corresponding to their respective stiffness. A damping coefficient can also be added proportional to the mass of a node. The total damping is equal to

$$\boldsymbol{C} = \mu \boldsymbol{M} + \lambda_{\mathrm{a}} \boldsymbol{K}_{\mathrm{axial}} + \lambda_{\mathrm{b}} \boldsymbol{K}_{\mathrm{bending}} + \lambda_{\mathrm{t}} \boldsymbol{K}_{\mathrm{torsional}} \tag{5.36}$$

## 5.8. Response statistics

Ocean waves are a stochastic phenomenon, meaning that it is impossible to make an exact prediction on how a sea state will look like. In time domain, sea states can be simulated by deriving a time signal of the surface elevation and thus the velocity potential of waves from an energy density spectrum. In order to do this, a random set of phases with a uniform distribution should be given to the waves. To account for the stochastic nature of sea states, the set of phases that is given to the waves can be varied, based on different outcomes of the uniform distribution. A convergence study can be done on the results in order to account for the randomness of the process. In frequency domain, the phase of the input and response is not accounted for. Therefore, a different approach must be taken.

### 5.8.1. Statistical approach in frequency domain

To be able to calculate with stochastic phenomena such as waves in frequency domain, statistics must be applied. A convenient way to describe a sea state is to use a statistical description of its waves. A wave field can be characterised as a narrow banded frequency spectrum. Furthermore, the water surface elevation follows a Gaussian distribution, meaning the probability of occurrence of a surface elevation varies around a mean value (the waterline) by a given standard deviation $\sigma$ [23]:

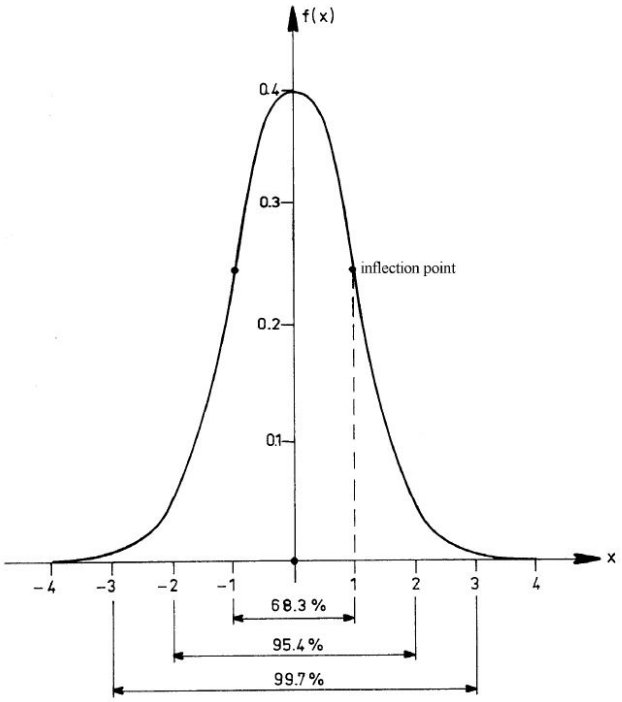


**Figure 5.11:** Gaussian probability density function with a standard deviation of 1 [23]

Because of these two characteristics of a sea state, the probability density function of wave amplitudes in a sea state follows a Rayleigh distribution,

$$f(x) = \frac{x}{\sigma^2} \cdot \exp\left\{-\left(\frac{x}{\sigma\sqrt{2}}\right)^2\right\} \tag{5.37}$$

where $x$ is the wave amplitude and $\sigma$ the standard deviation. The probability density function gives a probability of the occurrence of a wave amplitude. A key characteristic of the probability density function is that by integrating it, the probability that the wave amplitude occurs in the sea state can be found. Therefore, to find the chance that a wave amplitude will be the largest in a sea state, the distribution can be integrated up to that wave amplitude. From an engineering perspective, an interesting quantity is the probability of the exceedance of a highest possible wave amplitude. To find the probability that the wave amplitude $\zeta_a$ in a sea state exceeds a chosen threshold value $a$, the Rayleigh distribution can be integrated from that amplitude onwards:

$$\begin{aligned} P\{\zeta_a > a\} &= \int_a^\infty f(x) \cdot dx \\ &= \frac{1}{\sigma^2} \int_a^\infty x \cdot \exp\left\{-\left(\frac{x}{\sigma\sqrt{2}}\right)^2\right\} \cdot dx \\ &= \exp\left\{-\frac{a^2}{2\sigma^2}\right\} \end{aligned} \tag{5.38}$$

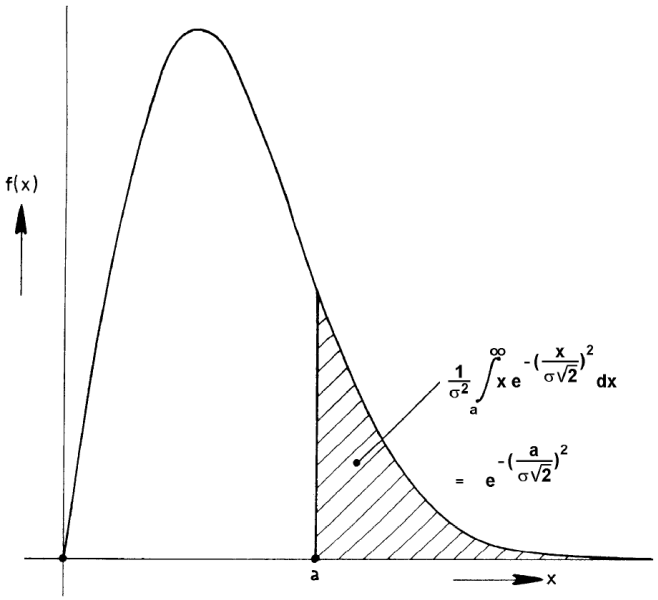


**Figure 5.12:** Rayleigh distribution and the probability of exceedance of a threshold value [23]

Equation 5.38 can be conveniently rewritten as a function of the significant wave height $H_s$, which is equal to $4\sigma$, and the maximum wave height $H_{max}$:

$$P\{H > H_{max}\} = \exp\left\{-2\left(\frac{H_{max}}{H_s}\right)^2\right\} \tag{5.39}$$

To find the most probable maximum wave height for a given period, the number of waves in that period is of importance. This can be expressed as $N_{cycles}$, which relates to the number of waves. The most probable maximum wave is defined as the wave height that will be exceeded once for the duration of interest. The most probable maximum can be found by stating that the probability that this maximum is exceeded, is equal to 1 divided by the amount of waves:

$$\exp\left\{-2\left(\frac{H_{max}}{H_s}\right)^2\right\} = \frac{1}{N_{cycles}} \tag{5.40}$$

The number of cycles is determined by the zero crossing wave period, and the duration of the reference period:

$$N_{cycles} = \frac{T_{reference}}{T_{z,wave}} \tag{5.41}$$

Because in frequency domain there is a linear relation between the input and the output, a wave spectrum and the spectrum of a system property, the output will have the same statistical properties as the input. That means that any output property of the system that is modeled will be a Gaussian process, and the amplitudes of the output property will follow a Rayleigh distribution. As mentioned before, the output spectrum of a system property can be used to calculate the SDA, which is analogous to the significant wave height. Analogously to the most probable maximum wave height, the significant double most probable maximum (SDMPM) of any system property can be found. The SDMPM of a response parameter $X$ can be found by the integration of the Rayleigh distribution and written as:

$$\exp\left\{-2\left(\frac{X_{SDMPM}}{X_{SDA}}\right)^2\right\} = \frac{1}{N_{cycles}} \tag{5.42}$$

To determine operational limits, the significant single MPM (SSMPM) of a system property is used, which is the most probable maximum amplitude, equal to half the SDMPM. This gives an intuitive measure of a safe boundary for a system property. For example, when observing relative motions during

the mating phase of a component, it gives the maximum allowable excursions a component can make with respect to its docking point in order for it to be installed. A clearance between two objects can also be expressed as an SSMPM, as it is equal to the difference between the static clearance and the minimum allowable clearance between the two objects.

As the maximum amplitude of the response is used, it is more convenient to also express the response as an amplitude as well. This is done by using the significant single amplitude (SSA), which is equal to half the SDA. Equation 5.42 can be rewritten so that a relation is formed between the SSA and the SSMPM:

$$X_{SSMPM} = X_{SSA}\sqrt{\frac{1}{2}\ln N_{cycles}} \tag{5.43}$$

### 5.8.2. Operability

The statistics of a response parameter can be used to determine the operability of the operation. Operability is defined as the maximum wave height at which the SSMPM of a response parameter reaches a threshold value. Operability can therefore be used to find the most limiting factors of an operation, and define its safe working limits. The result is a curve that represents the maximum wave height at a given peak periods, below which the operation can take place safely. Operability curves usually feature the operability of several response parameters, and the operability is found below all thresholds.

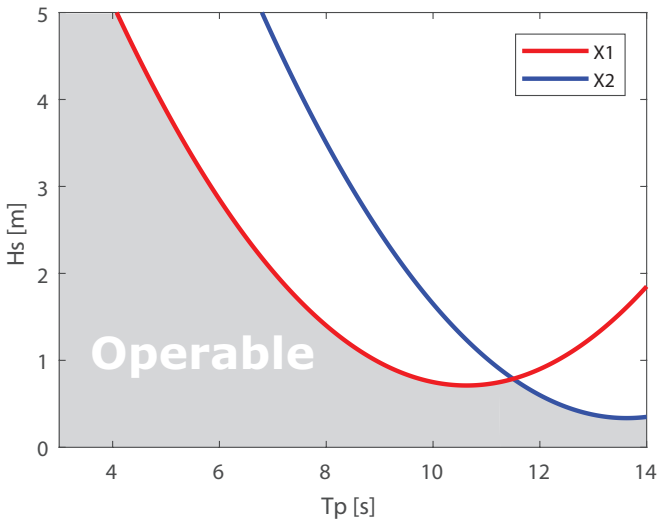


**Figure 5.13:** Example operability curve

To find the SSMPM of a system property through frequency domain, a spectral approach can be used. The output spectrum can be calculated through the RAO of the system property and the input wave spectrum, which is given for a combination of peak period and significant wave height. The spectral moment of the output spectrum can then be used to calculate the SSA of a system property. Through the number of cycles, the SSMPM of the system property is then calculated. To find the operability, this process is repeated for a given number of combinations peak periods, and can also be done for multiple wave headings. Since frequency domain calculations are inherently linear, the process is performed for a unit wave height and scaled linearly to other wave heights. A schematic representation of the calculation is shown in figure 5.14.

To obtain operability data from time-domain simulations, simulations with different wave heights and corresponding wind speeds are performed for a range of peak periods. For each simulation, the SSA is computed as $2\sigma$, and it is scaled to an SSMPM through the number of cycles relevant for the response variable. For each peak period, the wave height for which the response limit is reached is found by interpolating between the SSMPM values of the response corresponding with the simulated wave height and wind speed.

*For every Tp...*

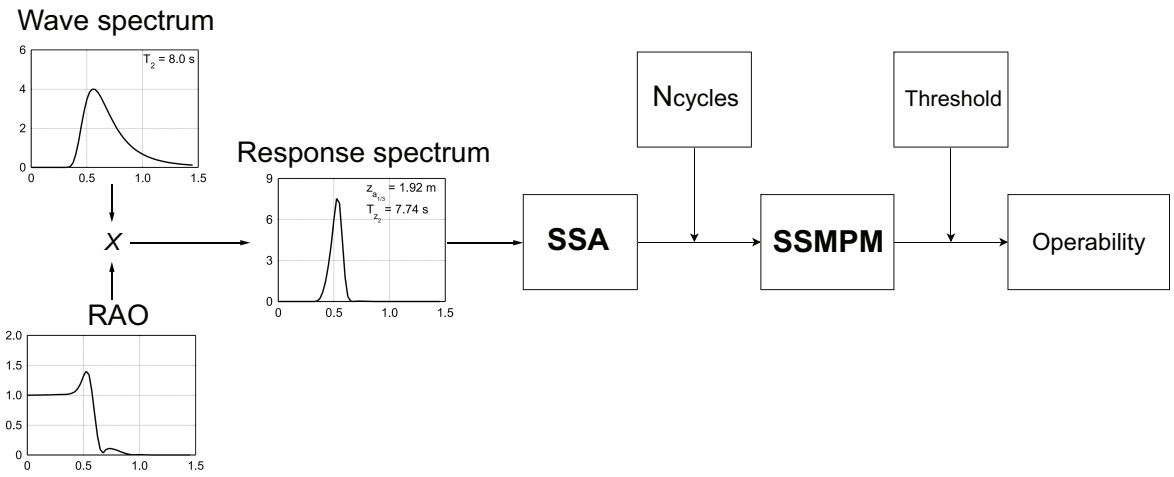


**Figure 5.14:** Diagram of spectral and statistical approach of finding operability through frequency domain

# 6

# Model description

Models are made of the floating wind turbine, the support vessel and the OSCC, that are sufficiently accurate to be used for a dynamic analysis. This is done by including all aspects of the turbine, floater and vessel that influence the dynamics of the system in the model. In the following sections, the floating turbine that is used is described, and the TLP is designed based on its motion characteristics. A simplified model of the support vessel is also presented.

## 6.1. Floating wind turbine

As mentioned in section 2.1, the wind turbine generators (WTGs) that will be used in floating wind are likely to have a higher power rating than WTGs currently used. To make a representative model of the component exchange operation, the WTG used in the model is chosen to have a power rating of 15 MW. The 15 MW IEA reference turbine, of which all relevant data is publicly available, is selected as a model WTG as it has a power rating that is realistic for use in floating wind.

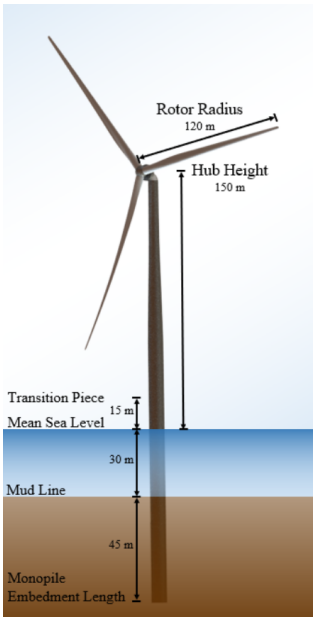


**Figure 6.1:** The bottom-fixed version of the IEA 15 MW reference turbine [51]

Some general information about the reference turbine is given in table 6.1, but more information can be found in the reference document and the corresponding GitHub page [51] [18]. As the model will be for a maintenance operation, the rotor will not be turning, and no further detail is provided in this thesis on the power production properties. The tower of the turbine is adapted from the design of the

bottom-fixed tower to meet the needs for a tower on a TLP. This will be further explained in subsection 6.1.2.

**Table 6.1:** Turbine properties

| *Property* | *Value* | *Unit* |
|---|---|---|
| Hub height | 150 | m |
| RNA mass | 949.8 | mT |
| Blade length | 115.0 | m |
| Blade mass | 66.0 | mT |

### 6.1.1. Blade loads

For reference, the aerodynamic loads on the blade are examined. The lift and drag can be computed through the BEM methodology. The aerodynamic load will be different along the blade, due to its varying shape and chord size. This can result in a moment around the lifting point of the blade. A local axis system is defined in the center of mass of the blade, in which the loads on the blade are computed. The blade pitch is defined as its orientation around the y-axis. The pitch of the blade is in this model defined to be zero in its feathered position with the leading edge of the blade pointed in negative x-direction.

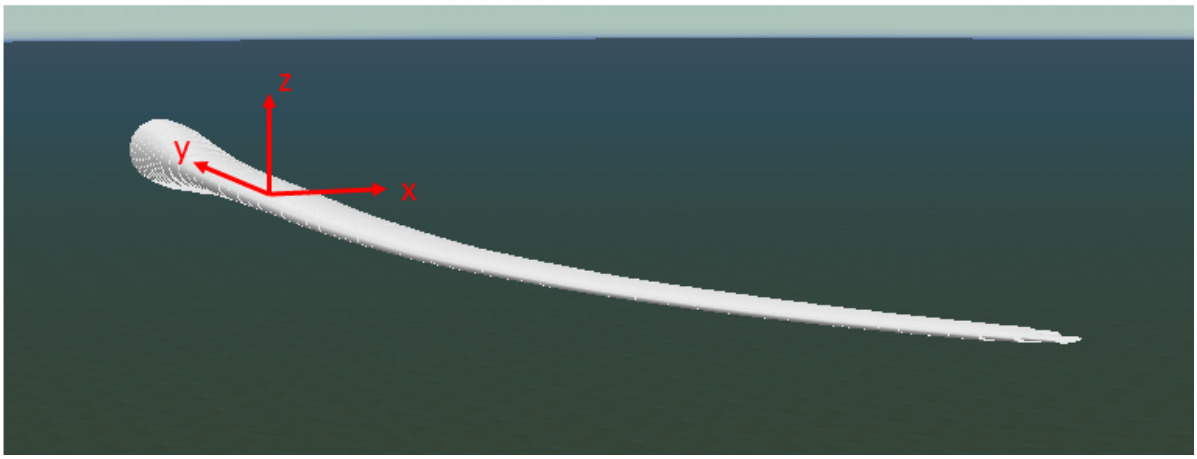


**Figure 6.2:** Local axis system of the lifted blade

The loads in the local axis system are shown in figure 6.3, for a variation of the pitch of the blade and the inflow angle of the wind. The inflow angle is defined as the angle the wind direction makes with the x-axis, in the x-y plane. The inflow angle is zero when the wind direction is exactly aligned with the x-axis. It can be seen that the forcing on the blade is at its minimum in its feathered position. The force in x-direction and z-direction becomes less for larger inflow angles, as the aerodynamic load on the blade is calculated for the wind speed parallel to the airfoils the blade. This is a consequence of the BEM theory that is used. This is a non-conservative result since the actual loads will likely be higher, since the component of the wind parallel to the length of the blade will also result in loads on the blade, which are not taken into account through BEM theory. This could especially lead to higher forces in y-direction and an extra moment around the x-axis. It can be seen that the moments on the blade are close to zero for the feathered position. There is a small moment around the z-axis for the feathered position, which will rotate the blade in yaw. To minimize the dynamic excitation of the blade under wind loads, the blade will be installed in its feathered position and is modeled as such.

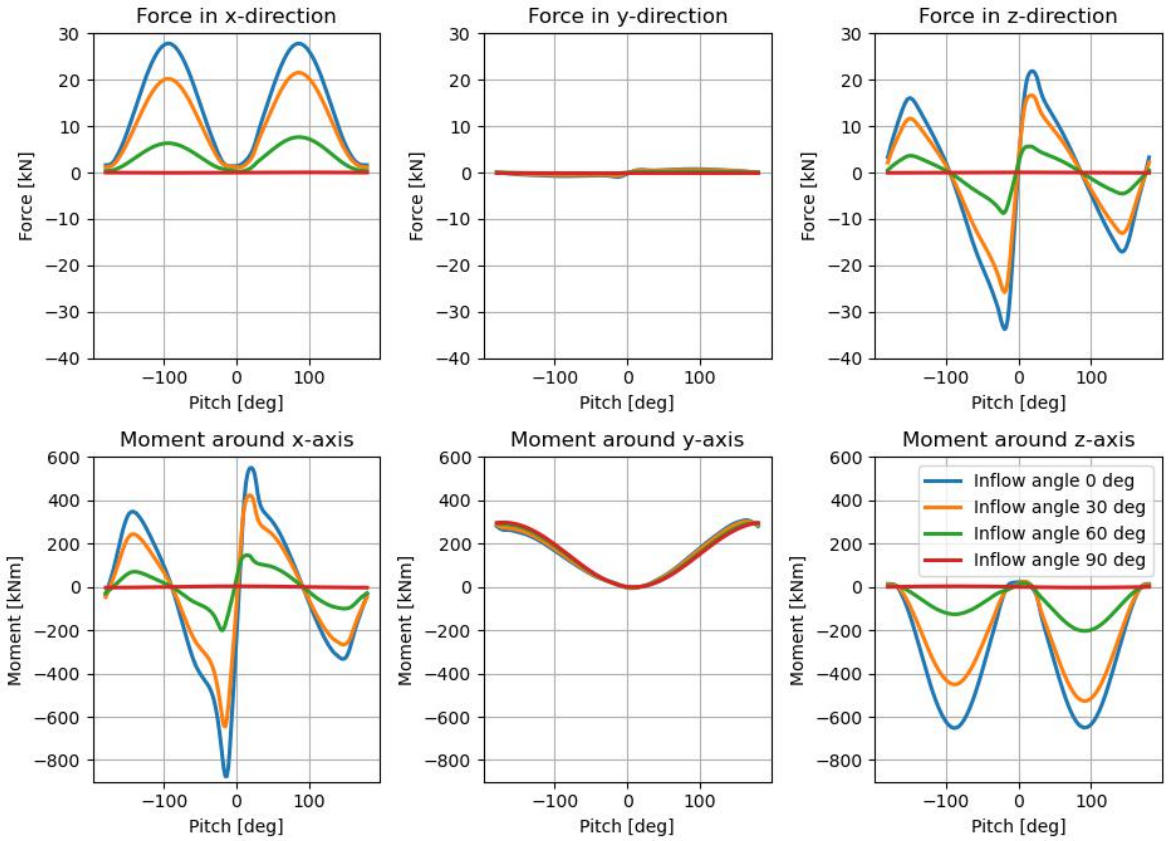


**Figure 6.3:** Loads on a single blade for a constant wind speed of 10 m/s

During lifting, the blade's pendulum motion will be excited by the force in its local x-direction. The pendulum mode of the blade will therefore be excited less for larger inflow angles of the wind. The force in z-direction is parallel to the hoisting cable, which will reduce its tension but it will not influence the dynamics of the blade in a major way, as the force is not high enough to overcome the mass of the blade. The moment around the x-axis and z-axis will excite the blade's pitch and yaw, respectively. It can be seen that there is a large increase in the loads that influence the dynamics of the blade, for different pitch angles. This also shows that it is non-conservative to only model the incoming wind as a parallel flow without accounting for turbulence, as turbulence can cause a relative pitch of the blade to the incoming wind. This can greatly increase the wind loads and therefore excite the dynamics of the blade.

### 6.1.2. Tower stiffness

The pitch and roll modes of a TLP that hosts a WTG are coupled with the first tower bending mode of the WTG [4]. The tower bending stiffness is therefore important for the placement of the roll and pitch natural frequencies of the system. Through a frequency domain approach, a tower is designed which is appropriate for the reference turbine on the modeled TLP. This is done in order to correctly model the natural frequencies of the TLP, as this will have a major influence on the dynamics of the system as a whole.

WTG towers are designed to withstand fatigue damage accumulated over the lifetime of the WTG, and great care is taken in avoiding fatigue damage. In the course of a component's lifetime, fatigue can lower its structural resistance and can cause it to fail under loads it normally would not. Fatigue is caused by gradual damage done to the tower when it is subjected to time-varying stresses. Fatigue damage grows with each stress cycle, and when the stress cycles are of a higher magnitude more damage is done.

Resonance can cause great fatigue damage because it creates large stress cycles in the tower. Resonance is the phenomenon where the natural frequency of the structure is close to the frequency of the loads it is subjected to, and the deformations of the structure are amplified greatly, which in turn leads to high-magnitude stress cycles.

The natural frequencies of a WTG are determined by the stiffness of its tower and foundation, and its top mass. The wall thickness of the tower is an important design choice in placing the natural frequencies of the WTG. A higher wall thickness will lead to a stiff tower, and increase its natural frequency. To avoid fatigue damage, a the natural frequency of the first bending mode of the WTG should be placed outside of the frequency range of potential excitation sources, such as wind and wave loads and excitations from the WTGs rotor.

To map the excitation frequencies relevant for the WTG, a power spectral density (PSD) plot can be used. It describes the energy contained at a certain frequency of an excitation source, forming a spectrum that defines at which frequencies the load is applied. Wind and wave loads can be described by an API and a JONSWAP spectrum, respectively. Rotor excitations can be subdivided between excitations coming from the rotational frequency of the entire rotor (1P), and the blade passing frequency (3P). These excitations can be caused by for example irregularities in the wind speed around the WTG, or influence of the tower on the aerodynamics of the blades. The frequency range of the 1P and 3P regimes is determined by the rotational frequency of the WTG, and therefore turbine specific. However, a general classification is given to the areas before, between and after the 1P and 3P regime. This has to do with the placement of the first natural frequency of the WTG. The area below the 1P regime is called soft-soft, as it would lead to a soft tower and foundation of the WTG, as its stiffness is low in order for it to have a low natural frequency. The area above the 3P regime is called stiff-stiff, as it would lead to a stiff tower and foundation of the WTG, in order for it to have a high enough natural frequency. The area in between the rotor excitation frequencies is called soft-stiff, as it is a compromise between both ends. Wave loads usually fall around the 1P frequency regime, depending on the period of the sea state. Wind loads are very low frequent, and fall in the soft-soft area.

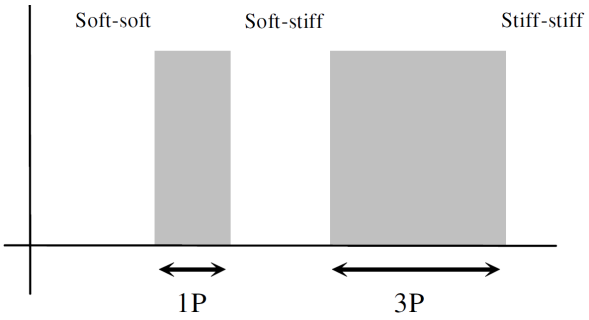


**Figure 6.4:** Rotor excitation frequencies [43]

A soft-soft configuration of the WTG would lead to overly large displacements of the WTG due to the decreased stiffness of the tower, and a stiff-stiff configuration would require too much steel, making the WTG more expensive. The roll and pitch natural frequencies of a TLP should ideally be placed in between the 1P and 3P frequencies [4]. This favours the choice for a soft-stiff tower, as the coupling between the modes will ensure that the pitch and roll natural frequencies will then also be placed in the soft-stiff area.

The natural frequency in roll and pitch of the TLP should be placed towards the 3P frequency regime to avoid wave loads. The natural frequency of the tower with the RNA on top is therefore placed at the edge of the 3P frequency regime of the reference turbine, at 0.25 Hz. To obtain a tower with such a natural frequency, the wall thickness of the tower of the bottom-fixed IEA 15 MW reference turbine is scaled such that its natural frequency is equal to 0.25 Hz. Exact data on the wall thickness and diameter of the tower used in the model is given in appendix C. The natural frequency of the tower with the RNA included is shown in figure 6.5.

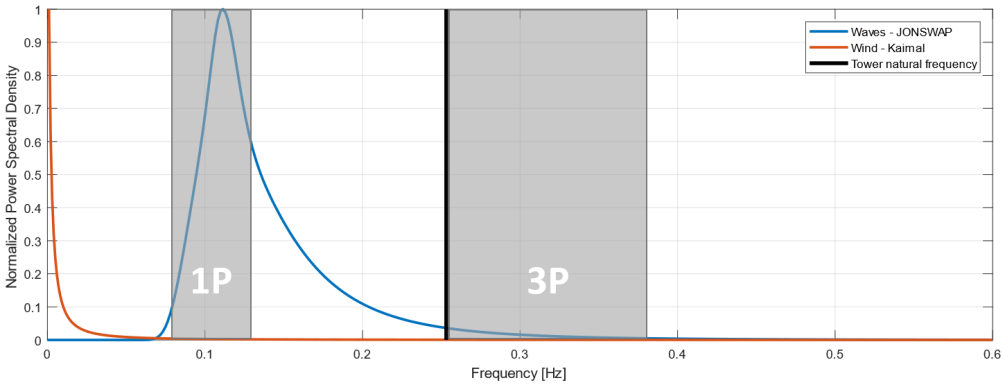


**Figure 6.5:** Placement of the first natural frequency of the tower with respect to the excitation frequencies of the reference turbine

The resulting mass of the tower is 962.5 mT. The original tower mass of the reference turbine is 860 mT. In summary, all mass properties and radii of gyration of the turbine that are used in the model are given in table 6.2. The center of gravity of each component is given with respect to the interface height of the turbine, 15 meters above the waterline.

| | ***CoG*** | ***Mass*** | ***rxx, ryy, rzz*** |
|---|---|---|---|
| Rotor | [-12.3, 0, 134.45] m | 180 mT | 41.3, 29.2, 29.2 m |
| Nacelle and hub | [-5.17, 0, 133.68] m | 769.8 mT | 3.7, 3.9, 3.8 m |
| Tower | [0, 0, 41.01] m | 962.5 mT | 38.8, 38.8, 0.7 m |
| WTG | [-3.17, 0, 92.70] m | 1911.2 mT | 49.9, 49.3, 10.5 m |

**Table 6.2:** Center of gravity and buoyancy of system components with respect to the interface height of the TLP, 15 meters above the water level

### 6.1.3. Damping

Structural damping is added to the tower in accordance with the Orcina model of the 15 MW IEA reference turbine, in which the Rayleigh damping coefficients of the reference turbine tower are obtained through an aeroelastic simulation [32]. In order to reduce the computational time needed to run a simulation, a simplification is made to model the blades of the turbine as rigid bodies. However, in reality the blades also account for a certain amount of structural damping. This damping is also included in the Orcina model, which has been obtained through an aeroelastic simulation of the blades. A comparison of the transient response of the simplified model and the model with the fully flexible rotor has been done in order to verify the amount of damping in the system. The tower bending modes of both models have an almost equal damping ratio of 1.05 %, and the simplification is therefore deemed valid. The result of the assessment of the transient response can be found in appendix C.

## 6.2. Tension-leg platform

A Tension-leg Platform for the 15MW IEA reference turbine is modeled to support the dynamic analysis of the component exchange. The TLP is modeled for a water depth of 150 meters, as this is seen as a suitable water depth for this floater type [3]. A generic floater shape, with three pontoons and a single column, is taken as a starting point. From Bachynski and Moan, it becomes clear that this shape is a viable option for a TLP design [4]. For modeling purposes, one tendon is attached to each pontoon, and although there will likely be more tendons per pontoon for redundancy purposes in reality, it is assumed this is a reasonable approximation as long as the tendon stiffness is chosen correctly. As the aim of this thesis is to do a dynamic analysis with the TLP as a starting point, the most important aspect of the TLP is that the motion characteristics are realistic, as they will influence the motion characteristics of the system as a whole. The aspects of the TLP that are required in order to model its dynamics are discussed in the following subsections.

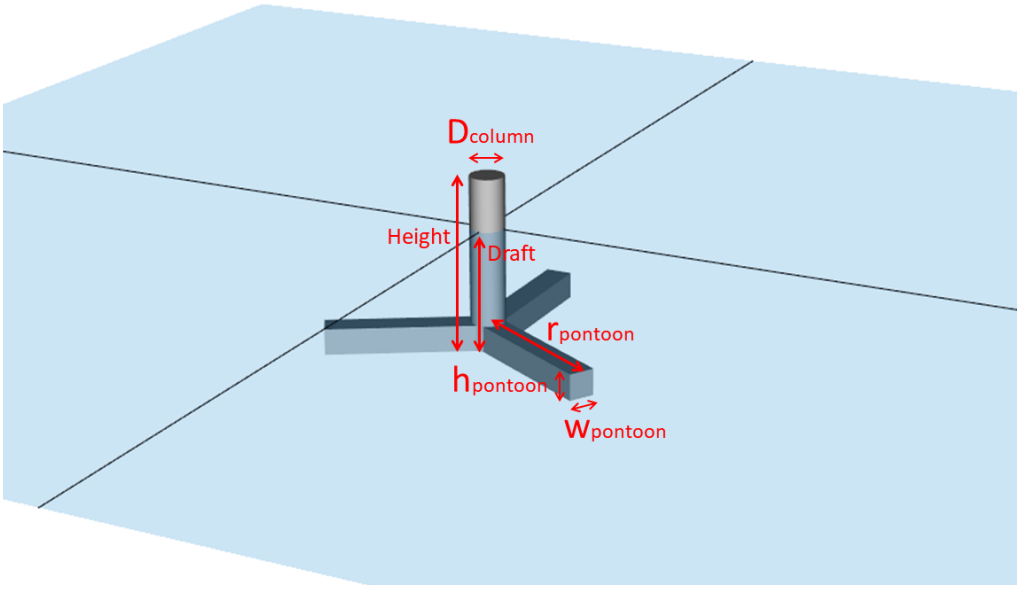


**Figure 6.6:** Shape of the Tension-Leg Platform

### 6.2.1. Hydrostatics

The hydrostatic equilibrium of a TLP is determined by its buoyancy properties and its mooring configuration. As explained previously, the TLP makes use of taut tendons which provide a reaction force to its buoyancy in order to keep it in its position. The center of buoyancy of a TLP is below its center of gravity, and the TLP has a small waterplane area. This means that a TLP has a negative metacentric height, and is unstable by itself. The stability of the TLP is ensured by the tendons, which provide a restoring moment to the platform. There is an equilibrium between the buoyant forces on the TLP, the mass of the TLP and WTG and the tendon forces. The vertical component of the tension in the tendons, assuming a number of three massless tendons, can be calculated through the hydrostatic properties of the TLP:

$$T_{\text{tendon,vertical}} = \frac{1}{3} g(\rho \nabla_{\text{TLP}} - M_{\text{WTG}} - M_{\text{TLP}}) \tag{6.1}$$

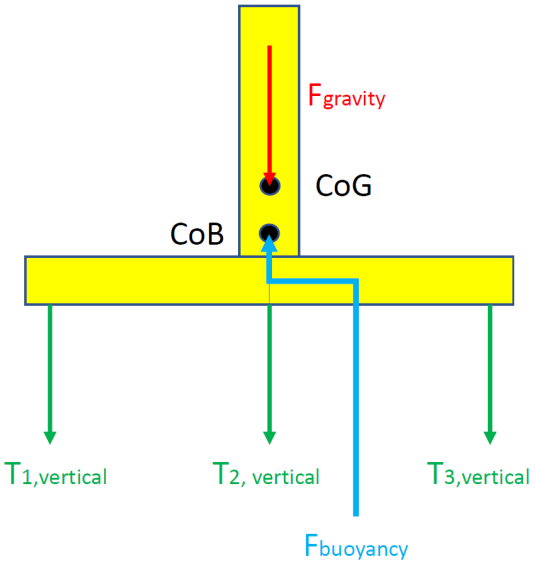


**Figure 6.7:** Balance of vertical forces on the TLP

The results of the hydrostatic properties of the TLP are summarized in table 6.3. Indicative values for the displacement, mass and center of gravity of the TLP were given by Heerema Engineering Solutions, which are used in the model. It should be noted that in its equilibrium, the tension in the tendons of the TLP is not exactly equal due to the off-center center of gravity of the WTG. As the center of gravity of the RNA is placed slightly towards the rotor, the tension in the tendon closest to it will be slightly lower than in the other tendons. As there is no ballast system present in the TLP itself, this will be the case for any orientation of the RNA.

**Table 6.3:** Geometric and hydrostatic properties of the tension-leg platform

| *Property* | *Value* | *Unit* |
|---|---|---|
| Draft | 35 | m |
| Height | 50 | m |
| Column diameter | 10 | m |
| Pontoon radius | 42.5 | m |
| Pontoon width | 7.5 | m |
| Pontoon height | 7.5 | m |
| TLP mass | 4150 | mT |
| TLP displacement at draft | 9161.5 | mT |
| Center of Buoyancy (from keel) | 7.87 | m |
| Center of Gravity (from keel) | 11.81 | m |
| WTG mass | 1911.3 | mT |
| Tendon tension vertical | 10.76 | MN |

### 6.2.2. Hydrodynamics

To compute the hydrodynamics of the TLP, first-order potential theory is used. For a TLP with a column diameter of 10 meters, it can be deduced from figure 5.7 that drag becomes negligible for wave heights lower than 2.5 meter. As precise offshore operations are usually performed at relatively low sea states, it is assumed to be a reasonable approximation to not model drag and assume potential theory for the model of the TLP. However, viscous damping can have a significant effect. The quadratic viscous damping is large compared to linear radiation damping for TLPs [3], and only the latter is accounted for using potential theory. Therefore, potential theory is chosen for modeling of the added mass and radiation damping of the TLP, and Morison elements with a drag coefficient of $C_d = 0.7$ and an equivalent diameter equal to the column diameter and pontoon width are added to the column and pontoon to account for viscous drag and damping, in accordance with Bachynski and Moan [4].

The potential coefficients of the TLP are calculated using WAMIT. To discretize the shape of the TLP, a rectangular mesh is used on the column and pontoon, and a curvilinear mesh is used on the ends of the column. A mesh sensitivity study is performed on the panel size of the mesh of the TLP. It is found that a mesh which has a panel size of around 2x2 meters yields a sufficiently accurate result. The final mesh that is used in WAMIT is shown in figure 6.8a, and the results of the mesh sensitivity analysis are given in appendix C. The axis system is given for reference of the degrees of freedom of the TLP. Different wave headings can be established based on the coordinate system of the TLP. The convention used for the incoming wave headings used for the TLP is shown in figure 6.8b.

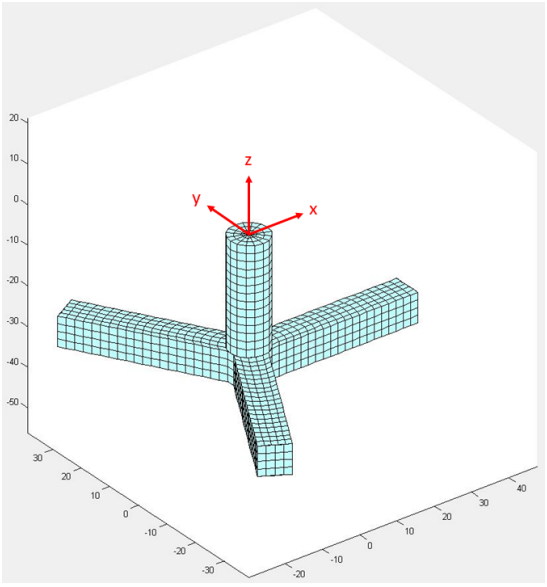


**(a)** Final mesh of the TLP used in the calculation of its potential coefficients

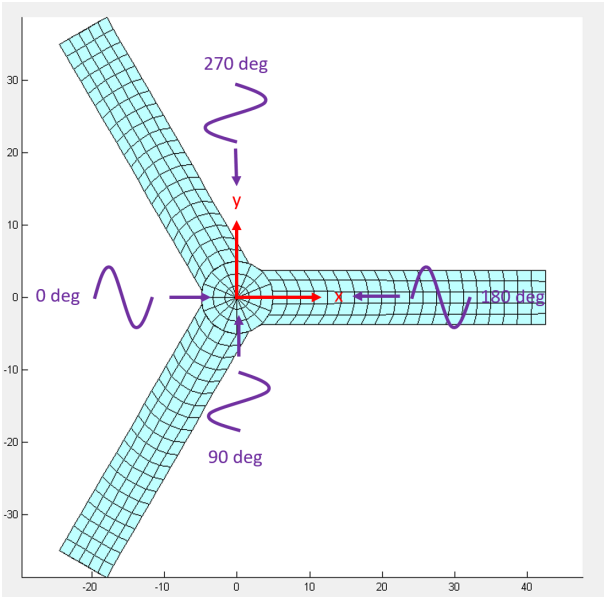


**(b)** Definition of incoming wave headings on the TLP

**Figure 6.8:** Mesh and coordinate details of the TLP

The results of the WAMIT run for the added mass and damping coefficients are given in figure 6.9 and 6.10. As the TLP is symmetric, the results in surge and roll are equal to the results in sway and pitch, and therefore only one of the two is given. It can be seen that there is a large dependency of the radiation damping on the frequency of oscillation of the TLP, as the damping coefficients approach zero at high and low frequencies. The added mass coefficients also vary over the frequency range, but approach a constant value for high frequencies.

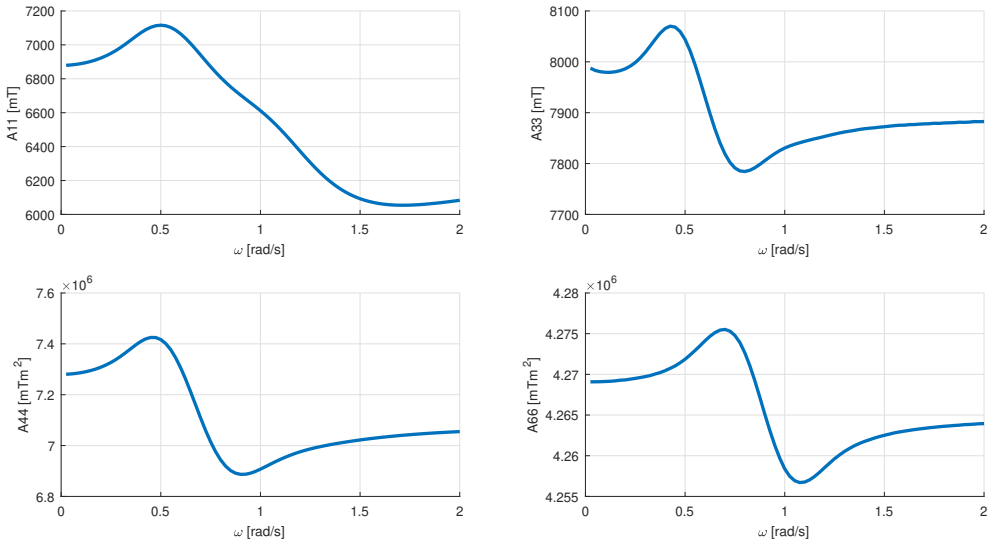


**Figure 6.9:** Added mass coefficients of the TLP in relevant degrees of freedom

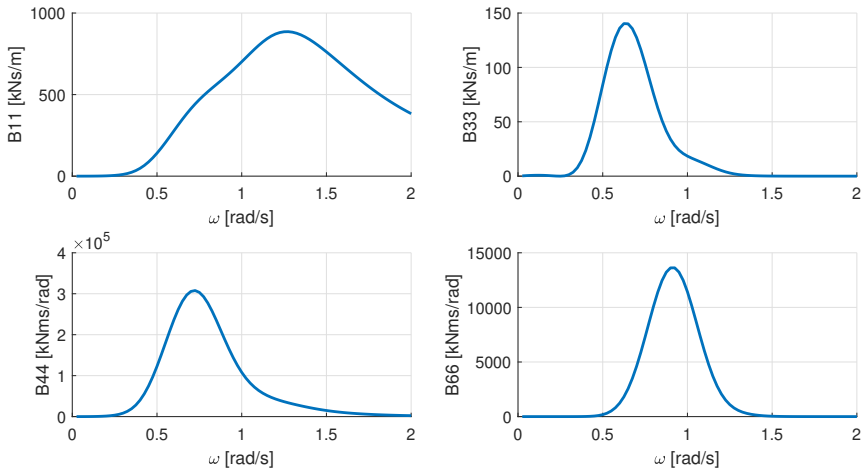


**Figure 6.10:** Radiation damping coefficients of the TLP in relevant degrees of freedom

Next to the potential coefficients, the first-order potential flow wave loads are also extracted from WAMIT. Figure 6.11 shows the first-order wave load amplitudes for a set of incoming wave headings. It can be seen that for wave loads, there is again a large dependency on the wave frequency. The maximum wave loading on the TLP occurs between 0.5 to 1 rad/s, which are typical wave frequencies. In surge and roll, a larger incline of the incoming waves leads to a decrease in forcing, and the opposite is true for sway and pitch. There is a small difference in the heave forcing for different orientations, which can be caused by coupling effects with other degrees of freedom or the asymmetry of the legs in a certain incoming wave heading. The 45 and 90 degree incoming wave heading show forcing on the TLP in yaw, due to its asymmetric projected area in the direction of the incoming waves.

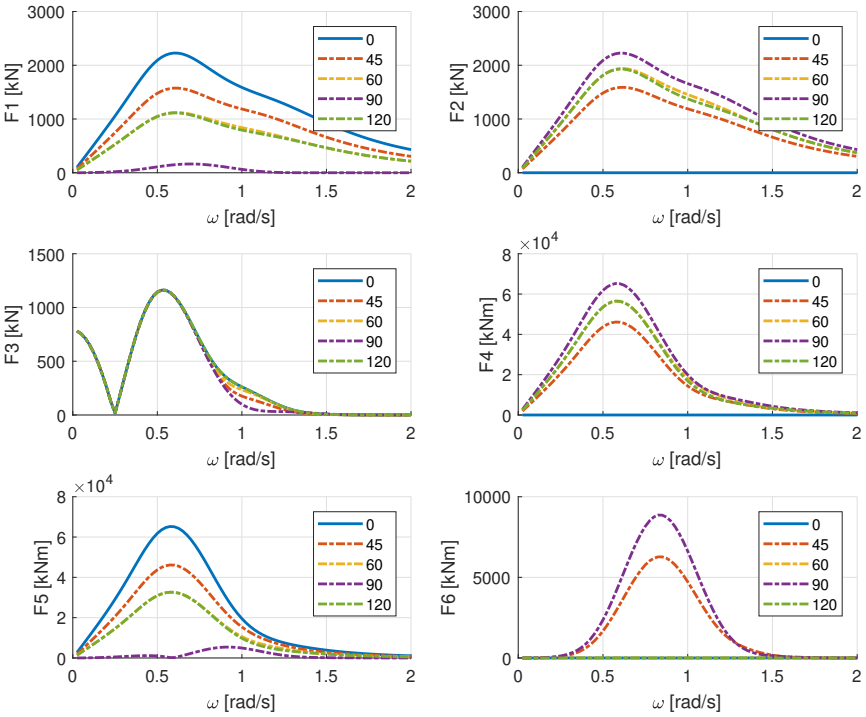


**Figure 6.11:** First-order potential flow wave load amplitudes on the TLP

### 6.2.3. Mooring

The TLP is moored to the seabed using taut mooring lines referred to as tendons. From project experience at Heerema Engineering Solutions, it is suggested to incorporate an angle in the tendon design. An angle in the tendons can enable the focal point of the rotation of the system to lie at hub height of the WTG, which reduces the motions in the nacelle. This has a positive influence on the requirements on components in the nacelle, and the reduced motions and accelerations of the nacelle will likely lead to lower maintenance due to lower loads on equipment.

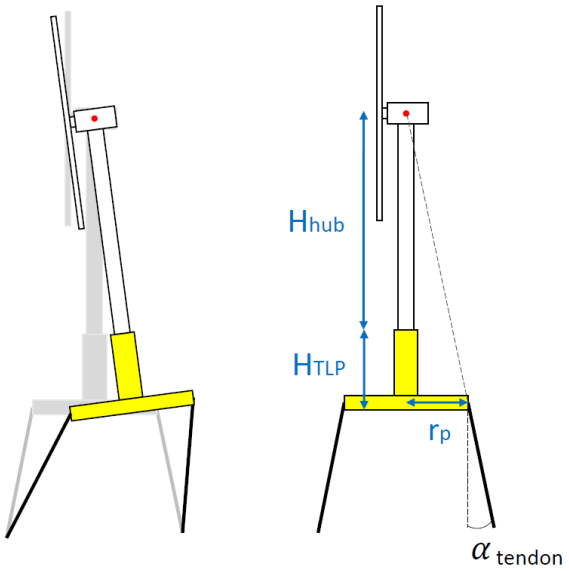


**Figure 6.12:** The angle in the tendon configuration leads to the focal point of the rotation of the TLP being at hub height

This angle can be determined through the geometry of the TLP and the WTG. To enable the focal point of the rotation of the TLP to be at nacelle level, the tendon angle should be such that when the tendons are extrapolated, they should intersect at the nacelle. It can therefore be expressed as:

$$\alpha_{\text{tendon}} = \arctan \frac{r_p}{H_{\text{TLP}} + H_{\text{hub}}} \tag{6.2}$$

For the TLP and WTG used in this thesis, with a height of 50 meters and a hub height of 150 meters respectively, this angle comes down to 12.97 degrees. As a result, the tension in a single tendon can be deduced from the required vertical tension to keep the system in equilibrium:

$$T = \frac{T_{\text{vertical}}}{\cos \alpha_{\text{tendon}}} \tag{6.3}$$

As the vertical tension is equal to 10.76 MN, the total equilibrium tension in a single tendon is equal to 11.04 MN.

#### Tendon stiffness

The stiffness of the tendons is an important factor in the dynamics of the TLP. There is no concensus yet in literature on which material is best suitable for a tendon, although hollow steel pipes, synthetic wire ropes and chain moorings are investigated as options [4]. Because the aim of the model of the TLP is only to accurately model its motion characteristics, the tendons are assumed to be massless springs, with a stiffness to be freely chosen. The stiffness of the tendons is expressed as $EA$, to link the spring stiffness to material stiffness with the material's Young's modulus $E$ and axial area $A$. The structural deflection of a material can be expressed as a function of its Young's modulus, area, unstretched length $l_0$ and the tension $T$ applied to it:

$$\delta l = l_0 \frac{T}{EA} \tag{6.4}$$

This equation bears resemblance to the equation for the stretch of a spring. This supports the assumption that the tendons can be modeled as springs, as their stiffness $EA$ acts as a spring constant. As the waterdepth, the desired draft of the TLP and the tendon tension are known, the unstretched tendon length can be expressed as a function of $EA$. First, the tendon stretch can be expressed as the desired length $L$ minus the unstretched tendon length:

$$T = EA\frac{\delta l}{l_0} = EA\frac{L - l_0}{l_0} \tag{6.5}$$

Rewriting this equation leads to the unstretched tendon length, and taking the desired length $L$ as the waterdepth minus the draft of the TLP, the following equation is found:

$$l_0 = \frac{L}{1 + \frac{T}{EA}} = \frac{\text{waterdepth} - \text{Draft}}{1 + \frac{T}{EA}} \tag{6.6}$$

It can be proven analytically that the stiffness in surge, sway and yaw direction resulting from the mooring of a TLP, depends mostly on the tendon tension. The stiffness resulting from the tendons in other degrees of freedom, depends on their stiffness, $EA$ [39]. The stiffness in these degrees of freedom determines, among other parameters, the natural frequencies of the system. Table 6.4 gives an overview of which tendon properties are dominant in the natural frequency of each degree of freedom of the FOWT.

**Table 6.4:** Dominant tendon property in natural frequency

| ***DoF natural frequency*** | ***Dominant tendon property*** |
|---|---|
| Surge, sway, yaw | Tension |
| Heave, roll, pitch | Stiffness |

As all other parameters that influence the natural frequencies of the system, the hydrodynamics, weight, waterdepth and WTG are already fixed, the tendon stiffness can be chosen freely in order to obtain the desired natural frequency in every degree of freedom. In order to place the natural frequencies of the TLP, and therefore accurately model its motion characteristics, a modal analysis is performed of the TLP with the WTG on top. The mooring stiffness $EA$ is varied, in order to determine the influence of the mooring stiffness on the natural frequencies.

The modal analysis is performed with a flexible tower modeled as a beam with a stiffness corresponding to its structural properties, and a rigid tower. This is done to visualise the coupling between tower bending and the roll and pitch from the TLP/ The result is shown in figure 6.13. As expected from the analytical analysis of TLP mooring, the biggest change in natural period can be observed in heave, roll and pitch. The coupled roll and pitch tower mode can also clearly be seen, in the large difference in natural period when including a flexible tower in roll and pitch. It can be seen that the natural period goes down for a higher tendon stiffness, and therefore the natural frequency goes up. To place the natural frequency of the system in roll and pitch as far away from wave frequencies as feasible, an $EA$ of 12 GN is chosen, after which the curve of the tendon stiffness influence flattens out.

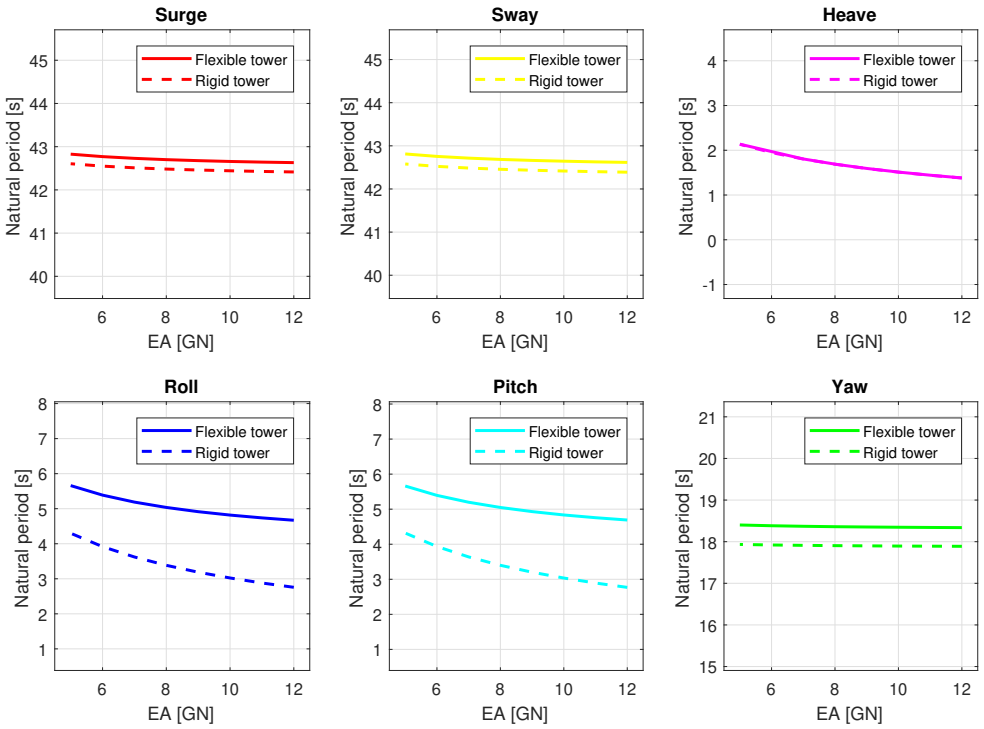


**Figure 6.13:** Sensitivity study of the natural frequencies of the system to the tendon stiffness through modal analysis

Through equation 6.6, the unstretched tendon length can now be calculated. The tendon properties are summed up in table 6.5 for the equilibrium draft of the TLP.

**Table 6.5:** Tendon properties

| ***Tendon property*** | ***Symbol*** | ***Quantity*** |
|---|---|---|
| Unstretched length | $l_0$ | 117.895 m |
| Stiffness | $EA$ | 12 GN |
| Angle | $\alpha_{\text{tendon}}$ | 12.97 deg |
| Average tension at equilibrium draft | $T$ | 11.04 MN |
| Average stretch at equilibrium draft | $\delta l_{avg}$ | 0.1085 m |

The resulting stiffness matrix from the mooring is computed in accordance with the equations for taut mooring systems from Al Solihat [39], and given in equation 6.7. It can be seen that the stiffness in the tension-dominated surge and sway modes is relatively low when compared to the stiffness-dominated mode in heave. The same can be seen for the low stiffness in yaw, compared to the high stiffness in roll and pitch. The coupling between surge, sway, roll and pitch is also visible through the off-diagonal terms, which results in the rotational displacement that keeps the RNA in place for a surge and sway displacement. The coupling term between surge and roll is negative due to the conventions of the axis system.

$$\mathbf{K} = \begin{bmatrix} 7.97MN/m & 0 & 0 & 0 & -150GNm/rad & 0 \\ 0 & 7.97MN/m & 0 & 150GNm/rad & 0 & 0 \\ 0 & 0 & 290MN/m & 0 & 0 & 0 \\ 0 & 150GNm/rad & 0 & 174GNm/rad & 0 & 0 \\ -150GNm/rad & 0 & 0 & 0 & 174GNm/rad & 0 \\ 0 & 0 & 0 & 0 & 0 & 0.82GNm/rad \end{bmatrix} \tag{6.7}$$

### 6.2.4. Natural frequencies and motion characteristics

The system characteristics of the TLP and WTG can be presented in frequency domain by their natural frequencies, mapped against possible excitation sources. The natural frequencies of the system are plotted in figure 6.14, including the rotor excitation frequencies, wave loads and wind loads. It can be seen that the pitch and roll natural frequency falls in between the rotor excitation regimes with some margin. This mode will be largely excited by wave loads. The natural frequencies of surge and sway fall in the excitation frequencies of wind loads, and will therefore be excited by low-frequent wind loads. Heave and yaw of the TLP are mostly out of range of any excitation sources.

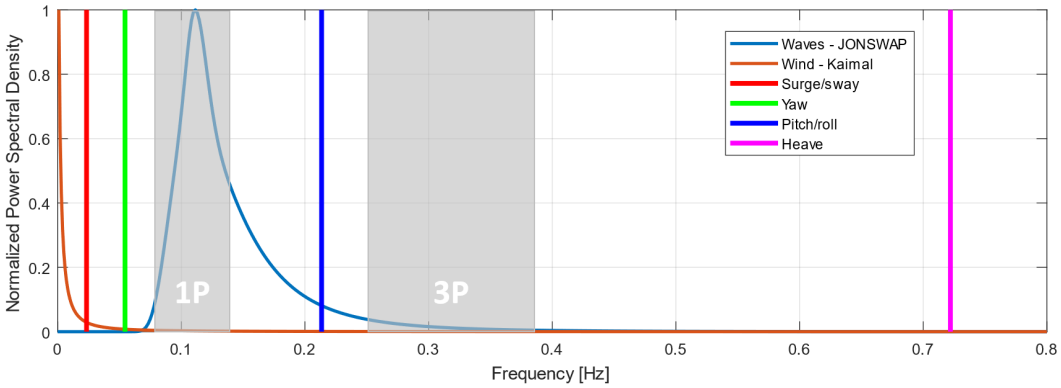


**Figure 6.14:** The natural frequencies of the TLP with the WTG

The mode shapes of the TLP and WTG in surge and roll are shown in figure 6.15. As the sway and pitch mode shapes are equal to the surge and roll shapes, they are ommitted. The yaw and heave mode shapes are pure rotation and displacement, so their mode shape is straightforward. The effect of the tendon angle can be seen in the mode shape in surge, as the RNA does not displace out of its original location. The tower bending and roll coupling can be seen in the roll mode shape. It can be seen that most of the displacement comes from the tower bending instead of the roll of the TLP. This also shows that there is little damping in the roll and pitch mode. The main source of damping in the model is hydrodynamic radiation and viscous damping. The amount of hydrodynamic damping depends on the velocity of the TLP, and as the displacement of the TLP in the roll and pitch mode is small, the amount of damping is also small. Therefore, structural damping in the tower becomes more important for the roll and pitch mode.

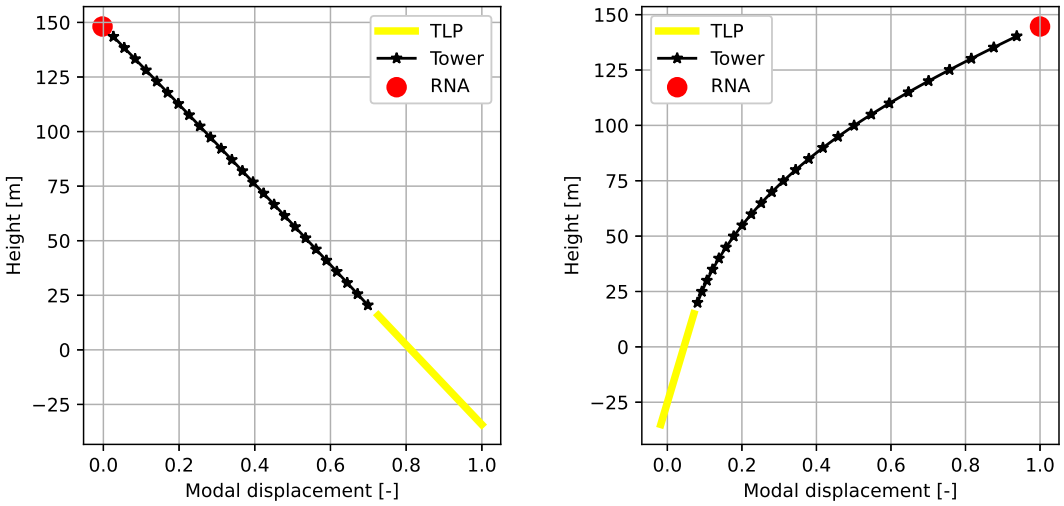


**(a)** Surge mode shape

**(b)** Roll mode shape

**Figure 6.15:** Mode shapes of the TLP and WTG in surge and roll

#### Higher-order wave loads

Moored structures such as TLPs are subject to loads due to higher-order, non-linear wave effects. Higher-order effects can lead to excitation at frequencies higher or lower than normal wave forces, and are therefore relevant for surge, sway and heave displacements. There is little hydrodynamic loading in the yaw degree of freedom, so higher-order wave loads will also have little effect. Important non-linear wave effects of higher order are low-frequent wave drift forces, difference- and sum-frequency forces, and higher-order forces due to steep waves that cause a structural response of the TLP.

Difference- and sum-frequency forces are hydrodynamic forces that arise due to the nonlinear interaction of waves with different frequencies. This nonlinear interaction can produce excitation at new frequencies equal to the difference or sum between the original frequencies. For TLPs for floating wind turbines, second-order theory is important for high-frequency resonant pitch or heave motions due to sum-frequency effects, also known as springing. This can affect the response in these modes, but it has been shown by Moan and Bachynski that the response of a TLP in due to sum-frequency effects is an order of magnitude lower than the response due to linear wave loads [3]. The same research shows that sum-frequency effects are more important for fatigue in the tendons due to the increase in standard deviation in the tension, but this is not of relevance for this thesis.

Low frequent surge motion could be excited by wave drift forces and difference frequency forces. Wave drift forces are caused by a mean force resulting from the reflection of incoming waves. This force varies at a low frequency by interaction between irregular waves, which form envelopes of higher and lower amplitude. It is assumed that low frequent wind loads due to drag on the turbine will have a larger effect on the TLP.

These second-order effects are not accounted for in the hydrodynamic model of the TLP. This will lead to an underestimation of low-frequent and high-frequent motions of the TLP. This should be considered in the results, and if there are results that have a particular sensitivity at these frequency ranges, further investigation is required.

Third-order potential theory is also relevant for TLPs for floating wind turbines, in order to compute ringing responses [3]. Ringing responses occur in severe seas, where large transient structural deflections can occur in the tendons at frequencies much higher than the wave frequency, usually after a high, steep wave [5]. As this model of a TLP is for a maintenance operation, severe sea states are not expected. Therefore it is considered to be a reasonable approximation to model the TLP without any third-order effects.

## 6.3. Support vessel

A simplified model of the support vessel is created in order to support the dynamic analysis of the operation. Indicative values for the dimensions and vessel cranes are taken from the Jumbo Fairplayer [29]. The vessel's dimensions, mass properties and hydrostatic terms are given in table 6.6. Its radii of gyration are computed as $r_{xx} = 0.42B_{vessel}$, $r_{yy} = 0.25L_{vessel}$ and $r_{zz} = 0.25L_{vessel}$ in accordance with *ITCC* [20]. The vessel's hull shape is computed as a box with a chamfered bow and stern, as seen on the Jumbo Fairplayer. The edges are filleted to account for the hydrodynamic shape of the reference vessel.

**Table 6.6:** Vessel properties

| ***Property*** | ***Value*** |
|---|---|
| Length | 144 m |
| Breadth | 27 m |
| Height | 16 m |
| Draft | 8 m |
| Mass at draft | 31880 mT |
| $r_{xx}$ | 11.34 m |
| $r_{yy}$ | 60.48 m |
| $r_{zz}$ | 60.48 m |
| KB | 4.0 m |
| BM | 7.6 m |
| KG | 5.0 m |
| GM | 6.6 m |

### 6.3.1. Hydrodynamics

Potential theory is used to compute the hydrodynamics of the vessel. A WAMIT run is performed of the vessel at its draft. A mesh sensitivity analysis is run in order to determine the effect of the panel size on the result. The full mesh sensitivity analysis is given in appendix C. The final mesh used is shown in figure 6.16, and has 2867 panels.

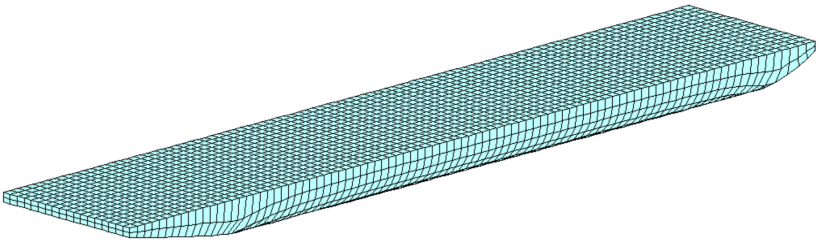

**Figure 6.16:** Mesh used to compute the hydrodynamics of the support vessel

#### Viscous roll damping

As potential theory is used to describe the hydrodynamics of the vessel, viscous effects are not taken into account. As the loads on the vessel are inertia dominated in all degrees of freedom, this is a reasonable approximation. However, viscous roll damping has a significant effect on the response of ship-shaped bodies [6]. It is chosen to add an amount of viscous roll damping relative to the critical damping of the vessel in roll. As a base case, 5 % of critical damping is assumed. As the natural period of roll of the vessel is equal to 12.8 seconds including the added mass, the critical damping can be calculated:

$$B_{c4,4} = 2\sqrt{\mathbf{C}_{4,4}(\mathbf{M}_{4,4} + \mathbf{A}_{4,4}(T = 12.8s))} \tag{6.8}$$

The critical damping in roll is equal to 7.52e+06 kNm*s/rad. The viscous roll damping is then calculated as follows,

$$B_{v4,4} = 0.05 * B_{c4,4} \tag{6.9}$$

and is equal to 3.76e+05 kNm*s/rad.

#### Dynamic positioning

The dynamic positioning of the vessel is modeled as a set of springs. As dynamic positioning systems compensate low-frequent motions, a set of springs is chosen that leads to a natural period of 100 seconds in surge, sway and yaw. In order to compute the stiffness of the set of DP springs, the vessel's

mass and added mass at a wave period of 100 seconds are used. The DP spring stiffness calculation can be found in appendix C.

### 6.3.2. Response

To get insight into the dynamic behaviour of the vessel, its response is examined by means of its RAOs in heave, roll and pitch for different wave headings. The wave headings with respect to the vessel's orientation are shown in figure 6.17.

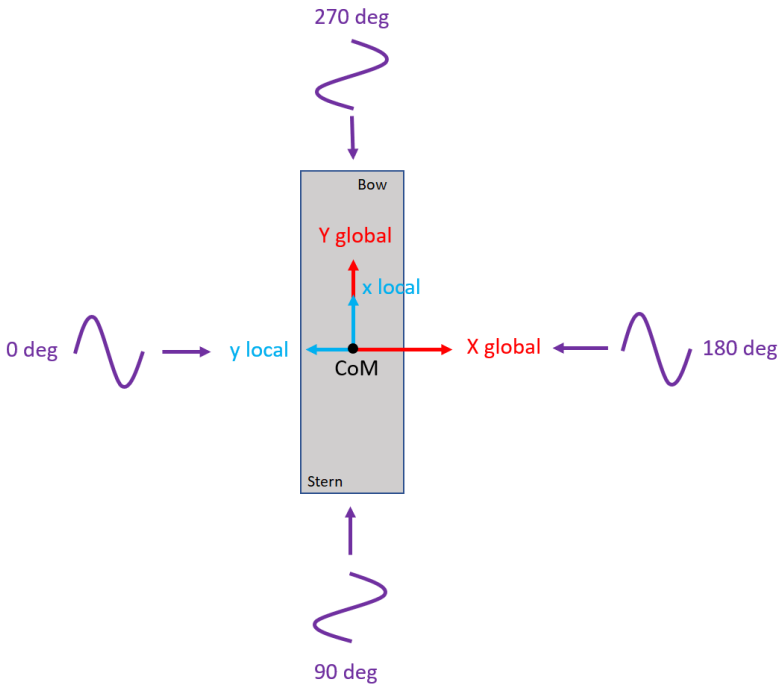


**Figure 6.17:** Wave headings with respect to the support vessel

The natural periods of the vessel in its degrees of freedom are given in table 6.7. These periods are plotted together with the RAOs in figure 6.18.

**Table 6.7:** Natural periods of the support vessel

| ***DoF*** | ***Natural period*** |
|---|---|
| Surge | 100 s |
| Sway | 100 s |
| Heave | 8.5 s |
| Roll | 12.8 s |
| Pitch | 11.3 s |
| Yaw | 100 s |

It can be seen that the RAOs have a peak at the natural period of the vessel in the corresponding degree. The response of the vessel in roll becomes negligible with waves incoming from 90 degrees. Contrary to this, the response in pitch only slightly decreases when the incoming wave heading is 90 degrees, and the peak in the RAO shifts to a higher period. The RAO's are verified based on assets of the supervising company. As these RAOs are confidential, this verification is not included in the public version of this thesis.

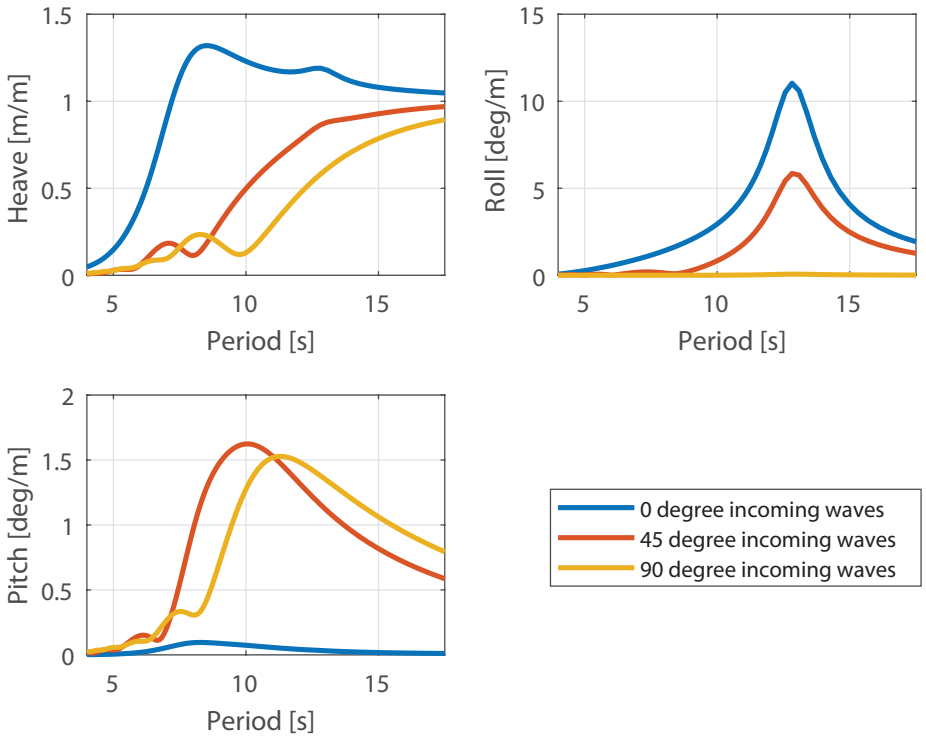


**Figure 6.18:** RAOs in heave, roll and pitch around the center of mass of the support vessel for three different wave headings

## 6.4. OSCC

The OSCC is modeled through a combination of rigid body elements such as the base and the crane, and a flexible lattice with a bending and torsional stiffness. The base is assumed to be connected rigidly to the TLP, and the lattice is clamped at its base. In its compressed mode, the OSCC is modeled as one rigid body. Important properties of the OSCC that are used in the model are given in table 6.8. The frontal area of the lattice and crane are used to calculate drag due to wind loads. The yoke that is used to lift the blade is also included in the table

| *Property* | *Value* |
|---|---|
| Base diameter | 20 m |
| Lattice height | 140 m |
| Lattice bending stiffness | 100 GNm$^2$ |
| Lattice torsional stiffness | 24.3 GNm$^2$ |
| Lattice frontal area | 1.3 m x 140 m |
| Crane boom length | 37 m |
| Crane boom mass | 200 mT |
| Crane frontal area | 77 m$^2$ |
| OSCC total mass | 1021.1 mT |
| Yoke mass | 80 mT |

**Table 6.8:** Modeled properties of OSCC

The mass properties of the OSCC in different operational modes are given in table 6.9. The local axes system of the OSCC has the same orientation as the global axes system, and has its origin in the center of the OSCC's ring, coinciding with the centerline of the tower when it is installed.

| | ***CoG*** | ***rxx, ryy, rzz*** | unit |
|---|---|---|---|
| SCC compressed | [-0.14, -2.94, 23.0] | 18.7, 19.9, 12.4 | m |
| SCC extended | [-1.61, -9.14, 67.24] | 60.1, 59.2, 11.9 | m |

**Table 6.9:** Mass properties of the self-climbing crane

## 6.5. Model summary

A sketch of the all system components, including the coordinate system and the conventions for wind and waves that is used, is shown in figure 6.19. To model different stages of the operation, the hoist wire length, crane slew angle and position of the vessel are varied.

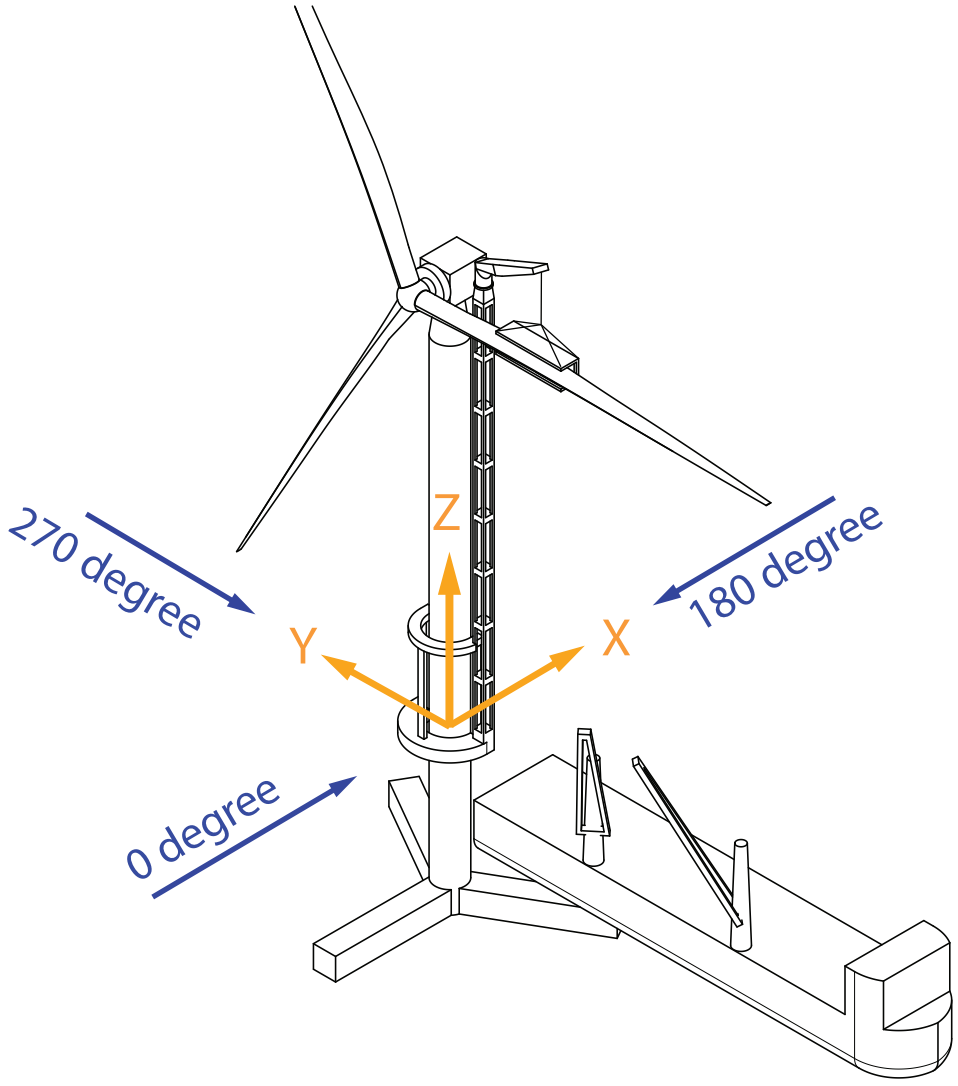


**Figure 6.19:** Sketch of all components in the model, with the appropriate coordinate system and wave and wind directions

The floater, turbine, support vessel and OSCC are modeled in the dynamic analysis software packages OrcaFlex and LiftDyn, which are described in more detail in subsection 5.2.3. Due to differences in the available modeling options, there are some differences between the models in OrcaFlex and LiftDyn. LiftDyn does not allow for modeling of beam elements. To accurately model the natural period of the TLP in roll and pitch and its influence on the response in LiftDyn, the tendon stiffness was changed to obtain a similar response in roll and pitch as the OrcaFlex models. A verification of the adjusted frequency domain model and time domain model is given in appendix C, where the horizontal

displacement of the RNA is studied for both models. Furthermore, a small amount of damping is added to the line-up tool in OrcaFlex, as otherwise the blade would experience undamped oscillations. In reality, this damping could come from friction in the line-up tool connection. A sensitivity study on the damping values is given in appendix C, and around 1.15 % of critical damping is added to the model. The differences between the LiftDyn and OrcaFlex models are summed up in table 6.10.

**Table 6.10:** Differences in LiftDyn and OrcaFlex models

| | ***LiftDyn*** | ***OrcaFlex*** |
|---|---|---|
| Dynamic solution method | Frequency domain | Time domain with modal analysis |
| Tower | Rigid body | Beam element with bending and torsional stiffness<br>Connections to the lattice |
| Tendons | EA = 4.1 GN<br>*To compensate for rigid tower* | EA = 12 GN |
| Lattice | Rigid body | Beam element with bending and torsional stiffness |
| Hydrodynamics | Potential theory | Potential theory and Morison elements |
| Environmental conditions | Wave only | Wind and waves |

To obtain the dynamic response of the system, wind and wave loads are applied to the system. Wind loads are applied to the blade through the BEM methodology, and to the tower, rotor, RNA and OSCC in the form of aerodynamic drag. A summary of all the loads applied to the system is given in table 6.11. The drag coefficient on the tower is obtained from the verified Orcina model of a 15 MW turbine [32], and this drag coefficient is also applied to the RNA and crane boom for simplicity. The drag coefficient on the lattice is taken to be equal to 1.8, in accordance with wind-tunnel tests on lattice structures [16]. To model drag on the rotor, the load that was found on a single blade through the BEM methodology was used. This load is multiplied by the number of blades in the rotor to find the total drag, and a drag coefficient and area are applied that correspond with that load. An off-center center of volume is applied to the case of a 2-blade rotor, so the eccentric drag load on the tower is accounted for.

**Table 6.11:** Loads applied to components in the model

| ***Component*** | ***LiftDyn*** | ***OrcaFlex*** |
|---|---|---|
| TLP | Hydrodynamic load - Potential theory | Hydrodynamic load - Potential theory<br>Hydrodynamic load - Morison elements |
| Vessel | Hydrodynamic load - Potential theory | Hydrodynamic load - Potential theory |
| Tower | - | Aerodynamic drag<br>$C_D = 1.2$, A = 1176 m$^2$ |
| RNA | - | Aerodynamic drag<br>$C_D = 1.2$, A = 100 m$^2$ |
| Crane boom | - | Aerodynamic drag<br>$C_D = 1.2$, A = 77 m$^2$ |
| Lattice | - | Aerodynamic drag<br>$C_D = 1.8$, A = 182 m$^2$ |
| Rotor 3 blades | - | Aerodynamic drag<br>$C_D = 1$, A = 115 m$^2$ |
| Rotor 2 blades | - | Aerodynamic drag<br>$C_D = 1$, A = 77 m$^2$<br>Center of volume: [0, -23.9, 0] |

# Part III

# Research

# 7

# Static and dynamic behaviour of the loaded TLP

In this chapter, the effect of the OSCC on a Tension-Leg Platform is examined. Its influence on the tendon tension and natural frequencies of the system is addressed. The tendon tension is assessed to find the minimum tension in a tendon under the load of the OSCC. The influence of the OSCC on the natural frequencies of a TLP is researched to find its influence on the dynamics of the system. These are then analyzed in order to study the occurrence of snap loads in the tendons, which occur when the tension in a tendon reduces to zero.

## 7.1. OSCC orientation

The orientation of the OSCC on the floater influences the distribution of the tension in the tendons. When the center of mass of the OSCC is placed above a pontoon of the TLP, the other tendons provide the restoring moment, and minimum tension is observed in the pontoon above which the center of mass is placed. In order to prevent snap loads, a good distribution of the tension in the tendons is preferred, which will lead to a higher minimum tendon tension. To quantify this effect, the orientation of the OSCC on the TLP is varied. Two orientation angles can be defined, the slew angle of the crane and the orientation of the base of the OSCC with respect to the floater.

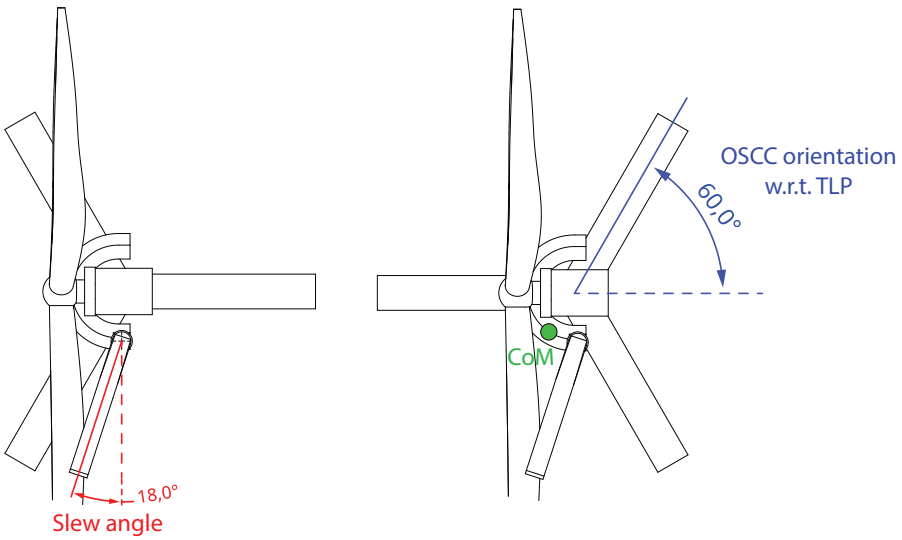


**Figure 7.1:** Definition of crane slew angle and OSCC orientation and the location of the CoM of the OSCC

The tension in the tendons is computed for the case of the extended OSCC with a blade and a yoke being lifted by the crane, as this will result in the highest overturning moment on the TLP. The mass of

the crane is not equally distributed, and its center of gravity is not at the centerline of the base. This will result in an overturning moment on the crane and floater. Its relevant mass properties are given in table 6.9.

The statics are computed with the static solvers of AGES and OrcaFlex, and the results are cross referenced between the two to check their validity. In figure 7.2, the minimum tension in all tendons is plotted for varying orientations of the OSCC, with two slew angles. It can be seen that the highest minimum tension is reached for an orientation of the OSCC of 60 degrees, where its center of mass lies in between two tendons. The uneven distribution between the tension in the tendons leads to an offset in pitch and roll of the TLP. The effect of the orientation of the OSCC on the pitch and roll of the TLP is shown in figure 7.3. The angular offset of the TLP is also at a minimum at the orientation of the OSCC for which the tension is most distributed over all tendons. It is therefore favourable to place the OSCC on the TLP in a specific orientation, at 60 degrees. From the geometry of the TLP, it can be deduced that this leaves three possible OSCC orientations. This limits the possibilities of weathervaning, and environmental loads should be assessed from multiple directions.

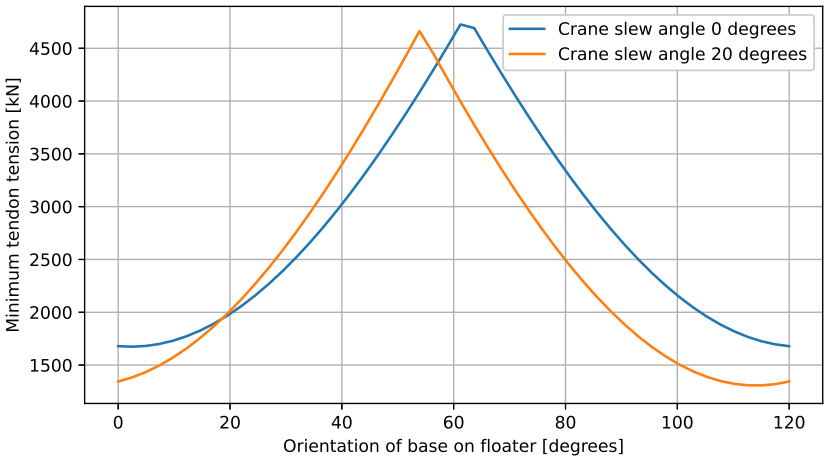


**Figure 7.2:** Minimum tendon tension for different orientations of the OSCC

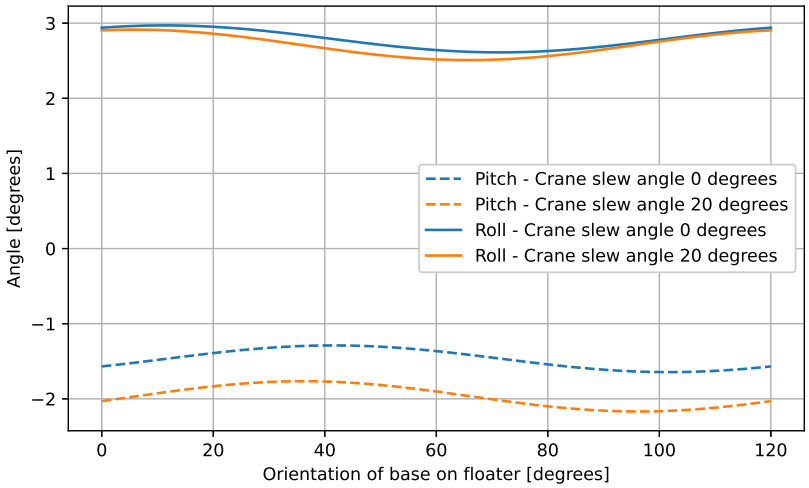


**Figure 7.3:** Roll and pitch of the TLP for different orientations of the OSCC

## 7.2. Statics of a loaded TLP

To understand the static behaviour of the TLP under the load of the OSCC, the tension in each tendon and the rotational displacement of the TLP is studied. The static equilibria of different operational stages of the OSCC are analyzed, from its docking to the lifting of a blade. The displacement of the floater in heave is found to be minimal. The high stiffness of the tendons causes them to deform only slightly under a load, and the TLP therefore does not see a significant displacement in heave. The OSCC mainly influences the tension of the tendons. The resulting tendon tensions are shown in figure 7.4.

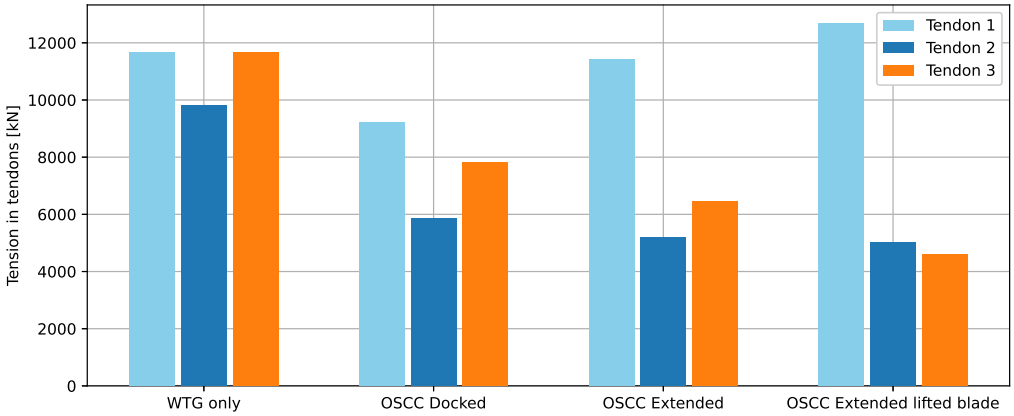


**Figure 7.4:** Static tendon tension for different operational stages of the OSCC

The uneven tendon tension due to the off-center center of gravity of the RNA can be observed in the WTG only loadcase. It can be observed that the average tendon tension is reduced when the OSCC is docked onto the TLP. When the OSCC is in its extended mode and the crane is slewed outward, the center of gravity of the OSCC shifts up and further away from the TLP's centerline. This results in a more uneven distribution of the tendon tension, due to the increased overturning moment from the gravity of the OSCC. When a blade is lifted, this overturning moment increases further. This leads to the minimum static tendon tension that is to be expected during the operation. The tension in the tendon that is affected most, is reduced by 60.5 % when the overturning moment from the weight of the OSCC is at its maximum.

The uneven tension in the tendons translates to a static rotational offset of the TLP. The roll and pitch angle of the TLP under the same operational stages of the OSCC is plotted in figure 7.5. For readability of the figure, the offset in pitch has been shown as the absolute offset, but through the definition of the axis system it should be negative as the turbine pitches forward. It can be seen that there is a small static offset in pitch of the TLP without the OSCC docked, without any roll. This is because the center of gravity of the RNA only has an off-center component in x-direction. Analogously to the uneven tendon tension, the roll and pitch angles increase for an increasing overturning moment of the OSCC. As the center of gravity of the OSCC has the largest off-center component in y-direction, it follows that the largest offset of the floater is in roll.

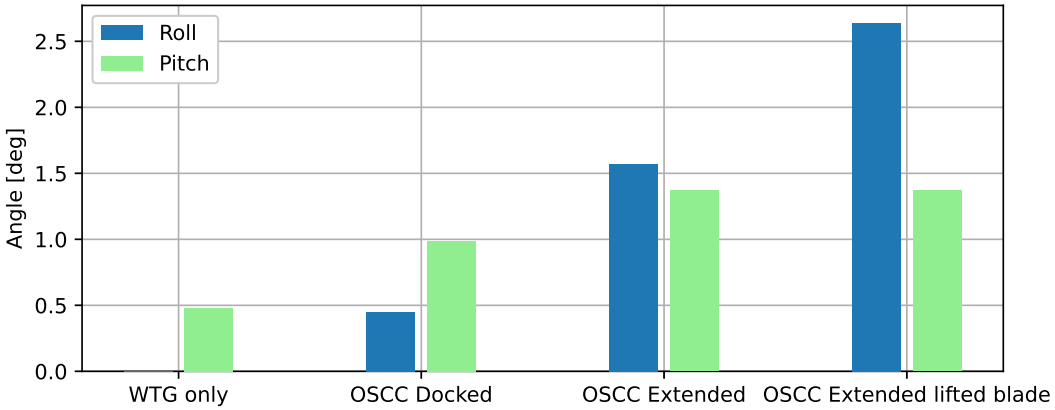


**Figure 7.5:** Static rotational offset of the TLP for different operational stages of the OSCC

## 7.3. Dynamics of a loaded TLP

The OSCC influences the dynamic behaviour of the TLP and WTG. To understand its influence on the natural frequencies of the system, a modal analysis is performed. Next, simulations are performed to assess the possibility of the occurrence of snap loads in the tendons under influence of the OSCC. The analyses are done in OrcaFlex to accurately capture the influence of the TLP's behaviour in roll and pitch through including the tower bending mode.

### 7.3.1. Modal analysis

As mentioned before, it can be proven analytically that the natural frequencies in surge, sway and yaw depend on the tendon tension. The stiffness is proportional to the tension in the tendons. The higher the tension in the tendons, the higher the natural frequencies. It follows that the natural frequencies of these modes will be reduced when the crane is docked. As the natural frequency of a system depends on its stiffness $k$ divided by its mass $m$ or in the case of rotation its moment of inertia $I$, the mass of the crane that is introduced on the floater also lowers the natural frequencies.

$$\omega_{nat} = \sqrt{\frac{k}{m}} \quad \text{or} \quad \omega_{nat} = \sqrt{\frac{k}{I}} \tag{7.1}$$

As a result, the natural frequencies in surge, sway and yaw shift closer to the excitation spectrum of the wind. The floater will therefore be more susceptible to wind loads in these degrees of freedom when the OSCC is docked.

The natural frequencies in roll, pitch and heave will also be lower with the OSCC docked on the TLP. This is due to the extra mass introduced to the system, without any extra stiffness. Furthermore, the coupling between the lattice and the tower through the tower connection influences the natural frequencies in roll and pitch. Because of the tower connections, the lattice moves together with the tower, and their bending modes are coupled. Because the first bending mode of the tower is coupled with the natural frequencies in roll and pitch, the bending stiffness of the lattice also influences the natural frequencies in roll and pitch.

The natural frequency of the tower and lattice is determined by their bending stiffness and top mass. The natural period of a cantilever beam with a top mass can be derived through modal analysis and shown to be proportional to the square root of the top mass $M$ divided by the bending stiffness $EI$ of the beam [2]:

$$T_{nat} \propto \sqrt{\frac{M}{EI}} \tag{7.2}$$

The bending stiffness of the lattice is relatively low compared to the bending stiffness of the tower, which has an average bending stiffness of 2340 GNm$^2$, compared to 100 GNm$^2$ of the lattice. The lattice has a natural period in combination with the top mass of the crane of 15.0 seconds, compared to 3.75 seconds of the tower. When the tower and lattice are connected, a relatively low amount of stiffness is added to the tower, but the top mass of the crane contributes significantly. Intuitively, the connection of the tower and lattice leads to an increase of the natural period of the tower bending mode, and therefore an increase of the roll and pitch natural period of the TLP.

The effect of the bending stiffness of the lattice on the natural period of the system in roll and pitch is shown in figure 7.6. The top mass of the crane and the mass of the lattice are kept constant. Trough the coupling of the bending mode of the tower and the roll and pitch natural frequency, the natural period of the two modes should roughly follow the relation $T_{nat} \propto \sqrt{\frac{1}{EI}}$, in accordance with equation 7.2. It can be seen that the natural period of the system does indeed decrease with an increased bending stiffness of the lattice in a non-linear manner.

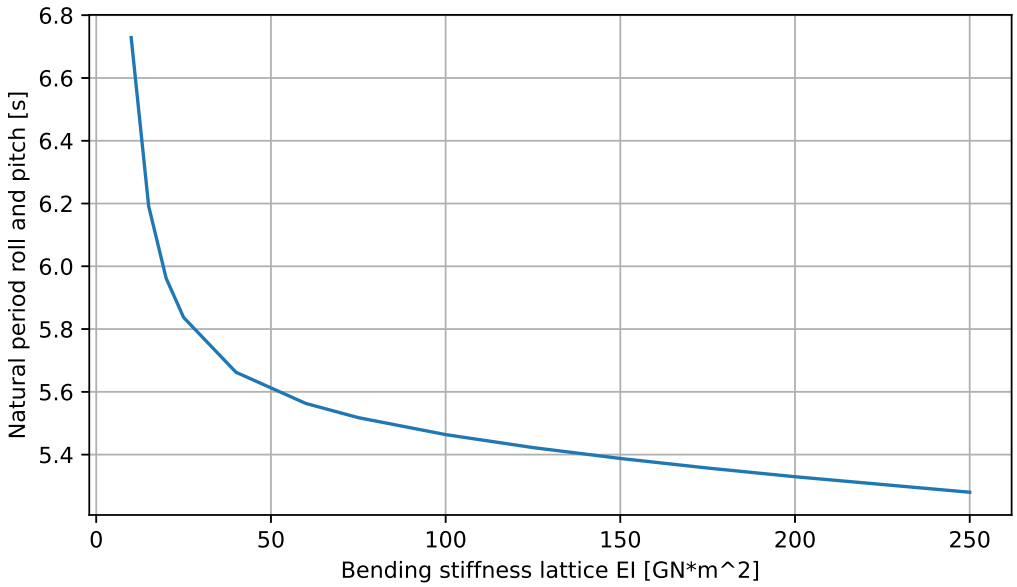


**Figure 7.6:** Natural period of the system in roll and pitch for a varying bending stiffness of the OSCC's lattice

As the natural period in bending also depends on the top mass of the structure, the influence of the crane mass on the natural period of the TLP is also studied. The lattice stiffness is kept constant at 100 GNm$^2$. From equation 7.2, it follows that the natural period of the lattice itself increases proportional to the square root of the crane mass, $T_{nat} \propto \sqrt{M}$. However, it can be seen in figure 7.7 that the natural period in roll and pitch increases linearly with the top mass. This shows that the top mass of the crane not only affects the natural bending period of the lattice and tower, but also increases the moment of inertia of the system which leads to a higher natural period, which explains the linear influence of the top mass on the natural period in roll and pitch.

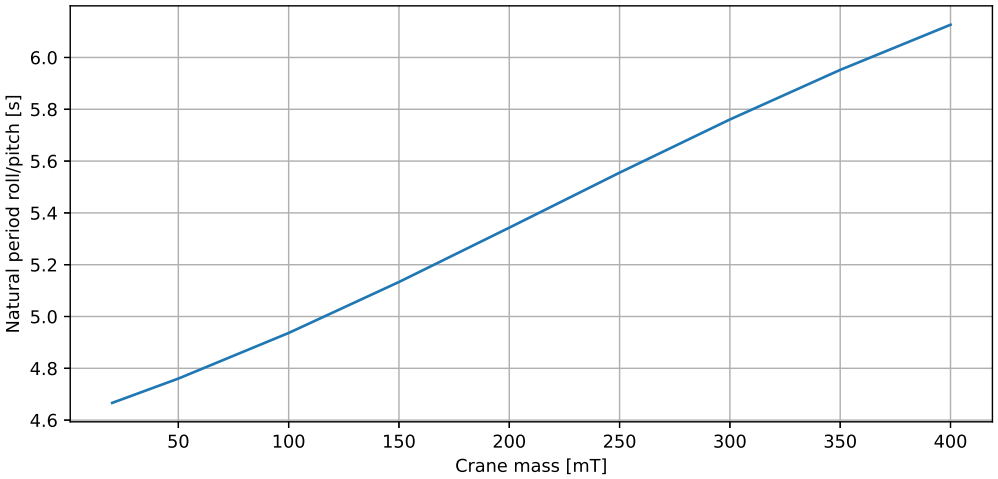


**Figure 7.7:** Natural period of the system in roll and pitch for a varying top mass of the OSCC's crane

The influence of the OSCC on all natural frequencies of the TLP is shown in figure 7.8. The natural frequencies in surge, sway and yaw are lowered through the reduction in tendon tension and the increase in mass of the system, and shift closer towards wind excitation frequencies. The natural frequency in roll and pitch is lowered because of the connection between the lattice and the tower and the increase in mass of the system, and is shifted closer to wave excitation frequencies. The natural frequency in heave is also lowered because of the increase in mass of the system, but is still far away from environmental excitation spectra.

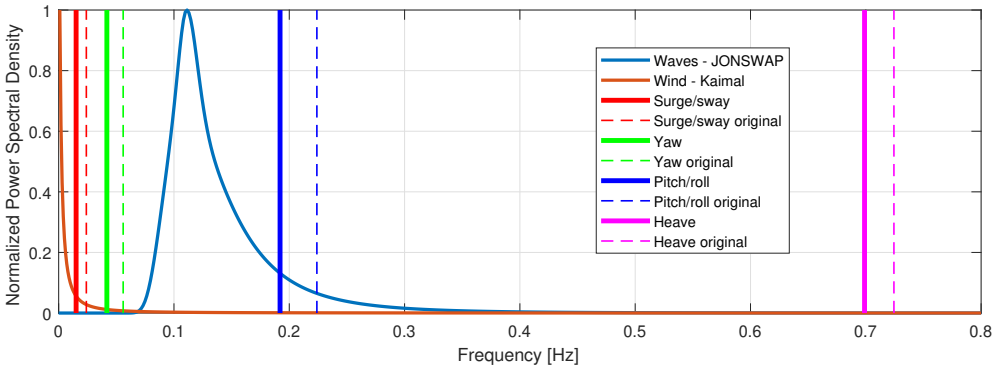


**Figure 7.8:** Results of the modal analysis of the TLP and WTG with the OSCC

The shift of the natural frequency in roll and pitch towards wave excitation frequencies, reduces the effect of sum-frequency forces on the response in this mode. As the frequency is excited more by first order wave loads, the relative contribution of sum-frequency loads will be less. Furthermore, sum-frequency effects are more apparent at higher frequencies, which will also reduce the absolute effect of sum-frequency loads on the roll and pitch motion. As the TLP's stiffness in surge has been reduced by the OSCC, it will become more susceptible to difference-frequency and low-frequent wave drift forces. It should be noted that this is not captured in the results since first order potential theory is used.

## 7.4. Snap loads

The tendons of a TLP are subject to oscillations in tension, due to movement of the platform. A snap load occurs when tension is applied instantly to an untensioned tendon due to oscillations of the TLP. It can therefore be said that a snap load occurs when the tension in a tendon drops to zero. A snap

load results in shock on the line material and considerably reduce the fatigue life of a tendon [17]. They should therefore be avoided for any operational stage of the OSCC. Since the tension in the tendons is reduced by the OSCC, it follows that there is a higher likelihood for snap loads with the OSCC docked onto the turbine.

Simulations of sea states with varying combinations of peak period and wave height are performed, taking into account the wave breaking limit. Since wind leads to an offset of the TLP off its equilibrium position, it increases the tension in the tendons due to their restoring force. Therefore, no wind is simulated in order to assess the scenario with minimal tendon tension.

### 7.4.1. Parked WTG

As a base case, the parked WTG on the TLP is assessed. Figure 7.9 shows the PSD of the TLP in pitch. It can be seen that the wave spectrum is represented, as well as a peak at its natural frequency. Figure 7.10 shows the PSD of tension in a tendon. The peak lies at the natural frequency in roll and pitch of the system. The roll and pitch modes of the TLP directly stretch the tendons and are in the range of wave frequencies, and therefore they have a large influence on the tendon tension.

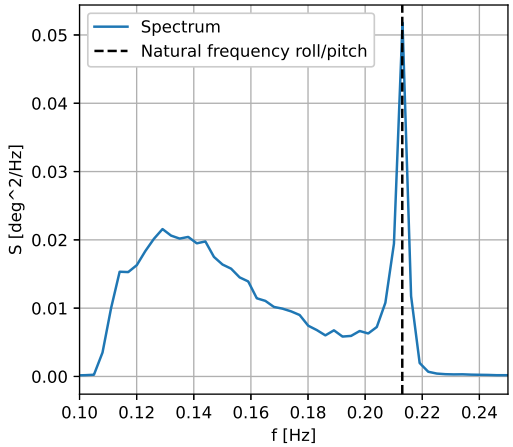


**Figure 7.9:** PSD plot of the TLP's pitch

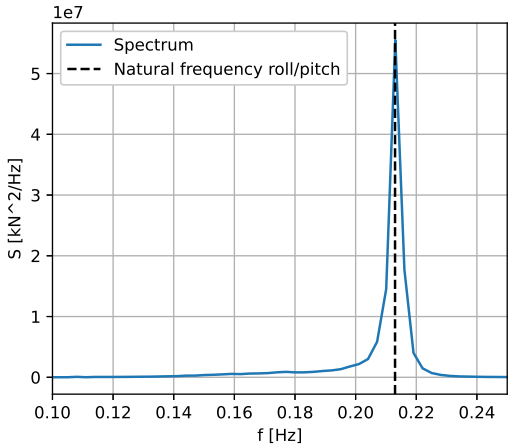


**Figure 7.10:** PSD plot of the tendon tension

To assess the possibility of snap loads, a three hour most probable minimum of the tendon tension has been taken trough the standard deviation of three-hour time-domain simulations, as this is the reference period of the operational stages for which the minimum tendon tension is computed. The results are plotted in figure 7.11. It can be seen that the tendon tension has a minimum around its natural period in roll and pitch, which is in line with the previous results. There is an increasing trend in the minimum tendon tension for periods higher than the roll and pitch natural period.

Some peaks in can be observed in the minimum tendon tension at peak periods higher than 8.5 seconds. From the spectral density graphs of the tendon tension from these simulations, it was seen that it is still the roll and pitch mode that causes the most oscillations in the tendon tension. The peaks are caused by a transient response of the tower to displacements caused by the TLP. The amount of damping for this mode is small, as there is little hydrodynamic and structural damping, and no aerodynamic damping due to the fact that the rotor is not operational. The transient oscillations of the tower bending mode are damped out very slowly, causing the tower to oscillate continuously. As the tower bending mode is coupled with the roll and pitch mode of the TLP, which has a large influence on the tendon tensions, the transient excitations of the tower cause a peak in the tendon tensions. The transient response has more effect on the tendon tension for higher wave periods, as there is more time in between waves which means there is more time for transient oscillations of the tower.

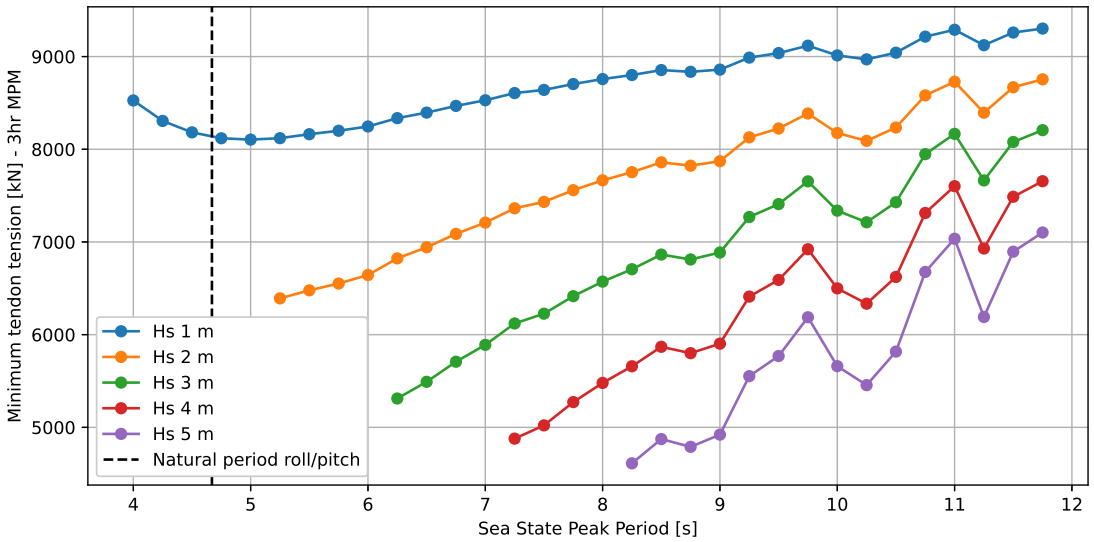


**Figure 7.11:** Three-hour most probable minimum tendon tension under different sea states during the parked condition of the WTG, without the crane

### 7.4.2. Operational OSCC

To analyse the occurrence of snap loads when the OSCC is docked and operational, the in-place condition of the OSCC is simulated when it is performing blade installation. As the OSCC is loaded with a blade and a yoke, the overturning moment on the WTG is at its maximum for this loadcase. This will lead to the most uneven distribution of the tension between the tendons and therefore the lowest equilibrium tendon tension during the operation, so this case is simulated.

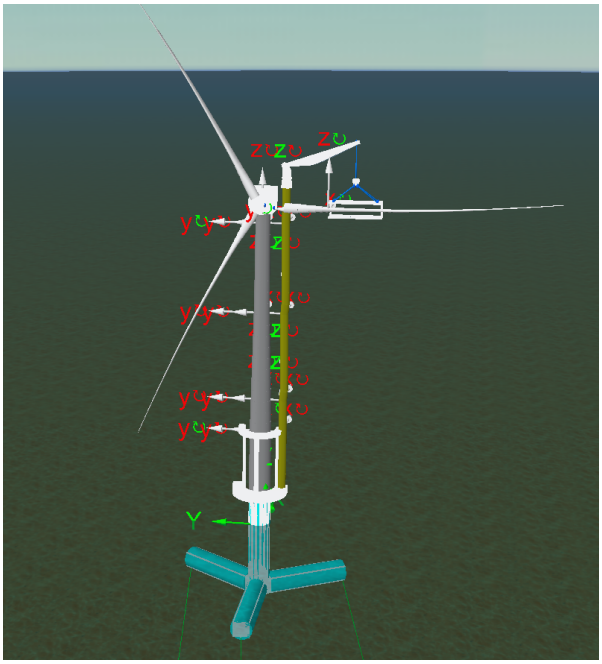

**Figure 7.12:** OrcaFlex model of the blade installation, for which the minimum tendon tensions are computed

The results of the simulations are plotted in figure 7.13. It can be seen that the natural period in roll and pitch has shifted to a higher period. Similar to the case of the parked WTG, the minimum tendon tension occurs for sea states with a peak period around the natural period in roll and pitch. Snap loads can occur for sea states with a significant wave height of 2.5 meters, and a peak period close to the

natural period in roll and pitch. It can be seen that due to the increase in natural period in roll and pitch, sea states with a higher peak period have more influence on the tendon tension as compared to the case of the WTG only.

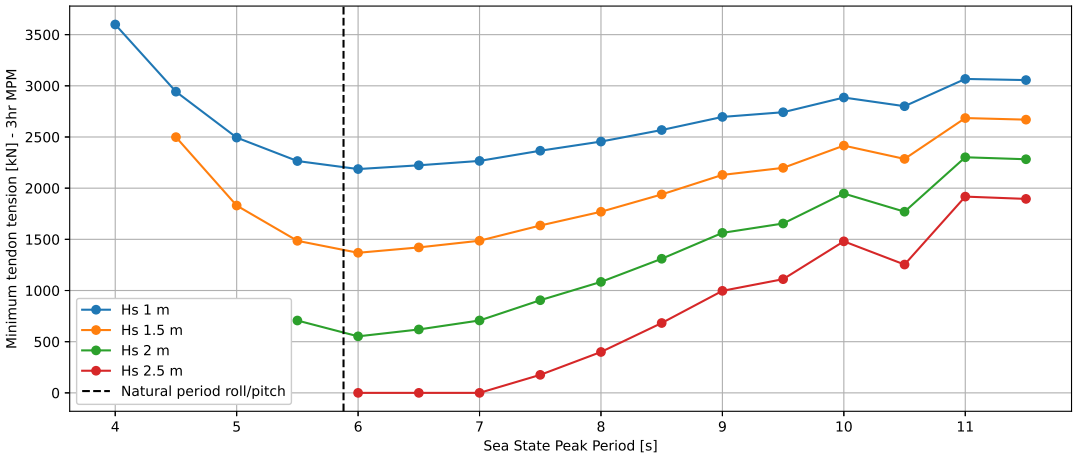


**Figure 7.13:** Three-hour most probable minimum tendon tension under different environmental conditions during blade lifting

# 8

# Response assessment of the operational sequence

In this chapter, the response of the system dynamics during the critical stages highlighted in chapter 4 is studied. The effect of two tugger line configurations during the installation of the OSCC is shown, and the influence of the design choice of the position of the line-up tool is assessed. The response is first studied based on the wave-induced RAOs that are obtained through frequency domain analysis in LiftDyn. Next, the response of the blade while it is lifted is studied further through time-domain simulations in OrcaFlex, where wind loads are included.

## 8.1. OSCC installation

For reference, the points of interest on the OSCC and the TLP between which the relative motion has been assessed are shown in figure 8.1. The global axis system is given in which the RAOs are computed. The yaw motion of the OSCC around the global Z-axis is assumed to be relatively small and less critical than the other rotational and translational motions with respect to the TLP, because the yaw motion of the vessel is controlled by its DP system. Constraints have been added to the crane blocks which prevent rotation about the Z-axis, as this otherwise leads to an unconstrained rotation. Therefore the global Z-rotation of the OSCC is left out of the RAOs. In reality, the yawing motion of the OSCC could be limited by taglines attached to the OSCC and controlled from the vessel, and the use of two lifting points on the OSCC also adds some stiffness in yaw.

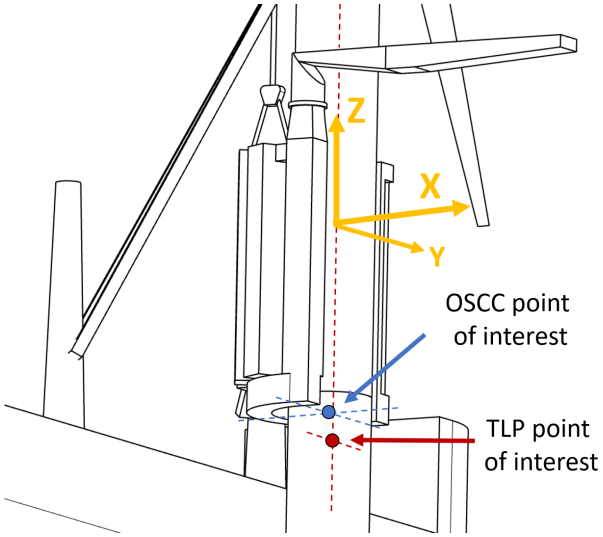


**Figure 8.1:** The points of interest between which the RAOs are computed

The RAOs of the OSCC's motions with respect to its docking point on the TLP in the global axis system are shown in figure 8.2. It can be seen that the motions of the TLP have little influence on the RAOs, compared to the vessel's motions. Only a small peak around the roll and pitch natural periods of the TLP is visible. Most of the response is caused by coupling of the pendulum motion of the OSCC to vessel motions. Second pendulum motions, due to the rigging present between the OSCC and the crane tips, also cause a peak in the response. Second pendulum motions occur when the hoist cables above the crane block are oscillating in opposite phase of the hoist cables below the crane block, and have a higher frequency of oscillation than the normal pendulum motion.

The highest peak in the RAOs is observed in the global X-motion at a wave heading of 0 degrees, which is caused by the excitation of the pendulum motion of the OSCC by the vessel's roll motion. Furthermore, the vessel's pitch motions excite the pendulum motions of the OSCC in global Y-direction. Less rotational motion is seen in this case, since both lifting points give stiffness in this direction and prevent the OSCC from rotating. The pendulum motion also has a lower natural period because the stiffness in this direction is different than in global X-direction. It can be seen that the natural period of the second pendulum is higher than in X-direction. This causes it to be excited by the vessel's pitch motion, and the largest translational response in Y-direction can be seen at its natural period.

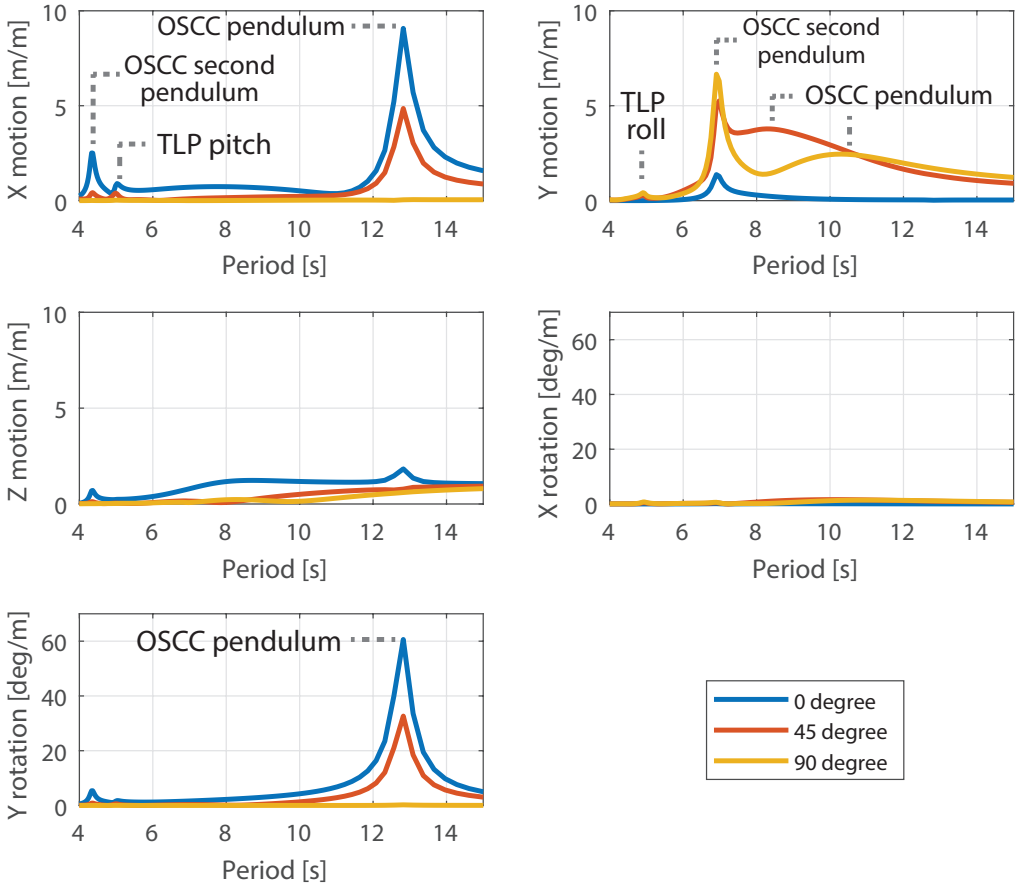


**Figure 8.2:** RAO of motions between the OSCC and TLP during installation

The effect of adding tugger lines to the OSCC to limit its motions during lifting is studied. The tugger lines are modeled as dampers with a damping coefficient of 15 mT*s, and are attached to the bottom of the OSCC as the displacement caused by pendulum motions will be the largest there. Two tugger line configurations are examined, where the tugger lines are attached either at the vessel cranes or at the deck of the vessel. The tugger line configurations are angled differently, and will therefore either mostly compensate global X-motion or global Y-motion. In configuration 1 the tugger lines make an angle to the global X-axis of 48 degrees, and in configuration 2 the lines make an angle to the global Y-axis of 8.5 degrees.

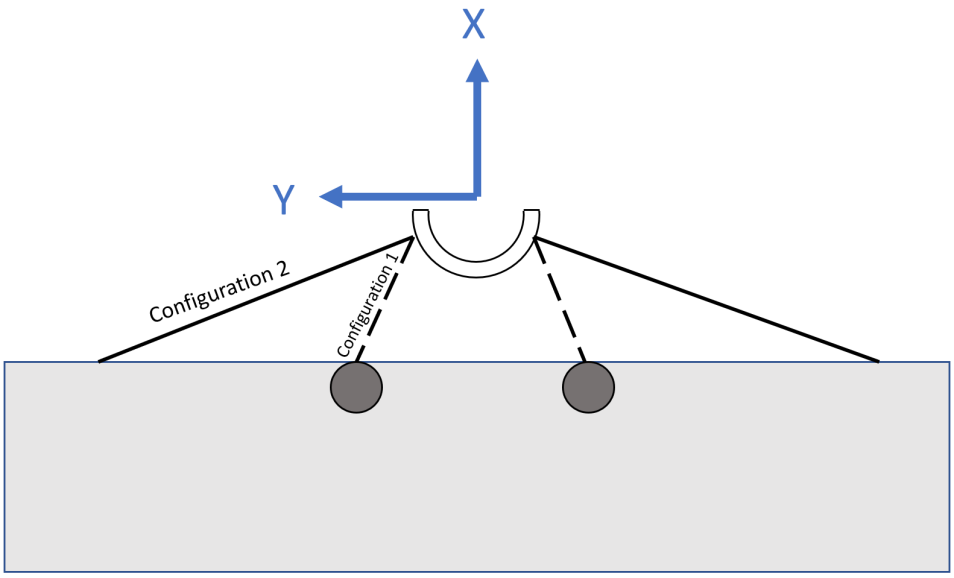


**Figure 8.3:** Modeled configurations of the tugger lines

The results of using tugger lines in the abovementioned configurations on the RAOs between the OSCC and TLP are plotted in figure 8.4 for a wave heading of 0 degrees, and in figure 8.5 for a wave heading of 90 degrees. Tugger line configuration 2 damps out motion in Y-direction, but causes an increase in motion in X-direction. Because of the angle in the tugger lines, the OSCC is also excited in X-direction even when the vessel is not excited in X-direction, as can be seen in figure 8.5. Tugger line configuration 1 damps out motion in X-direction when waves are coming into the beam of the vessel, but causes a slight increase in Y-motion when waves are coming into the bow of the vessel.

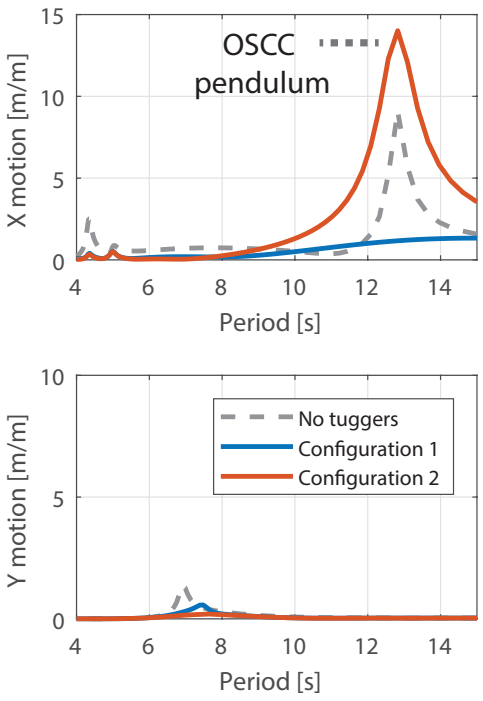


**Figure 8.4:** Influence of tugger line configurations on the response for a 0 degree wave heading

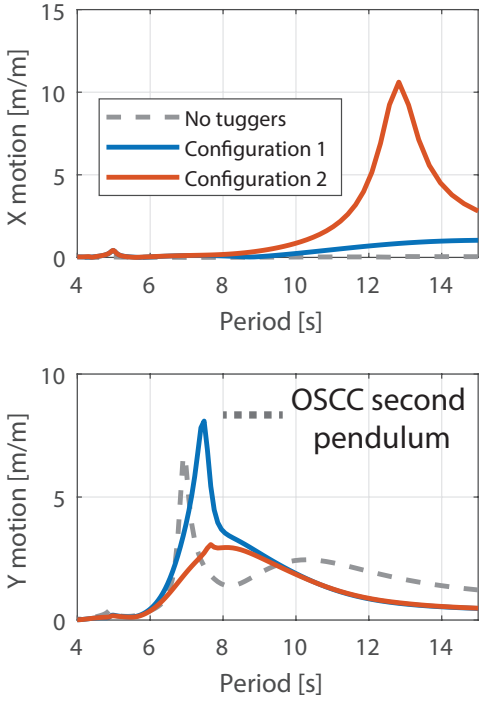


**Figure 8.5:** Influence of tugger line configurations on the response for a 90 degree wave heading

## 8.2. Blade removal

The operability of the decommissioning of the old blade is determined by the yoke attachment and blade setdown on the vessel. The wave-induced response of both steps is computed in the following subsections.

### 8.2.1. Yoke attachment

The RAOs of the free-hanging yoke with respect to the lift point on the blade are shown in figure 8.6. The yaw mode of the crane block is constrained artificially in the model, as there is no stiffness in this degree of freedom. It is therefore not included in the RAOs. The yoke is excited by crane tip displacements caused by roll and pitch motions of the TLP. The natural period of its inverse pendulum motion due to its rigging lies close to the roll and pitch natural periods of the TLP, which causes this mode to be excited. A peak can also be seen at the pendulum motion of the yoke. The distance between the crane tip and the center of mass of the yoke is 33 meters, which corresponds with a natural pendulum period of around 11.5 seconds. There is less motion of the TLP at this wave period, so it is excited less than the inverse pendulum.

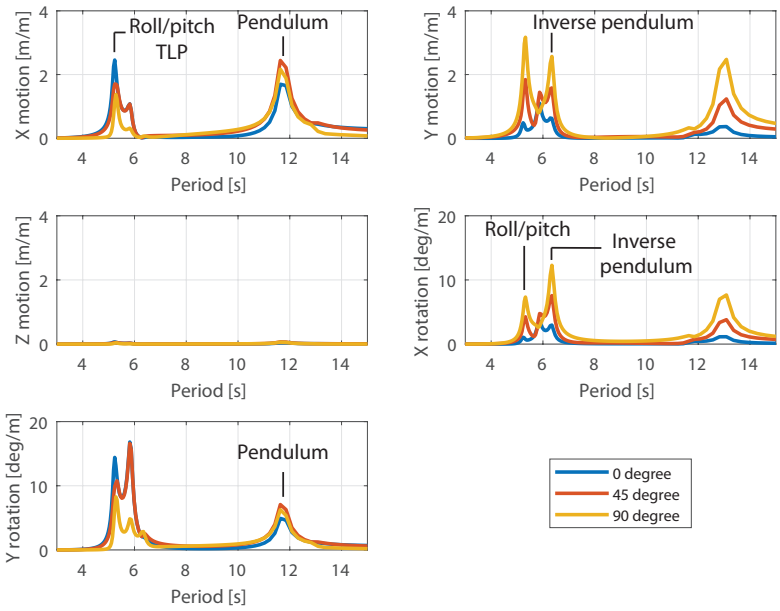


**Figure 8.6:** RAOs of the free hanging yoke with respect to the blade it is attached to

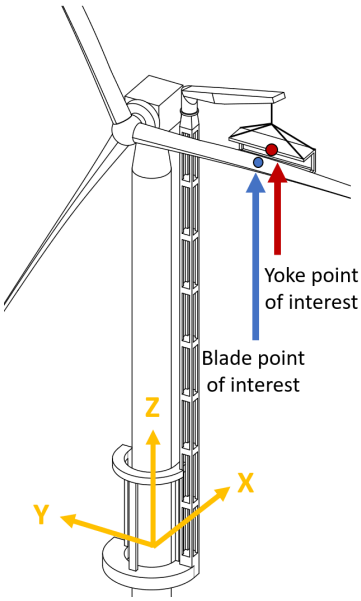


**Figure 8.7:** Points of interest between which the RAOs are computed

### 8.2.2. Blade setdown

The RAOs of the center of gravity of the free hanging blade with respect to its setdown point on the vessel are shown in figure 8.8. Again, the yaw mode of the crane block is constrained artificially in the model, so it is not included in the RAOs. It can be seen that at wave periods, most of the response comes from the vessel. Roll of the vessel causes a peak in X-motion when waves are coming in from the side of the vessel, but for bow and beam seas this effect is little. Vertical motion between the blade and its setdown point are caused by heave and pitch of the vessel, depending on the incoming wave heading. For a wave heading of 90 degrees, the least response of the vessel relative to the blade can be observed.

The inverse pendulum motions of the blade are excited by crane tip displacements resulting from roll and pitch motions of the TLP. The natural period of the first pendulum motion of the blade is high due to the long hoist cable, and lies outside of normal wave periods. It is therefore not present in the wave-induced RAOs.

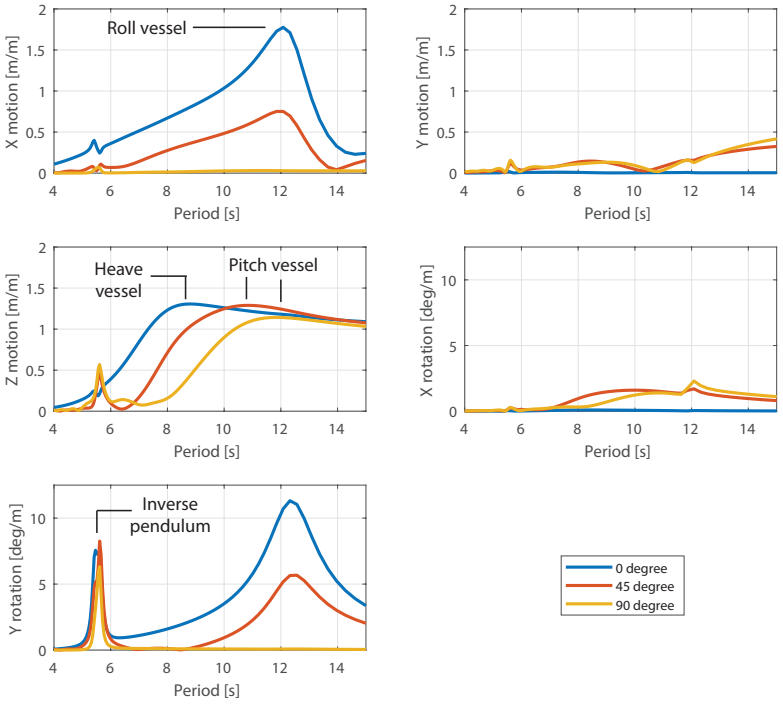


**Figure 8.8:** RAOs of the center of gravity of the blade with respect to its setdown point on the vessel

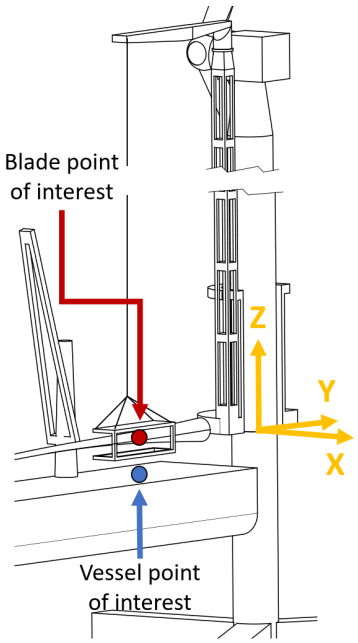


**Figure 8.9:** Points of interest between which the RAOs are computed

## 8.3. Blade installation

The RAOs of the blade root with respect to the hub during installation are shown in figure 8.10. The blade is free-hanging and the crane block is artificially constrained in yaw. The blade is excited through roll and pitch motions of the TLP, which induce the inverse pendulum motion of the blade. There is also a peak in response at the natural pendulum period of the blade. This natural period is slightly different in X and Y-direction, due to the different inertia properties of the yoke and blade in these directions.

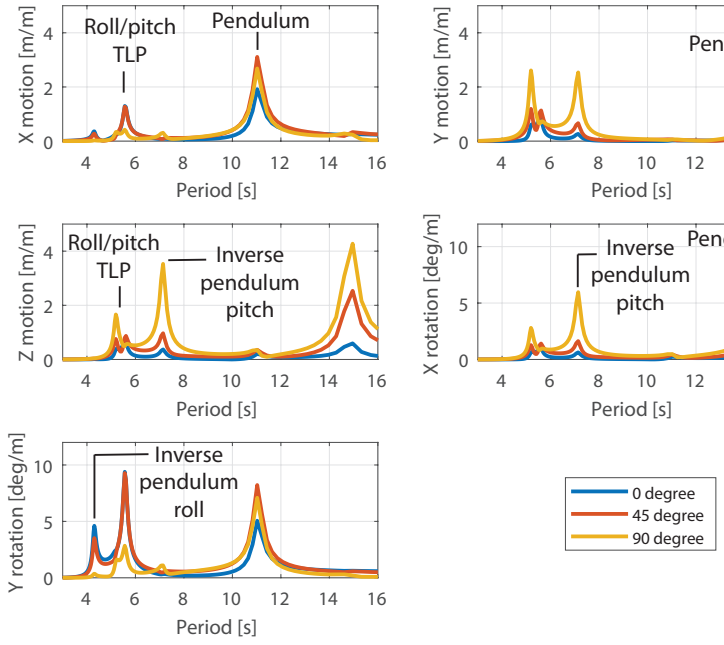


**Figure 8.10:** RAOs of the free hanging blade root with respect to the hub

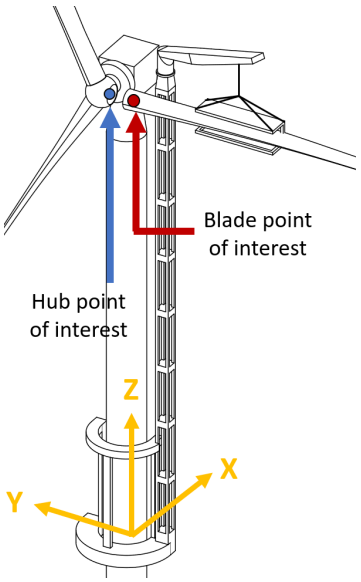


**Figure 8.11:** Points of interest between which the RAOs are computed

## 8.4. Influence of the line-up tool

Placing a line-up tool at the blade root or at the yoke alters the motion characteristics of the blade. The line-up tool creates a point of rotation on the blade, which changes the free pendulum mode to a yawing motion, as seen in figure 8.12. Due to the presence of the rigging between the yoke and the crane tip, an inverse yaw motion is also possible, analogously to an inverse pendulum motion.

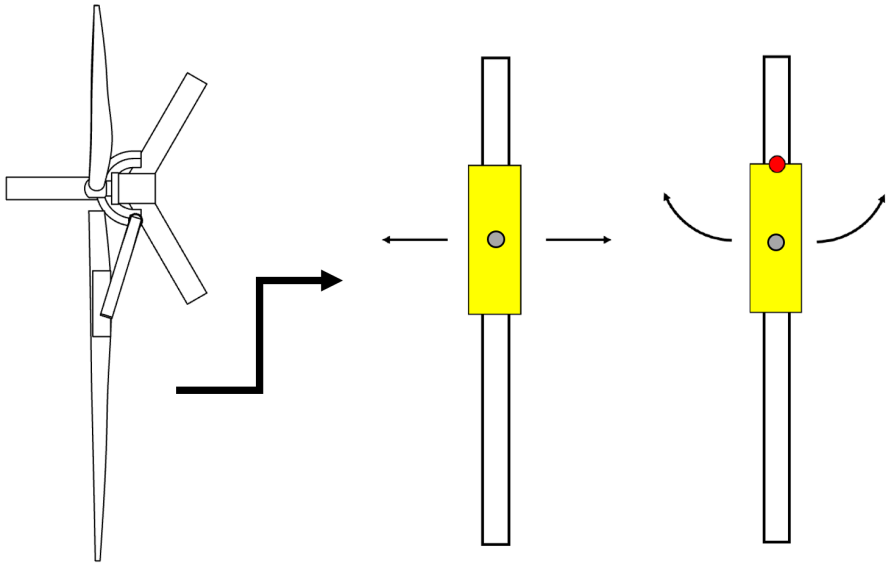

**Figure 8.12:** Pendulum motion of the blade or yoke that becomes a yawing motion under influence of the line-up tool

### 8.4.1. Stiffness from the line-up tool

To understand the dynamics of the blade when the line-up tool is attached, the stiffness in the yaw degree of freedom of the blade can be studied. A displacement in yaw causes a displacement of the hoisting point, $d_{hoist}$, as can be seen in figure 8.13.

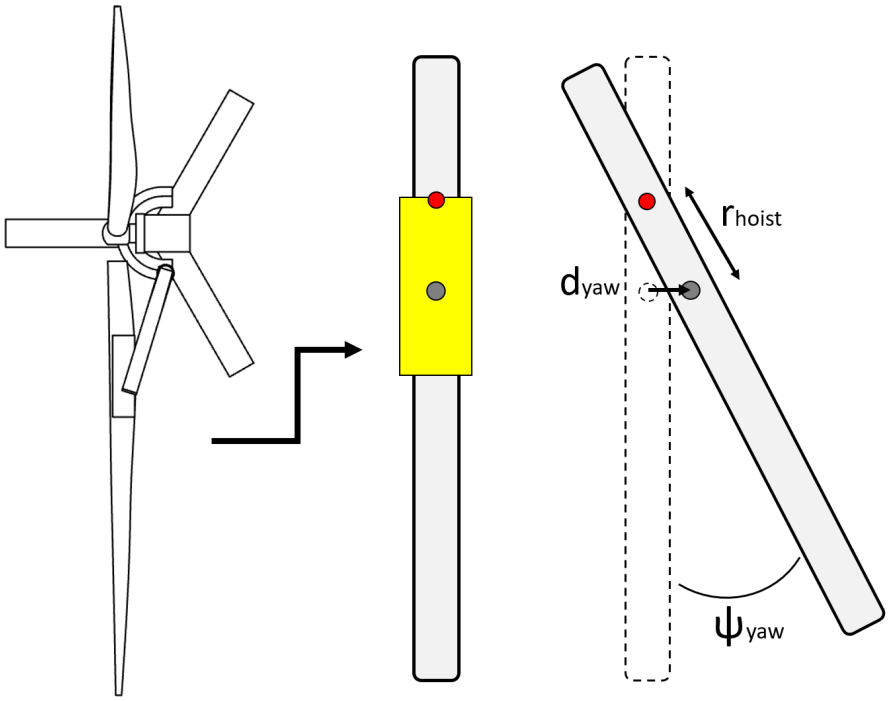


**Figure 8.13:** Displacement of the hoisting point due to a rotation in yaw

This displacement results in an angle in the hoisting cable, $\phi_{hoist}$, as can be seen in figure 8.14. This angle depends on the hoisting cable length, $l_{hoist}$. A horizontal component of the tension in the hoisting cable is created, which increases with the angle in the hoisting cable.

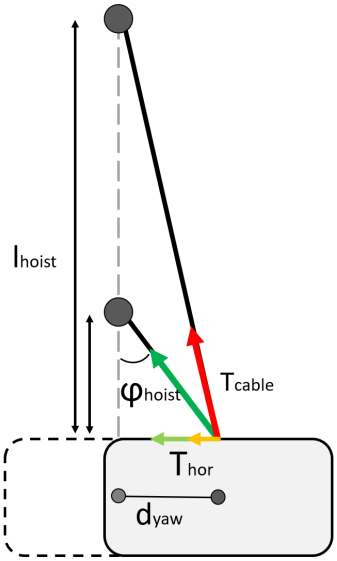


**Figure 8.14:** Horizontal tension component due to a displacement in yaw for different hoist cable lengths

The horizontal component of the tension in the lifting cable causes a restoring moment around the point of rotation in yaw. The magnitude of this moment depends on the distance of the hoisting point to the rotation point of the blade, $r_{hoist}$. The restoring moment in the yaw degree of freedom of the blade can then be expressed as:

$$\begin{aligned} M_{rest} &= r_{hoist} T_{hor} \\ &= r_{hoist} \sin(\phi_{hoist}) T_{cable} \approx r_{hoist} \phi_{hoist} T_{cable} \\ &= r_{hoist} \arctan(\frac{d_{yaw}}{l_{hoist}}) T_{cable} \approx r_{hoist} \frac{d_{yaw}}{l_{hoist}} T_{cable} \\ &= r_{hoist} \frac{\cos(\psi_{yaw}) r_{hoist}}{l_{hoist}} T_{cable} \approx \frac{r_{hoist}^2}{l_{hoist}} \psi_{yaw} T_{cable} \end{aligned} \tag{8.1}$$

As the blade is lifted at its center of mass, the hoisting cable tension is equal for both configurations of the line-up tool. Therefore, the stiffness in yaw is proportional to:

$$k_{yaw} \propto \frac{r_{hoist}^2}{l_{hoist}} \tag{8.2}$$

When the line-up tool attached to the blade root is used, the distance between the hoisting point and the point of rotation is larger than when the line-up tool is attached to the yoke. The line-up tool attached to the blade root will therefore result in a higher stiffness in yaw. When a blade is lifted at hub height, the stiffness in yaw will be higher than when a blade is lifted at deck level of the vessel. The case with the lowest stiffness in yaw is therefore the setdown of a blade at deck level with a line-up tool attached to the yoke.

### 8.4.2. Influence on the response

The influence of the line-up tool on the wave-induced RAOs during yoke attachment is shown in figure 8.15, for an incoming wave heading of 0 degrees. It can be seen that the pendulum motion of the yoke becomes a yawing motion, as the peak is now also visible in the global Z-rotation RAO. The yaw motion also causes a displacement of the yoke with respect to the blade in X-direction, and it can be seen that the yaw motion is coupled with a motion in roll as the peak is also visible in Y-rotation. The natural period of the yaw motion is higher than the pendulum mode of the yoke itself. A small amount excitation of the inverse yaw motion is present, which is excited by roll and pitch of the TLP.

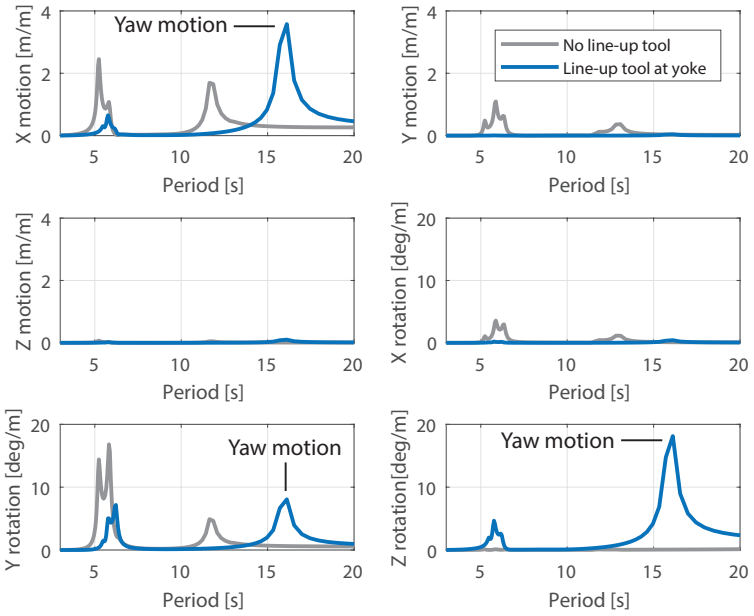


**Figure 8.15:** RAOs of yoke with respect to the blade with and without a line-up tool, for a wave heading of 0 degrees

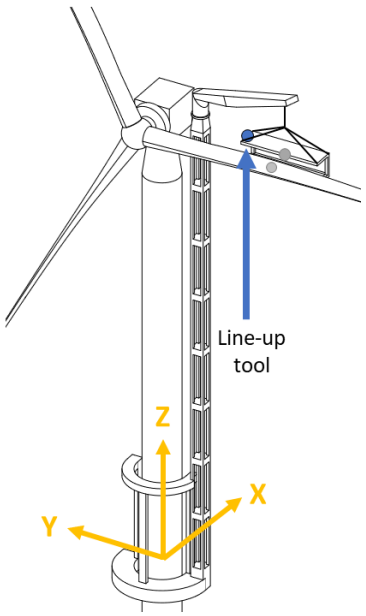


**Figure 8.16:** Placement of the line-up tool

The influence of the line-up tool during blade lifting is exemplified by the case of blade installation. The effect of placing a line-up tool at the blade root or at the yoke on the RAOs of the blade during installation is shown in figure 8.17. As the line-up tool constrains translational motion, there is no translational motion of the blade root with respect to the hub when the line-up tool at the root is used. Rotational motion of the blade root around the global Z-axis increases because of the yaw motion the line-up tool creates. Because this is coupled to a roll motion, the response in Y-rotation also increases. When the line-up tool is placed at the yoke, the yaw motion also causes response in X-direction of the blade root. It can be seen that the line-up tool at the yoke has a lower stiffness, as the natural period of the yawing motion it causes is higher than the line-up tool at the root. This exemplifies the relation given in equation 8.2.

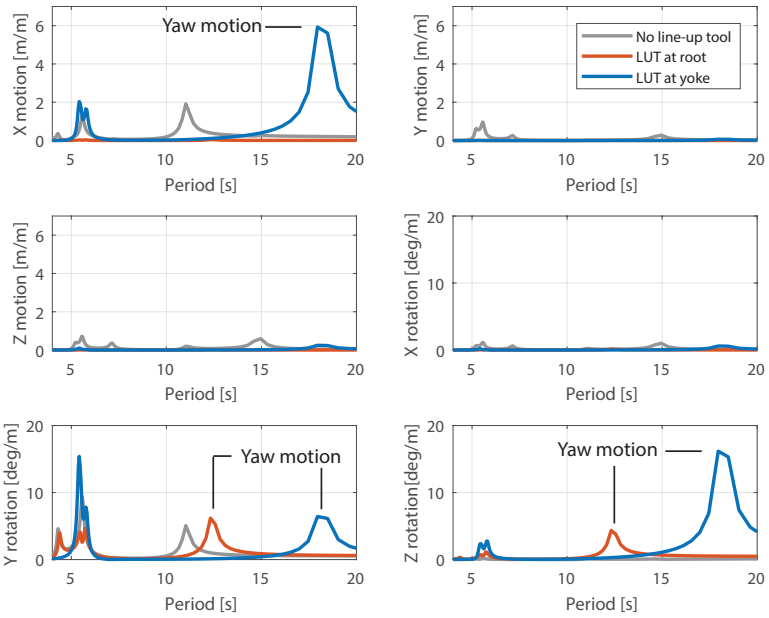


**Figure 8.17:** RAOs of blade root with respect to the hub for the different line-up tool configurations, for a wave heading of 0 degrees

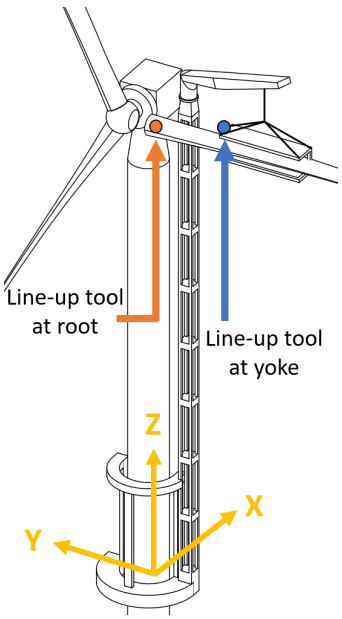


**Figure 8.18:** Placement of the line-up tool

## 8.5. Influence of wind

In the wave-induced RAOs of blade lifting with the line-up tool, it can be seen that the natural period of the yaw motion of the blade is relatively high, for both line-up tools. This is especially true during set-down of the blade, when the hoist cable is long and equation 8.2 shows that the stiffness in yaw will be low. Because the natural period of the yawing mode of the blade is above normal wave periods, it will not influence a frequency domain operability curve. However, high period wind loads will have a large effect on the yaw mode of the blade, as its natural period is high and it is susceptible to aerodynamic loads. Therefore, a more detailed time domain study is required in which aerodynamic loads are taken into account.

The blade is excited through motions of the crane tip. To better understand the motions of the lifted blade, the response of the system at the crane tip can be studied. A PSD of the response of the crane tip under environmental loading is shown in figure 8.19, obtained through time domain simulations of a blade lifting scenario. The peaks of the PSD show which frequencies are contained in the response, and show how much energy is contained in the response at that frequency. Wave induced motions are present, and a peak in response is caused by wave induced pitch motion of the TLP. At low frequencies, peaks in the response can be seen at surge and yaw frequencies of the TLP. These motions are induced by low-frequent wind loads on the WTG and the OSCC. Surge motion of the TLP is caused by aerodynamic drag on the WTG and OSCC. Yaw motion of the TLP is caused by the moment resulting from aerodynamic drag on the off-center components of the OSCC, such as the lattice and the crane, which result in a moment around the TLP which induces yaw. There is a clear distinction between wave and wind induced motions, as it can be seen that above 0.05 Hz there are almost no wind-induced motions, and below 0.075 Hz the motions of the TLP are only induced by wind.

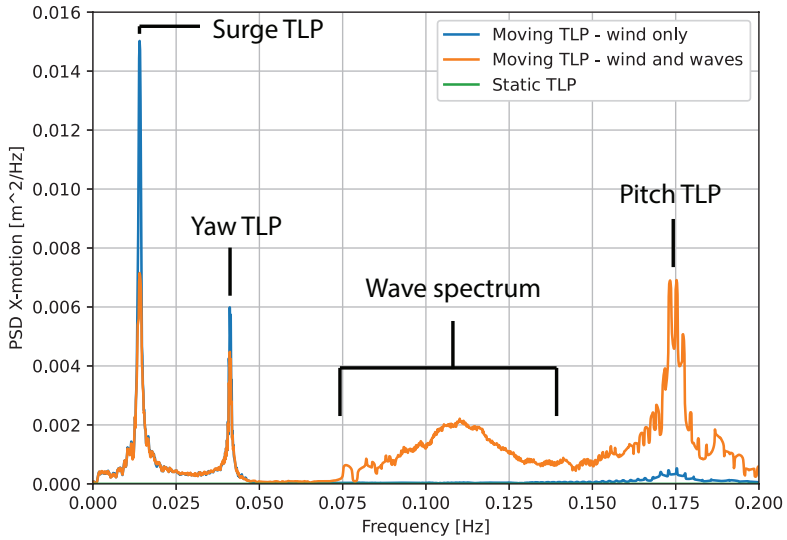


**Figure 8.19:** PSD of the X-motion of the crane tip under environmental loading, for a wind and wave heading of 0 degrees

### 8.5.1. Blade installation

The response of the blade in yaw during installation is studied through time domain simulations, in which wind and wave loads are considered. PSDs of the response with a line-up tool placed at the blade root and at the yoke are shown in figure 8.20a and 8.20b, respectively.

As a base case, the TLP is kept static, while wind loads are applied to the blade. A small peak around the natural period in yaw of the blade can be seen for both line-up tools. Because the blade is installed in a feathered position, the loads on the blade are low and there is little response in this load case.

When wind and wave loads are applied to the system and the TLP is not considered static, the response of the blade follows a similar pattern as the crane tip motions. It can be seen that for the

applied sea state, there is some wave energy contained at frequencies around the natural frequency in yaw of the blade with the line-up tool at the root. This causes a peak in the response at this frequency. Crane tip motions at this frequency excite the blade more than aerodynamic loading on the blade.

The crane tip motions are the same for both line-up tool configurations. The blade is excited more by crane tip motions when the line-up tool is placed at the yoke. This can be seen at pitch frequencies at the TLP, which excite the blade with the line-up tool at the yoke more. This is because the crane tip displacements are closer to the point of rotation when the line-up tool is at the yoke, which causes a larger angular displacement of the blade.

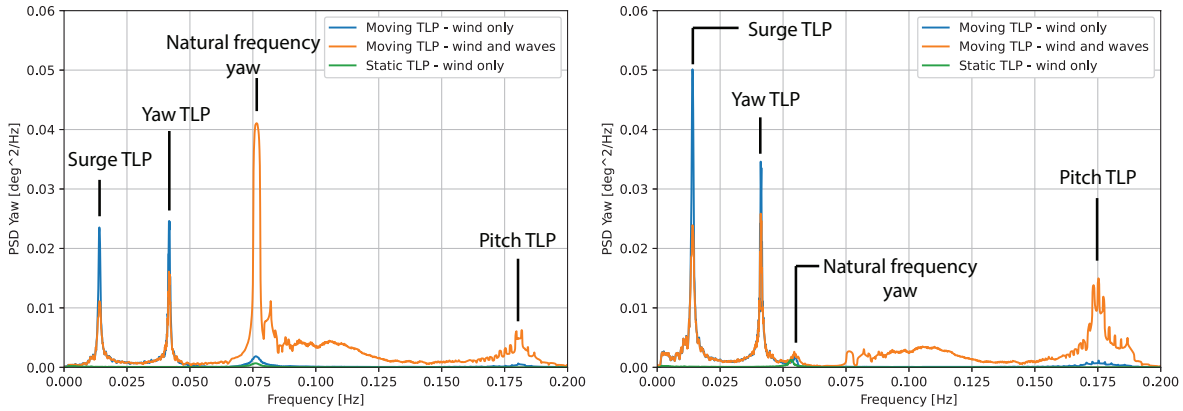


**(a)** Response with the line-up tool at the root

**(b)** Response with the line-up tool at the yoke

**Figure 8.20:** PSD of the response of the lifted blade in yaw under environmental loading during installation

## 8.5.2. Blade setdown

The response of the blade in yaw during setdown on the vessel is shown in figure 8.21. The vessel motions are not included, to be able to more clearly visualize the motion of the blade. It can be seen that the natural frequency in yaw has decreased due to the longer hoist cable. The natural frequency of the blade in yaw falls close to the natural frequency of the TLP in surge, when the line-up tool is placed at the yoke. This causes a large peak in the response of the blade due to resonance, and the response of the blade with the line-up tool at the yoke is larger than with the line-up tool at the root because of this. The response is dominated by wind-induced loads. Low-frequent crane tip displacements have more effect than low-frequent aerodynamic loading on the response of the blade, as can be seen from the relatively small response for a static TLP.

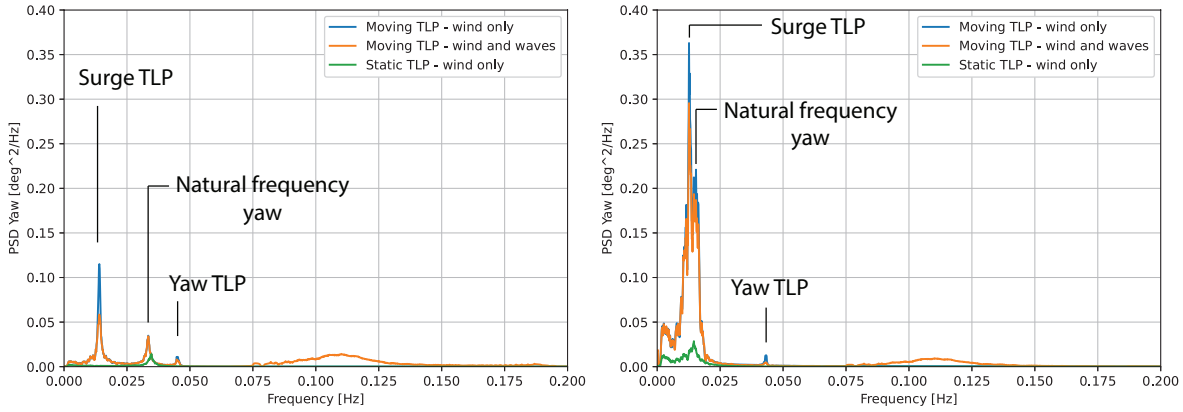


**(a)** Response with the line-up tool at the root

**(b)** Response with the line-up tool at the yoke

**Figure 8.21:** PSD of the response of the lifted blade in yaw under environmental loading during setdown

# 9

# Operability

In this chapter, the operability of the stages addressed in chapter 4 is assessed. The operability of the installation of the OSCC is assessed through frequency domain for waves only, as wave-induced vessel motions dominate the response. The operability of the blade exchange is assessed by the yoke attachment phase, the setdown of the blade on the vessel and blade installation in the hub. Wind and wave induced operability curves are generated of the operational steps in which a blade is lifted to account for its low-frequent response, through time-domain analyses using the IMCA wind-wave relation.

The operability of the blade setdown is assessed by focusing on the motions of the blade only, to get a more clear comparison between both line-up tool configurations. The response of the blade setdown at wave periods is dominated by vessel motions as has been shown through the RAO, and these would dominate the operability curve. As the type of support vessel might change due to operational requirements or constraints, it is deemed more valuable to only assess blade motions in order to get a neutral comparison between both line-up tools.

To limit the response of the lifted blade during the blade exchange, the OSCC can be installed on the TLP in a weathervaned orientation. In chapter 8 it was seen that aerodynamic drag on the OSCC's lattice causes a yaw response of the TLP, which excites the lifted blade. When the wind is coming in from the side of the WTG, this drag load does not cause a moment in yaw, which should decrease the response of the lifted blade. Moreover, this will decrease the aerodynamic loads on the blade itself, which also decreases its response.

As the amount of possible orientations of the OSCC on the TLP is limited due to its effect on the tendon tensions, a range of incoming wind and wave directions should still be considered, since the possibilities of weathervaning are limited. Due to the geometry of the TLP, a range of 60 degrees of incoming environmental load directions is taken into account around the optimal orientation of environmental loading coming from the side of the WTG. Assuming the wind and waves are coming from the same direction, the vessel would ideally install the OSCC with waves incoming to the bow.

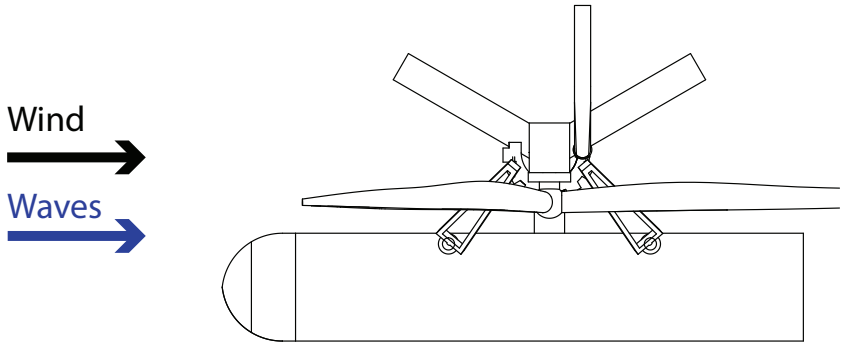


**Figure 9.1:** Orientation of the OSCC and vessel in a weathervaned position

## 9.1. OSCC installation

The operability curves of the installation of the OSCC are given in appendix D for a variety of incoming wave headings and both tugger line configurations. The best operability of the installation is found for a wave heading of 0 degrees and tugger line configuration 1, which corresponds to waves incoming from the beam of the vessel. The OSCC pendulum motion due to vessel roll is damped out the most for this heading and tugger line configuration. However, the operability in this orientation is very sensitive to the wave heading, as the vessel's pitch is excited when waves are coming in under a 30 degree angle with respect to the beam. To account for the possible spread in environmental loading, the vessel could install the OSCC with its bow in the waves, which results in a lower operability than for beam seas, but this way the operability is less sensitive to the wave direction. This also enables the OSCC to be installed in a more favourable position with regard to weathervaning. Using tugger line configuration 2 leads to an increase of the response of the OSCC in X-direction, due to the angle in the tugger lines. Therefore, it does not result in a higher operability than tugger line configuration 1.

The operability of the installation of the OSCC is shown in figure 9.2 for bow seas, using tugger line configuration 1. Crane clearance is limiting, due to the second pendulum motion of the OSCC. Global Y-motion of the OSCC is also limiting, which is excited through the vessel's pitch.

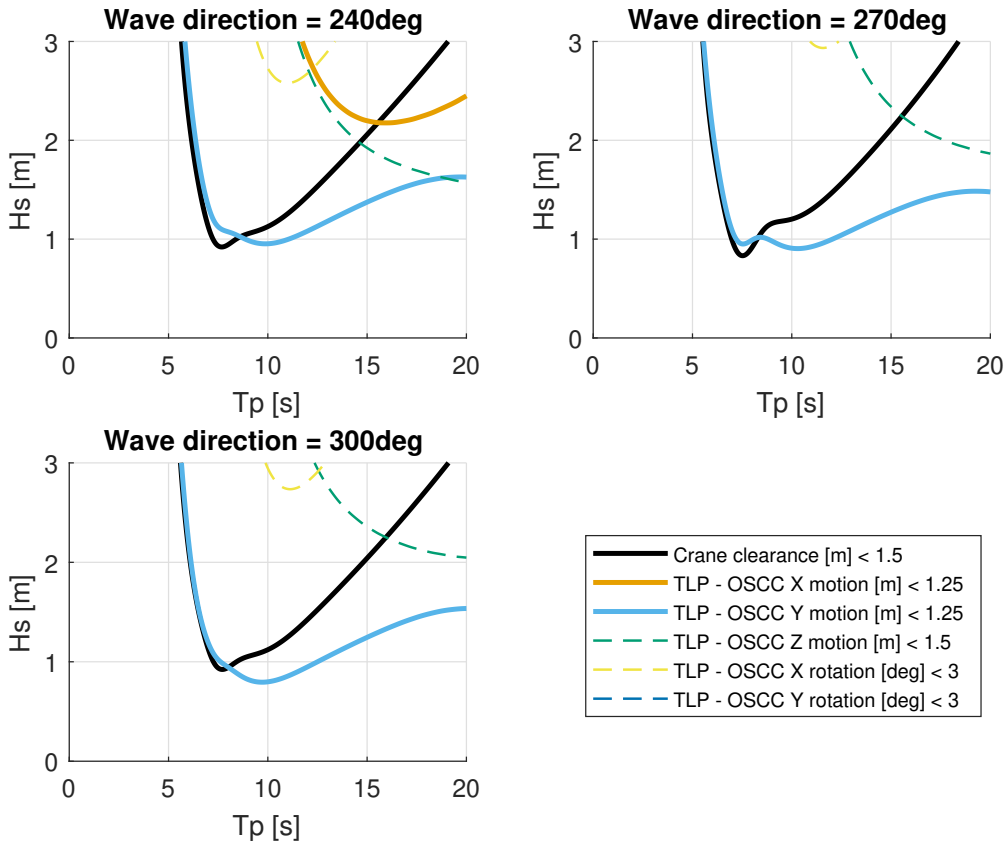


**Figure 9.2:** Operability of the installation of the OSCC on the TLP for beam seas

## 9.2. Seasickness

The operability regarding seasickness of the technicians that are required for the blade exchange is plotted in figure 9.3. It can be seen that motions at the RNA are most critical. The seasickness limit for horizontal acceleration is reached for sea states higher than 2 meters with a peak period close to the natural roll and pitch period of the TLP.

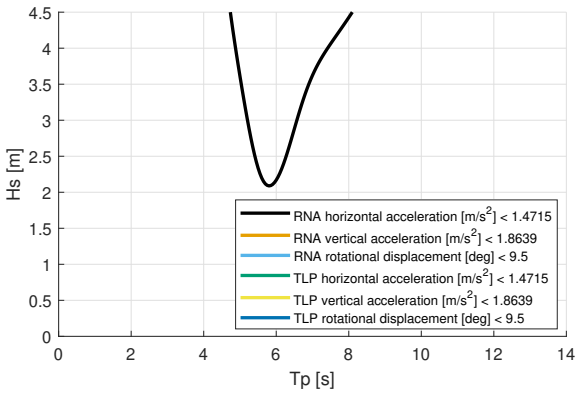


**Figure 9.3:** Operability regarding technician seasickness

## 9.3. Blade removal

The operability of the yoke attachment is given in figure 9.4. It can be seen that the operability of the free-hanging case is relatively low compared to with a line-up tool attached, and limited by the translational motions of the yoke. The wave direction is found to have little influence on the operability due to the limit on both X and Y-motion. The operability for 270 degree waves is used. A drop in operability is seen due to crane tip displacements at the natural period of the TLP in roll and pitch, which induce the second pendulum mode of the yoke. This causes the drop in operability for sea states with a peak period of 6 seconds. At higher peak periods, the pendulum motion of the yoke becomes limiting.

The line-up tool reduces these motions. The yawing mode of the yoke becomes limiting, which results in a limiting motion in global X-direction. The natural period of the yawing motion is relatively high compared to normal wave periods, and is therefore only excited by sea states with a relatively high peak period. The second yaw pendulum motion is excited around 6 seconds, but the magnitude of its response is less and it therefore has a higher operability limit than the normal pendulum.

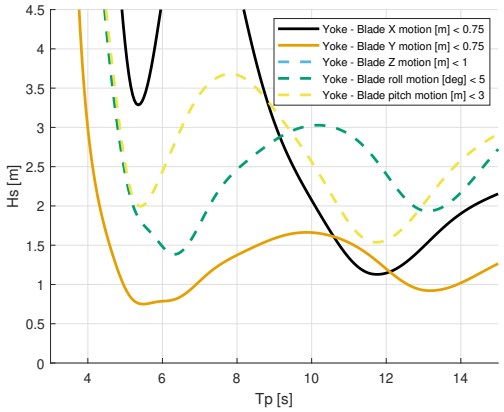


**(a)** Operability of the yoke attachment for the free-hanging case, for a wave heading of 270 degrees

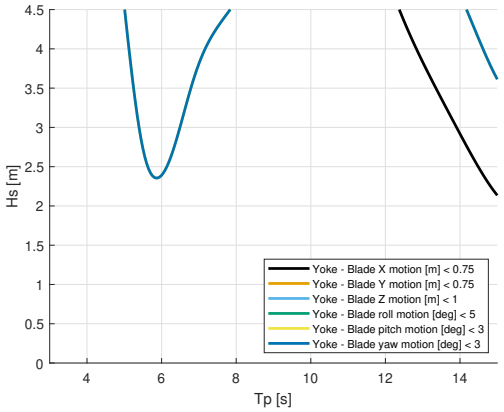


**(b)** Operability of the yoke attachment using the line-up tool, for a wave heading of 270 degrees

**Figure 9.4:** Yoke attachment operability with and without the line-up tool attached to the yoke

The wind and wave induced operability of blade setdown is shown in figure 9.5, for a wind and wave heading of 300 degrees as this leads to the largest response. Only the variables that reach an operability limit below 2.5 meter waves are shown. The yaw mode of the blade, excited through low-frequent wind loads, is limiting. In section 8, the response of the blade with the line-up tool at the yoke was shown to be larger in magnitude, which results in a lower operability. Wave loads also influence the operability. The yaw motion of the blade is excited by sea states with a high peak period, and the inverse yaw motion is excited around the natural period of the TLP in roll and pitch.

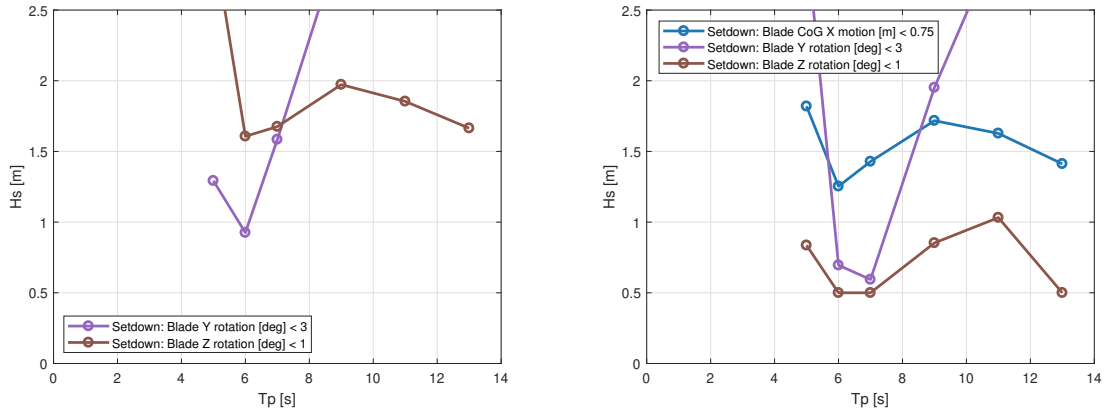


**(a)** Operability of blade setdown with the line-up tool at the root

**(b)** Operability of blade setdown with the line-up tool at the yoke

**Figure 9.5:** Wind and wave influenced operability of blade installation with both line-up tool configurations, for a wind and wave heading of 300 degrees

## 9.4. Blade installation

The wave-induced operability of the free-hanging blade installation is shown in figure 9.6. It can be seen that the in-plane motions of the blade root with respect to the hub are limiting. Sea states with peak periods close to the pitch and roll natural period of the TLP cause a drop in operability, due to the increased crane tip displacements and the excitation of the inverse pendulum of the blade. Sea states with higher peak periods excite the pendulum of the blade, which can also be seen in lower operability. It should be noted that the operability of this scenario will be lower when wind loads are included, as a response of the blade is expected at lower frequencies than wave loads.

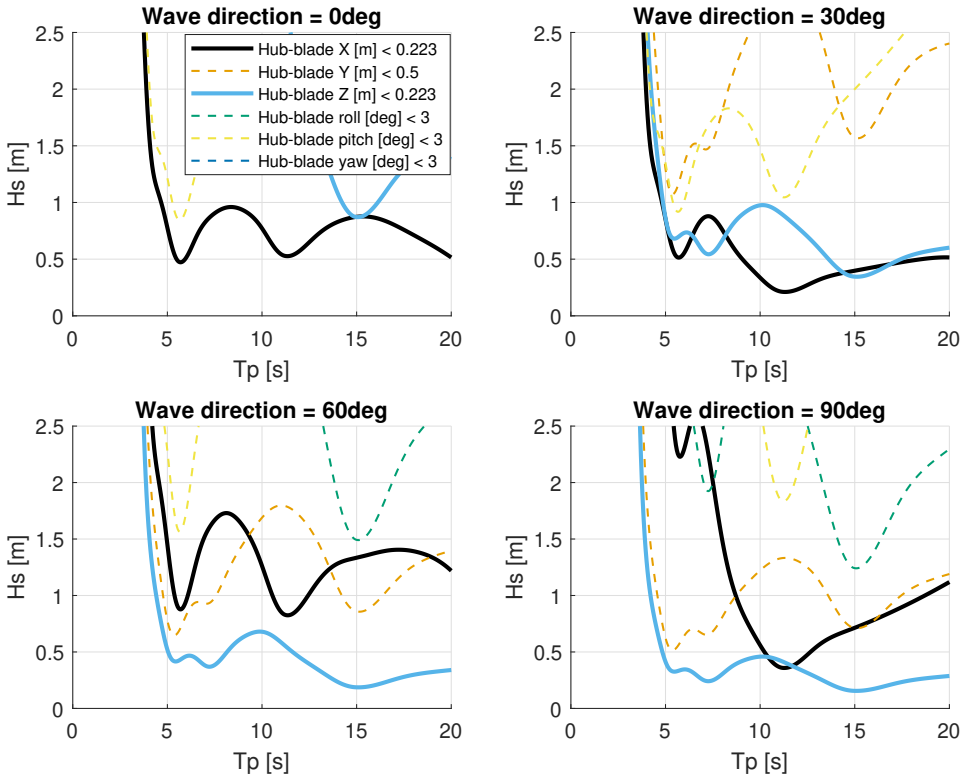


**Figure 9.6:** Operability of blade installation of the free-hanging case

The wind and wave induced operability of blade installation using a line-up tool is shown in figure 9.7. Only the response variables that have an operability limit below wave heights of 2.5 meters are shown. For both line-up tools, motions induced by the blade yaw pendulum are limiting. As was seen through the frequency response assessment of the blade motions, this mode is excited more for the line-up tool at the yoke. This translates in a lower operability for the line-up tool at the yoke, caused by translational motions at the blade root induced by its yawing motion. These motions are caused by low frequent wind loads, and by crane tip displacements through roll and pitch of the TLP.

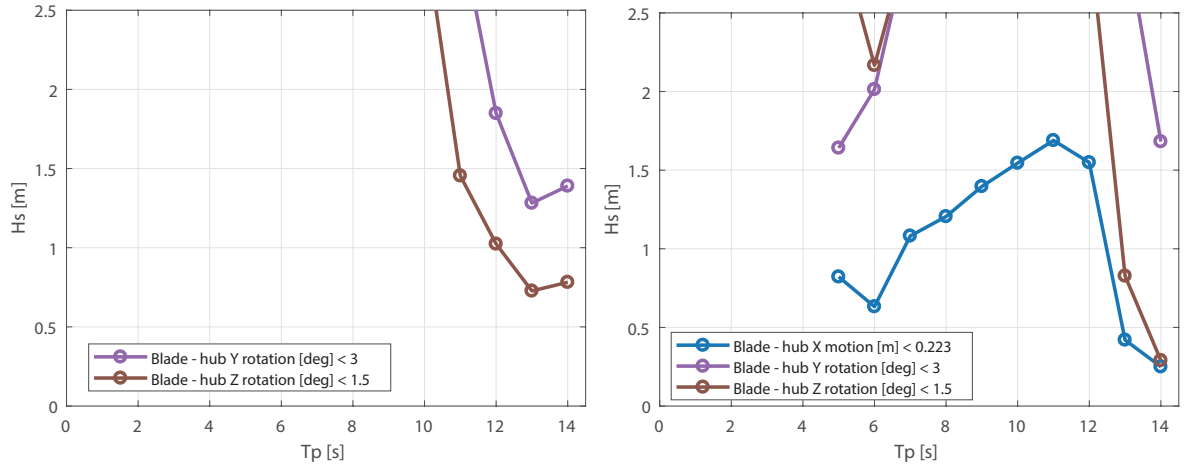


**(a)** Operability of blade installation with the line-up tool at the root

**(b)** Operability of blade installation with the line-up tool at the yoke

**Figure 9.7:** Wind and wave influenced operability of blade installation with both line-up tool configurations, for a wind and wave heading of 300 degrees

## 9.5. Operability comparison of both line-up tools

The operability of the blade exchange using the line-up tool at the root and the line-up tool at the yoke is compared. The operability of installation and setdown is combined for both configurations in figure 9.8. Only the limiting responses of each step are shown. It can be seen that using the line-up tool at the yoke results in lower operability, due to its low stiffness in yaw. When the line-up tool at the root is used, the free-hanging yoke attachment phase is the most critical.

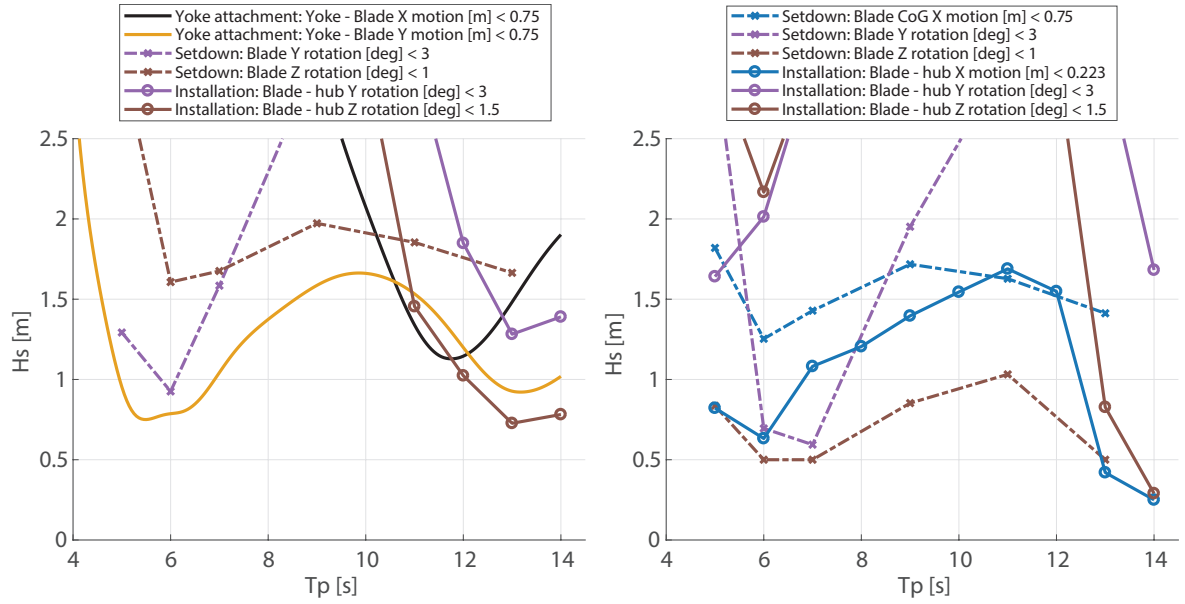


**(a)** Operability of a blade exchange with the line-up tool at the root

**(b)** Operability of a blade exchange with the line-up tool at the yoke

**Figure 9.8:** Wind and wave influenced operability of the blade exchange

# 10 Discussion

This chapter contains a reflection on the results and the modeling choices in this thesis. The key findings are summarized and the outcome of the research is discussed by means of its sensitivity to modeling choices and limitations of the model that was used.

## 10.1. Key findings

Installing the OSCC onto the TLP could be a bottleneck for the operation, due to a limited number of suitable vessels and low operability of the docking phase due to vessel motions. Once installed, the OSCC causes the floater to tilt. Due to its mass, unevenly lowered tension is observed in the tendons. This affects the dynamic behaviour of the TLP, making it more susceptible to low-frequent excitation sources such as wind. The design choices of the crane top mass and lattice stiffness also affect the dynamic behaviour of the TLP, in roll and pitch.

Due to the off-center center of mass of the OSCC, it must be installed on the TLP in a specific orientation. A sharp decrease in tendon tension is observed when the OSCC is placed on the TLP in a different orientation, and this could lead to snap loads in the tendons under dynamic conditions. The specific orientation of the OSCC on the TLP limits the amount of weathervaning that can be applied. This negatively impacts the operability of the blade exchange.

A line-up tool should be used to install the blade, as unguided blade installation leads to low operability and an unconstrained yaw mode of the blade. The line-up tool causes a yawing motion of the blade, and its ability to reduce motions of the blade depends on its stiffness in this degree of freedom. A lower stiffness is seen when the line-up tool is placed at the yoke, and when the hoist cable is long.

Crane tip motions excite the blade and yoke while they are being lifted. The crane tip moves due to wave induced motions, with a peak in the motion spectrum at the roll and pitch natural frequencies of the floater. Next to this, wind induced surge, sway and yaw of the floater also cause motions of the crane tip. Crane tip motions cause a larger response of the blade when the line-up tool at the yoke is used, because the hoisting point on the blade is closer to the point of rotation than when the line-up tool is placed at the blade root. Moreover, larger translational motions of the blade root are seen when the line-up tool is placed at the yoke, as the line-up tool at the root completely mitigates these motions.

Yoke motions during its attachment phase to the old blade are found to be limiting when the line-up tool is placed at the root. Lower operability of the blade exchange is found when the line-up tool is placed at the yoke. As this configuration leads to a lower stiffness in the yaw motion of the blade, the blade becomes susceptible to low-frequent excitations. Large dynamic amplification of the response of the blade is seen during setdown on the vessel, as its natural frequency is close to the surge natural frequency of the TLP. To a lesser extent, wind loads on the blade itself excite the blade. Furthermore, snap loads and seasickness are found not to occur under operable conditions.

## 10.2. Modeled operational stages and critical aspects

Not all operational stages and aspects of the OSCC were studied in this thesis, due to the time constraint for this work. It is plausible that the attachment phase of the line-up tool at the vessel's deck level can lead to additional operating limits, depending on the selected support vessel. This could affect the design choice of using a line-up tool at the root or at the yoke, as they will see different relative motions to the vessel. Similarly, vessel motions were left out of the operability results for the setdown of the blade on the vessel deck, which will also influence the operability once included. The operability should therefore be seen as indicative.

It is expected that the loads transferred onto the tower through the connections with the OSCC's lattice could be a critical element in the design of the OSCC as well. As mentioned before, WTG towers are not designed to cope with loads that do not come from the RNA. The loads in the tower connections are therefore deemed an important topic in order to get permission from a WTG manufacturer to operate the OSCC. A preliminary assessment was made on the loads in the tower connections. However, it was found that there are many variables that influence these. The bending stiffness of the lattice, the number of tower connections, having the point of rotation on the tower or lattice, the torsional and axial stiffness in the connection and the static heel or trim of the floater all influence the result in a major way. Within the scope of this thesis, the preliminary results were deemed too dependent on the input variables to be able to draw conclusions that can deliver any academic contribution.

For all analyses, it was assumed that the blade that is to be replaced is in good condition. However, the blade could also be damaged or partly broken. This could complicate its decommissioning, as it might be more difficult to place it safely on a vessel or attach a yoke to it.

It has also been assumed that the blade can be removed from its bearing when the RNA is tilted due to the OSCC. The bolts that connect the blade to its bearing will experience tension due to the mass of the blade and tilt of the floater, which could make it more difficult to undo the nuts on the bolts and impose a limit on the maximum allowable tilt of the RNA.

## 10.3. Sensitivity of the results

The outcome of the research depends on choices in the modeled configuration of the system and the analyses. The aspects that have a large influence on the results are discussed below.

### 10.3.1. Response limits

The relation between operability and the response limits is linear in frequency domain, and a similar relation exists in the time domain generated operability results. The results of the operability studies are therefore very sensitive to the limits assigned to the system's response. There is not much publicly available information on response limits during offshore operations. Where possible, limits were assessed based on available literature, but estimates had to be made for the limits on the OSCC installation, rotations of the blade, and the limits for yoke attachment. The operability of the blade exchange with the line-up tool at the blade root is limited by the operability of yoke attachment, which shows the results are sensitive to the chosen limits for this operation.

### 10.3.2. TLP design

The TLP in this thesis was designed on its natural frequencies only. The tendon stiffness and tower wall thickness were used as variables to place the natural frequencies. A natural frequency of the tower was set, after which the tendon stiffness was varied to obtain a natural frequency that corresponded with findings from literature. As the roll and pitch natural frequency are a combination of the tower stiffness and the tendon stiffness, a configuration with a stiffer tower and less stiff tendons could have yielded the same natural frequency, but a different response.

The response of the RNA of TLPs with a different distribution in tower stiffness and tendon stiffness is shown in figure C.11. The TLP used in this research has a relatively low response compared to TLPs with a stiffer tower. If a TLP with a softer tendon configuration and stiffer tower would have been used, a lower operability would have been found.

## 10.4. Modeling limitations

The modeling theory used in this research is only applicable under certain circumstances. Important simplifications and limitations of the modeling theory are discussed below.

### 10.4.1. Aerodynamic model and wind field

The aerodynamic loads on the blade are sensitive to the pitch of the blade. The results showed that for the pitch used during the blade installation, the loads on the blade were near-zero, as the wind field was entirely parallel. A three dimensional wind field could be generated with software packages like TurbSim. This could increase the loads on the blade due to variations in the inflow angle of the incoming wind. The response of the blade is expected to be higher in magnitude when this is accounted for, which could influence the results. More excitation at the natural period of oscillation of the blade is expected when a non-parallel wind field is modeled.

A limitation of the aerodynamic model used, is that it only computes the aerodynamic load that is caused by airflow perpendicular to the blade. As a result, the aerodynamic loads on the blade are near-zero when wind is flowing parallel to the length of the blade. However, this is not the case in reality. Accounting for this could more accurately show which installation orientation of the blade is best, and capture aerodynamic effects on the blade when wind is flowing across it. It is possible that for an incoming wind direction parallel to the length of the blade, there might be stabilizing effects for certain pitch angles of the blade.

### 10.4.2. Wind wave relation

There can be a large scatter in the correlation between wind speed and wave heights. When a developed sea state is encountered, the waves can be classified as swell and are generated by far-away wind fields, while there might be little wind in the area of measurement. When a fetch-limited sea state is encountered, the waves are generated by a local wind field. The wind-wave relation used in this thesis is calibrated for fully developed seas. Fetch-limited area's like the North Sea will see a different statistical relation between wind speed and wave height. In these type of area's, the encountered wind speed will be higher than presented in the IMCA wind-wave relation. This could impact the results, as the response of the system showed sensitivity to wind loads.

### 10.4.3. Second-order wave loads

Only first-order wave loads were accounted for in this research. As the TLP becomes more susceptible to low-frequent excitations under influence of the OSCC, it can be argued that low-frequent hydrodynamic loads such as difference-frequency and wave drift loads will also affect the dynamic behaviour of the TLP. As the response of the blade during lifting is also low-frequent, it can be expected that these loads will influence the dynamic behaviour of the blade, and that including low-frequent second-order wave loads will reduce the operability.

As mentioned before, sum-frequency effects could influence the standard deviation in the tendons, which could be important for assessing snap loads. Snap loads are shown not to occur near operational wave heights, and it is reasoned that including sum-frequency effects will not influence this conclusion. Sum-frequency effects have been shown to increase the standard deviation in tendon tension by around 6% [3], which is not enough to induce snap loads under operable wave heights. However, if a full understanding of the minimum tendon tension under influence of the OSCC is desired, sum-frequency effects should be included.

### 10.4.4. Hydrodynamic interaction

The hydrodynamic interaction between the vessel and TLP was not modeled. Under certain incoming wave headings, there could be wave shielding of the vessel, which could reduce the wave-induced response of the TLP. This would benefit the operability, and an optimal wave shielding configuration of the vessel during the component exchange could be of added value. However, a worst-case scenario in which there is no wave shielding was deemed a more appropriate scenario for this research.

# 11

# Conclusions and recommendations

In this chapter, the presented research is concluded based on the research questions presented in the problem statement. A judgement is given on the challenges and opportunities for onsite maintenance using the OSCC, and recommendations are given for future research.

## 11.1. Research questions

1. What are the constraints and requirements for a support vessel, and how does the support vessel influence the operation?

   The operational constraints were discussed in section 4.2, which shows that a two-crane vessel could perform the installation. An operational bottleneck of a limited number of suitable installation vessels was identified. In the response and operability plots, it can be seen that the vessel has a major influence on the operability. The operability of the installation of the OSCC is more limiting than the operability of the blade exchange for certain sea states. During setdown, the response is dominated by vessel motions at wave periods. When the operability of the line-up tool attachment at deck level of the vessel would also be included, it is possible that vessel motions also might limit the entire operability. Selecting a support vessel with better motion characteristics would increase the operability. However, this would mean a larger vessel has to be used which influences the business case.

2. What is the influence of the OSCC on the static and dynamic behaviour of a Tension-Leg Platform?

   a) *What influence does the OSCC have on the tension in the tendons of a TLP?*
   The tension in the tendons is lowered due to the mass of the OSCC, and its uneven center of mass causes uneven tension in the tendons. The OSCC's center of mass must be placed in between two tendons to obtain the most even distribution in tendon tension.

   b) *How are the natural periods of a TLP affected by the OSCC?*
   Due to the decrease in tendon tension, the natural periods of a TLP in surge, sway and yaw are increased and shift closer to the excitation spectrum of wind. The natural period in roll and pitch is influenced by the coupling of the lattice of the OSCC to the WTG tower, as their bending modes are coupled. The design choices of the crane top mass and lattice stiffness influence the dynamics of these modes.

   c) *Can snap loads occur in the tendons under sea states in which the OSCC can operate?*
   Snap loads are observed for sea states of 2.5 meters significant wave height, and a peak period around the natural period of a TLP in roll and pitch. Operability limits of the OSCC are reached before this wave height, so it can be concluded that snap loads will not occur under operable conditions for the OSCC.

In conclusion, a TLP is more susceptible to environmental loads due to the OSCC. A larger response was observed with the OSCC on the TLP due to increased drag on the structure, and the lowered natural frequencies of the TLP. This affects the operability of the blade exchange.

3. What is the operability of a blade exchange operation using the OSCC, based on the identified critical factors?

   The combined operability of the blade lifts using a line-up tool are shown in figure 9.8. It was seen that the line-up tool at the root provides better operability, due to the low stiffness in the yaw mode of the blade when using the line-up tool at the yoke. The operability of the OSCC installation was found to be more limiting than the blade exchange itself at certain sea states.

   a) *Is it necessary to control the motion of the blade during lifting, how can this best be done and how does this influence the operability?*
      The free-hanging blade sees a large translational response due to the crane tip displacements of the OSCC. Both line-up tools show better operability during installation. Moreover, the yaw mode of the blade is unconstrained without a line-up tool. This shows that the motions of the blade must be controlled using a line-up tool, and free-hanging blade installation is not possible. It can be concluded that using the line-up tool attached to the blade root is the best design choice.

   b) *What motions of the lifted blade or the turbine determine the operability?*
      Yawing motions of the blade were found to determine the operability of the blade lifts. These motions were mostly induced by crane tip displacements of the TLP. To a lesser extent, excitation of the blade at its natural frequency was seen which is caused by wind loads on the blade itself. However, this was relatively small due to the feathered position of the blade.

      Motions of the blade's yaw excited through surge, sway and yaw of the TLP influence the operability when wind is included in the environmental loads. Second pendulum motions of the blade's yaw motion and of the yoke are also found to be limiting, and are induced by the TLP's roll and pitch.

   c) *What means can be used to improve the operability?*
      Using a line-up tool at the root of the blade shows the highest operability. Yoke attachment becomes limiting, so improvements can be made in this phase. If the response limit on yoke installation can be improved, the operability improves. This could be done by installing bumpers on the yoke, which make it possible to attach it to the old blade under dynamic circumstances.

      Using a line-up tool at the yoke with increased stiffness in its connection could also improve the operability. This will make the blade less susceptible to low-frequent excitation, while having the advantage of using a line-up tool during yoke attachment. However, this will lead to large loads in the line-up tool, and the equipment must be designed to withstand these loads.

      Second pendulum motions due to the rigging in the yoke have a large influence on the operability. A longer or much shorter rigging could be used to place the second pendulum motion further away from TLP's roll and pitch periods. This would result in less dynamic amplification of this mode.

      The mass of the crane at the top of the lattice of the OSCC influences the roll and pitch natural period of the TLP. A drop in operability was seen due to this mode, as it excites the second pendulum mode of the blade and yoke. Using a lighter crane on top of the lattice places this period further away from wave periods. This will result in higher operability at wave periods that are commonly seen.

The stiffness of the lattice also influences the roll and pitch mode of the TLP. However, this influence is non-linear and mostly visible for very low bending stiffnesses of the lattice. Increasing the lattice stiffness would only slightly decrease the natural period, but due to the increased weight that comes with this it is expected that increasing the lattice stiffness only increases the natural period in roll and pitch.

If a maintenance operation with the OSCC is taken into account in the TLP design, the buoyancy of the TLP could be increased to increase operability during maintenance. This will make the degrees of freedom surge, sway and yaw less susceptible to wind loads, as the stiffness in these modes will be larger due to the increased tendon tension. The blade will therefore see less low-frequent oscillations. Increasing the tendon stiffness does not result in much better dynamic behaviour, as the curve for the natural period in roll and pitch flattens out after the selected stiffness.

Ballasting the OSCC so that it can be installed on a TLP in more than three orientations would increase the possibilities of weathervaning. The OSCC could be installed such that the yaw mode of the TLP is not excited by drag on the lattice of the OSCC. This would reduce the response of the blade and benefit the operability of the blade exchange.

## 11.2. Judgement

The wave height limits seen on operability are around 1 meter. As floating wind farms will be placed further offshore, the chance of encountering sea states with higher waves increases. This means that a blade exchange will be a calm weather operation. For unscheduled maintenance in winter season, relatively long waiting on weather windows can be expected. However, towing for maintenance can also be expected to be a calm weather operation. If the bottleneck of installation with regards to operability and vessel availability can be overcome, the OSCC would likely provide a quicker maintenance solution than a tow-back, due to the lengthy towing procedure and the disconnection and reconnection of the floater to its mooring lines and power cable.

The connection points of the OSCC to the floater and tower pose design constraints that must be accounted for early in the development of a floating wind farm. This means a developer of a floating wind farm must invest in a docking point on the floater, and potentially structural reinforcements in the tower. A developer therefore faces the choice of investing early on in a faster maintenance solution, or opting for less upfront expenditure and potentially higher operational costs. This choice will depend largely on if the business case of maintenance with the OSCC provides significant advantages over the alternatives.

With the operability figures from this thesis, the highlighted design choices that affect the operability, and the following recommendations for future research, the business case of the OSCC can be constructed in more detail and improved.

### 11.2.1. Feasibility of a blade exchange with the OSCC on other floaters

In this thesis, only a TLP was studied, as it is generally considered more difficult to displace this floater. However, the literature review also suggested that towing for maintenance of semi-submersibles and SPARs is a complex logistical process, and onsite maintenance might be better, if feasible.

The waterplane area of a SPAR is relatively small. It will therefore see a large vertical displacement when the OSCC is docked, of around 6 meters using a waterplane diameter of 15 meters, and even more when considering that the top of a SPAR is tapered to a smaller diameter. This will complicate installation of the OSCC. Furthermore, the height of the center of gravity of a SPAR will be increased when the OSCC is in its extended position. This will have a negative effect on the GM of a SPAR, making it less stable. This is problematic as a SPAR is ballast-stabilized, and there is little stiffness due to its mooring in roll and pitch. The lower GM will also influence a SPARs dynamic behaviour, especially in roll and pitch. These modes have shown to be important in the blade exchange on a TLP, as they can cause large crane tip displacements.

A semi-submersible floater with a center column would not work for the OSCC, as it is not possible to install it using the current installation methodology considering the outreach of the cranes. For a semi-submersible where the WTG is placed on one of the outer columns, ballast due to the weight of the OSCC will be necessary.

Motions induced by the crane tip displacements were found to have a large impact on operability. As a TLP is a relatively stiff system, these crane tip displacements can be considered relatively small. SPARs and semi-submersibles will see more excitation due to wave loads. This will induce more motion of the crane tip, especially at their roll and pitch periods. These periods are above wave periods for both semi-subs and SPARs. As these periods are higher, they will excite the first yaw pendulum of the lifted blade more, whereas a roll and pitch of the TLP excited the second pendulum mode. This could cause a larger response at these modes, depending on how much these modes are excited by environmental conditions.

## 11.3. Recommendations

In this section, recommendations are provided that could improve the model presented in this work, generate more understanding of the operation of the OSCC and its influence on a TLP, or contribute towards a better understanding of the business case of the OSCC.

### 11.3.1. Model improvement

#### TLP design

Several assumptions were made in the construction of the model of a TLP in this thesis, one of which was the tendon stiffness. A more thorough assessment of a realistic stiffness of the tendons with regards to available materials, after which the tower stiffness could be chosen based on the desired natural frequency, could be performed to get a more realistic representation of the dynamics of a TLP, especially with regard to the mode shape and response in roll and pitch. The selected EA of 12 GN results in a tendon diameter of 500 mm when using Fibremax, a commonly used material [14]. This could also translate in for example two tendons of 250 mm per leg. The required stiffness depends on the tendon length (EA/L), which depends on the waterdepth. Regarding the feasibility of such cables, conclusions could be drawn on suitable water depths for TLPs.

#### Environmental load modeling

As mentioned in section 10.4, simplifications were made in modeling the environmental loads. It was seen that the TLP is susceptible to low-frequent loads under influence of the OSCC, which makes low-frequent higher-order wave loads a point of future research. Generating a turbulent wind field would result in more accurate loads on the lifted blade, and the influence of turbulence on the response of the lifted blade could be studied. Higher fidelity aerodynamic simulations could be performed of the blade for different inflow angles of the incoming wind. The applied BEM methodology underestimates the aerodynamic effects on the blade for inflow angles parallel to the blade's length. As a larger inflow angle could result in higher operability because the yaw mode of the TLP would be excited less due to drag loads on the OSCC's lattice, a more thorough understanding of the aerodynamic loads on the blade when cross-flow is accounted for would be of added value. This could be done using CFD analyses of the blades of the reference turbine used in this thesis.

#### Modeled stages

The attachment of the line-up tool to the blade at deck level of the vessel remains a point of research, which will depend very much on the choice of vessel. Including it in the model will result in a better understanding of the operating limits of the OSCC, and the design choice of the line-up tool. Limits in this phase could be an argument for using the line-up tool at the yoke, as the vessel motions will be more amplified at the blade root. Important input to the business case could also be generated with regards to the vessel choice.

### 11.3.2. Future research on the OSCC

#### Tower connections

The loads in the tower connections are an important aspect in the interface between the OSCC and the WTG. Designing a tower connection layout and stiffness that result in the lowest static loads in the connections will be an important design aspect of the OSCC. To achieve this, boundary conditions could be formulated on the allowable displacement of the lattice and the allowable load on the tower. A sensitivity study on the stiffness in the tower connections, the height of the tower connections and the number of tower connections could be performed to generate insight into the design drivers and reach an optimal design.

In this research, the tower connections have been assumed to be fixed in rotation. It can be studied if having rotation-free tower connections would affect the loads that are seen. This could also affect the coupling of the tower bending mode to the lattice bending mode. If these can be uncoupled by having tower connections that are free in rotation, while still providing enough stiffness to the lattice, this could be beneficial for the system dynamics during the blade exchange.

#### Installation

Research towards new installation methodologies of the OSCC could contribute towards improving the operability of a blade exchange. Investigating the possibilities of using a larger dual crane installation vessel, which would reduce the motions seen during installation but also during setdown of the blade, could be worthwile. However, the business case needs to be kept in mind.

### 11.3.3. Future work on the business case

#### Logistical analyses

To gain a better understanding of the financial drivers behind floating wind maintenance scenarios, logistical analyses could be performed. Operability assessments of towing and a blade exchange using a floating vessel could be done to get a full understanding of the remaining maintenance scenarios. A logistical analysis of these maintenance scenarios and the OSCC, that takes their operability and duration into account, could help understand the effects of vessel costs, the resulting turbine downtime and vessel availability on the total cost of maintenance. Comparing the cost of maintenance using the OSCC to other solutions, could help in making a stronger business case and provide more certainty in the investment decision of a floating wind developer of using the OSCC as a maintenance solution.

# References


[1] Ampelmann. *E-Type*. 2023. URL: https://www.ampelmann.nl/systems/e-type (visited on 06/30/2023).

[2] Suzana Avila et al. “Numerical Modeling of the Dynamic Behavior of a Wind Turbine Tower”. In: *Advances in Vibration Engineering* 4 (July 2016).

[3] E. Bachynski. “Design and Dynamic Analysis of Tension Leg Platform Wind Turbines”. In: (2014).

[4] Erin E. Bachynski and Torgeir Moan. “Design considerations for tension leg platform wind turbines”. In: *Marine Structures* 29.1 (2012), pp. 89–114. ISSN: 0951-8339. DOI: https://doi.org/10.1016/j.marstruc.2012.09.001. URL: https://www.sciencedirect.com/science/article/pii/S0951833912000627.

[5] Erin E. Bachynski and Torgeir Moan. “Ringing loads on tension leg platform wind turbines”. In: *Ocean Engineering* 84 (2014), pp. 237–248. ISSN: 0029-8018. DOI: https://doi.org/10.1016/j.oceaneng.2014.04.007. URL: https://www.sciencedirect.com/science/article/pii/S0029801814001371.

[6] Subrata Chakrabarti. “Empirical calculation of roll damping for ships and barges”. In: *Ocean Engineering* 28.7 (2001), pp. 915–932. ISSN: 0029-8018. DOI: https://doi.org/10.1016/S0029-8018(00)00036-6. URL: https://www.sciencedirect.com/science/article/pii/S0029801800000366.

[7] Subrata Chakrabarti. *Handbook of Offshore Engineering*. Elsevier, 2005.

[8] J. Chung and G. M. Hulbert. “A Time Integration Algorithm for Structural Dynamics With Improved Numerical Dissipation: The Generalized-α Method”. In: *Journal of Applied Mechanics* 60.2 (June 1993), pp. 371–375. ISSN: 0021-8936. DOI: 10.1115/1.2900803. eprint: https://asmedigitalcollection.asme.org/appliedmechanics/article-pdf/60/2/371/5463014/371_1.pdf. URL: https://doi.org/10.1115/1.2900803.

[9] Heerema Marine Contractors. *Sleipnir*. 2019. URL: https://www.heerema.com/heerema-marine-contractors/fleet/sleipnir (visited on 06/20/2023).

[10] American Petroleum Institute. Production Department and American National Standards Institute. *Recommended Practice for Planning, Designing, and Constructing Fixed Offshore Platforms: Working Stress Design*. American Petroleum Institute, 1993. URL: https://books.google.nl/books?id=tFKUoAEACAAJ.

[11] DNV. “Floating Offshore Wind: The Next Five Years”. In: (2022).

[12] Catapult Offshore Renewable Energy. “Offshore wind Operations & Maintenance: a £9 Billion per year opportunity by 2030 for the UK to seize”. In: (2021).

[13] O. Faltinsen. *Sea Loads on Ships and Offshore Structures*. Cambridge University Press, 1990.

[14] Fibremax. *Fibremax Cable Calculator*. URL: https://fibremax.nl/cables/cable-configurator/ (visited on 08/01/2023).

[15] Fugro. *Decommissioning Blyth offshore wind farm*. URL: https://www.youtube.com/watch?v=wz9YrYk172E (visited on 12/05/2023).

[16] Christos T. Georgakis et al. “Drag coefficients of lattice masts from full-scale wind-tunnel tests”. In: 2009. URL: https://api.semanticscholar.org/CorpusID:110087181.

[17] Weiting Hsu et al. “Snap Loads on Mooring Lines of a Floating Offshore Wind Turbine Structure”. In: *Proceedings of the International Conference on Offshore Mechanics and Arctic Engineering - OMAE* 9 (June 2014). DOI: 10.1115/OMAE2014-23587.

[18] IEA Wind. *IEA-15-240-RWT*. 2021. URL: https://github.com/IEAWindTask37/IEA-15-240-RWT (visited on 04/04/2023).

[19] IMCA. “Specifications for DP Capability Plots”. In: (1997).

[20] ITCC. “Numerical Simulation of Capsize Behaviour of Damaged Ships in Irregular Beam Seas”. In: *ITTC – Recommended Procedures and Guidelines* ().

[21] Zhiyu Jiang. “Installation of offshore wind turbines: A technical review”. In: *Renewable and Sustainable Energy Reviews* 139 (Apr. 2021), p. 110576. ISSN: 1364-0321. DOI: 10.1016/J.RSER.2020.110576.

[22] J. M. Jonkman. “Dynamics modeling and loads analysis of an offshore floating wind turbine”. In: (2007).

[23] M. J. Journée, W. W. Massie, and R.H.M Huijsman. *Offshore Hydromechanics*. 3rd ed. 2015.

[24] Mert Kaptan et al. “Analysis of spar and semi-submersible floating wind concepts with respect to human exposure to motion during maintenance operations”. In: *Marine Structures* 83 (2022), p. 103145. ISSN: 0951-8339. DOI: https://doi.org/10.1016/j.marstruc.2021.103145. URL: https://www.sciencedirect.com/science/article/pii/S0951833921001969.

[25] Lagerwey. *Climbing crane*. 2015. URL: https://www.lagerwey.com/climbing-crane/ (visited on 12/03/2022).

[26] C.H. Lee. *WAMIT Theory Manual*. Report (Massachusetts Institute of Technology. Department of Ocean Engineering). Massachusetts Institute of Technology, Department of Ocean Engineering, 1995. URL: https://books.google.nl/books?id=fWKGHAAACAAJ.

[27] K. de Leeuw. “Single lift blade alignment for large offshore wind turbines”. In: (Dec. 2019).

[28] Liftra. *LT1200 - Self-hoisting crane*. URL: https://liftra.com/products/lt1200-self-hoisting-crane.html (visited on 10/31/2022).

[29] Jumbo Maritime. *Jumbo Fairplayer*. URL: https://www.jumbomaritime.nl/vessels/fairplayer/ (visited on 06/28/2023).

[30] J. McMorland et al. “Operation and maintenance for floating wind turbines: A review”. In: *Renewable and Sustainable Energy Reviews* 163 (July 2022), p. 112499. ISSN: 1364-0321. DOI: 10.1016/J.RSER.2022.112499.

[31] IFRI Centre for Energy Michael Cruciani. “The Expansion of Offshore Wind Power in the North Sea”. In: ().

[32] Orcina. *K03 15MW semi-sub FOWT*. 2023. (Visited on 06/30/2023).

[33] Orcina. *Line theory: Overview*. URL: https://www.orcina.com/webhelp/OrcaFlex/Content/html/Linetheory,Overview.htm (visited on 06/28/2023).

[34] Orcina. *Theory: Irregular frequencies*. 2023. URL: https://www.orcina.com/webhelp/OrcaWave/Content/html/Theory,Irregularfrequencies.htm (visited on 06/30/2023).

[35] Zhengru Ren et al. “Offshore wind turbine operations and maintenance: A state-of-the-art review”. In: *Renewable and Sustainable Energy Reviews* 144 (July 2021), p. 110886. ISSN: 1364-0321. DOI: 10.1016/J.RSER.2021.110886.

[36] Saipem. *Hywind*. URL: https://www.saipem.com/en/projects/hywind (visited on 03/04/2023).

[37] SenseWind. *Installing and servicing turbines*. URL: https://sensewind.com/ (visited on 09/06/2023).

[38] Matt Shields et al. “Impacts of turbine and plant upsizing on the levelized cost of energy for offshore wind”. In: *Applied Energy* 298 (Sept. 2021), p. 117189. ISSN: 0306-2619. DOI: 10.1016/J.APENERGY.2021.117189.

[39] Mohammed Khair Al-Solihat and Meyer Nahon. “Stiffness of slack and taut moorings”. In: *Ships and Offshore Structures* 11.8 (2016), pp. 890–904. DOI: 10.1080/17445302.2015.1089052. eprint: https://doi.org/10.1080/17445302.2015.1089052. URL: https://doi.org/10.1080/17445302.2015.1089052.

[40] M. Somoano et al. “Influence of turbulence models on the dynamic response of a semi-submersible floating offshore wind platform”. In: *Ocean Engineering* 237 (2021), p. 109629. ISSN: 0029-8018. DOI: https://doi.org/10.1016/j.oceaneng.2021.109629. URL: https://www.sciencedirect.com/science/article/pii/S0029801821010076.

[41] Spinergie. “Spinergie Offshore Wind Monthly Report, January”. In: (2023).

[42] Norwegian Petroleum Directorate Staff. *Regulations Relating to Loadbearing Structures in the Petroleum Activities*. Oljedirektoratet, 1998. ISBN: 9788272575006. URL: https://books.google.nl/books?id=jyA-PQAACAAJ.

[43] Jan van der Tempel. “Design of Support Structures for Offshore Wind Turbines”. In: (2016).

[44] Carbon Trust. “Floating Offshore Wind: Market and Technology Review”. In: ().

[45] Carbon Trust. “Floating Wind Joint Industry Project: Phase II Summary Report”. In: (2020).

[46] Carbon Trust. “Floating Wind Joint Industry Project: Phase III Summary Report”. In: (2021).

[47] H. Vallery, A.L. Schwab, and Technische Universiteit (Delft). *Advanced Dynamics*. Delft University of Technology, 2017. ISBN: 9789461868367. URL: https://books.google.nl/books?id=gUd8tgEACAAJ.

[48] Amrit Shankar Verma et al. “Impact assessment of a wind turbine blade root during an offshore mating process”. In: *Engineering Structures* 180 (Feb. 2019), pp. 205–222. ISSN: 0141-0296. DOI: 10.1016/J.ENGSTRUCT.2018.11.012.

[49] Vestas. *Vestas Offshore Blade and Gearbox Replacement*. URL: https://www.youtube.com/watch?v=pPeuHepz-J0&t=179s (visited on 12/05/2023).

[50] Wind watch. *Kincardine wind turbine taken to Rotterdam for maintenance*. 2023. URL: https://www.wind-watch.org/news/2023/06/01/kincardine-wind-turbine-taken-to-rotterdam-for-maintenance/ (visited on 06/20/2023).

[51] IEA Wind. “Definition of the IEA Wind 15-Megawatt Offshore Reference Wind Turbine”. In: (Mar. 2020).

[52] WindSpider. *Disruptive Self-Erecting Crane System Eliminating Need For Jack-Up Vessels*. 2022. URL: https://windspider.com/ (visited on 12/06/2022).

[53] Saeid Loftian Zi Lin Xiaolei Liu. “Impacts of water depth increase on offshore floating wind turbine dynamics”. In: *Ocean Engineering* 224 (2021).

# A

# Vessels suitable for the operation

Suitable vessels with one crane and dynamic positioning:

| *Company* | *Vessel Name* | *Length (m)* | *Breadth (m)* | *Draft (m)* | *DP* | *Crane 1 (t)* |
|---|---|---|---|---|---|---|
| Boskalis | Bokalift 1 | 216 | 43 | 8.5 | DP2 | 3000 |
| Boskalis | Bokalift 2 | 231 | 49 | 10 | DP2 | 4000 |
| COES Caledonia | Chuang Li | 198.8 | 46 | 8.5 | DP3 | 4500 |
| DEME Group | Orion | 216.5 | 49 | 11 | DP3 | 5000 |
| DEME Group | Green Jade | 216.5 | - | - | DP3 | 4000 |
| Goliath | Nor Goliath | 180 | 32 | 7.5 | DP3 | 1600 |
| Heerema | Aegir | 211 | 46.2 | 11 | DP3 | 5000 |
| Jan De Nul | Les Alizes | 236.8 | 52 | 10.5 | DP2 | 5000 |
| Saipem | Saipem 3000 | 162 | 38 | 9 | DP3 | 2177 |
| Saipem | Saipem Constellation | 178 | 46 | 10.5 | DP3 | 3000 |
| McDermott | Derrick lay vessel 2000 | 184 | 38.6 | 7.9 | DP3 | 2000 |
| Seaway 7 | Alfa Lift | 217.88 | 56 | 9.64 | DP2 | 3000 |
| Seaway 7 | Seaway Strashnov | 183 | 47 | 13.5 | DP3 | 5000 |
| Subsea 7 | Seven Borealis | 182.2 | 46.2 | 11.35 | DP3 | 5000 |
| Subsea 7 | Seven Champion | 142 | 40 | 6.5 | DP2 | 2200 |

Suitable vessels with two cranes and dynamic positioning:

| *Company* | *Vessel Name* | *Length (m)* | *Breadth (m)* | *Draft (m)* | *DP* | *Crane 1 (t)* | *Crane 2 (t)* |
|---|---|---|---|---|---|---|---|
| Jumbo | Fairplayer | 144.1 | 26.7 | 8.1 | DP2 | 900 | 900 |
| Jumbo | Javelin | 144.1 | 26.7 | 8.1 | DP2 | 900 | 900 |
| Jumbo/SAL | Lone | 160.6 | 27.91 | 9.01 | DP2 | 1000 | 1000 |
| Jumbo/SAL | Svenja | 160.6 | 27.91 | 9.01 | DP1 | 1000 | 1000 |

# B

# Response limits

## B.1. Blade alignment criterion

The alignment criterion for blade installation can be expressed as an SSMPM. Following from section 3.3, the SSMPM for a reference period of 1 minute is equal to 0.2 m. As the natural period of the blade's pendulum motion during installation is roughly 12 seconds, the SSA can be calculated through:

$$\exp\left\{-2\left(\frac{0.2}{X_{SSA}}\right)^2\right\} = \frac{1}{5} \tag{B.1}$$

The blade's SSA is equal to 0.223 m. This is used to express the SSMPM for a reference period of 30 minutes, using equation 5.43. The number of motion cycles is calculated using this reference period and an oscillation period of 12 seconds, resulting in 150 cycles.

## B.2. Reference periods

As the limit to a critical factor depends on the number of motion cycles that can occur, the reference period taken for an operation is of importance. Two reference periods are taken: 30 minutes and 3 hours. The 30 minutes reference period is taken for the final installation phase of components, and the 3 hour reference period is taken for clearances and the seasickness criterion. For the 30 minutes reference period, $N_{cycles}$ is taken to be 250, and for the 3 hours reference period $N_{cycles}$ is taken to be 1500. This corresponds with a zero-crossing period of 7.2 seconds. Although technically the number of cycles for each limit should be evaluated by its natural frequency, an assumption is made to make the number of cycles for each limit equal.

## B.3. Seasickness criterion

Table B.1 shows the threshold for motions humans are able to experience before experiencing motion sickness. The criterion for transit passenger is found to be the most fitting for technicians in a FOWT [24], as this best reflects the duration of the work and the work itself.

| Description | Vertical acc. (SSA) | Lateral acc. (SSA) | Rotational disp. (SSA) |
|---|---|---|---|
| Light manual work | $0.40$ g | $0.20$ g | $12.0°$ |
| Heavy manual work | $0.30$ g | $0.14$ g | $8.0°$ |
| Intellectual work | $0.20$ g | $0.10$ g | $6.0°$ |
| Transit passenger | $0.10$ g | $0.08$ g | $5.0°$ |
| Cruise liner | $0.04$ g | $0.06$ g | $4.0°$ |

**Table B.1:** Set of motion sickness criteria with regard to vertical and lateral accelerations and rotational displacement [24]

# C

# Model details

## C.1. Tower dimensions

The wall thickness of the tower for the floating wind turbine on the TLP is altered from the IEA 15 MW reference turbine in order to correctly place the natural frequency of the TLP and WTG combined. The tower outer diameter and wall thickness used in this thesis are shown in figure C.1 and C.2. The original wall thickness from the bottom-fixed IEA 15 MW reference turbine is shown for reference.

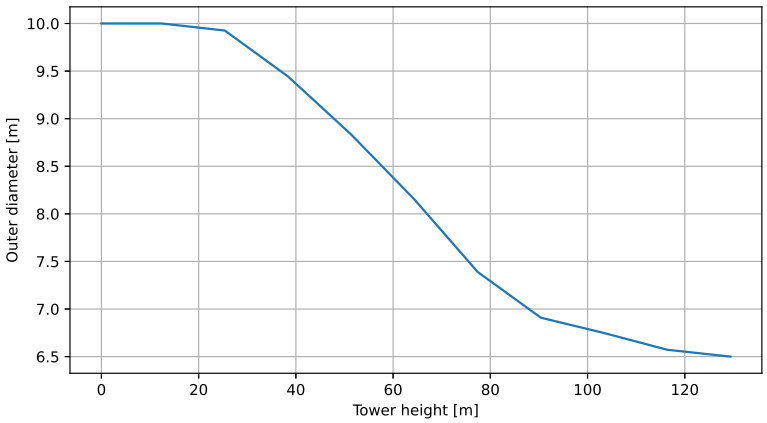


**Figure C.1:** Outer diameter of the tower

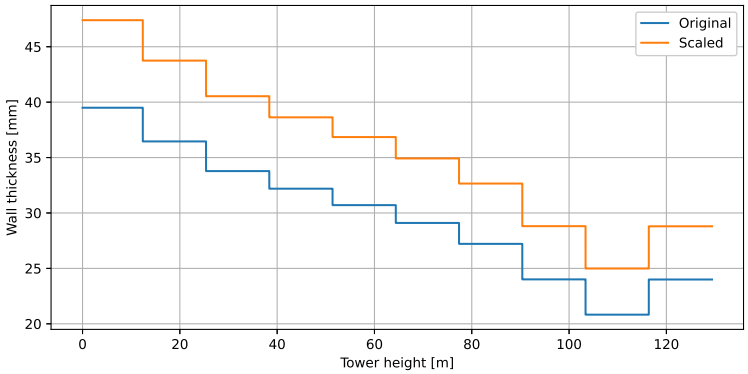


**Figure C.2:** Wall thickness of the tower

## C.2. Mesh sensitivity studies

A mesh sensitivity study is performed on the hydrodynamic modeling of the TLP. The results for different mesh sizes of the added mass is shown in figure C.3.

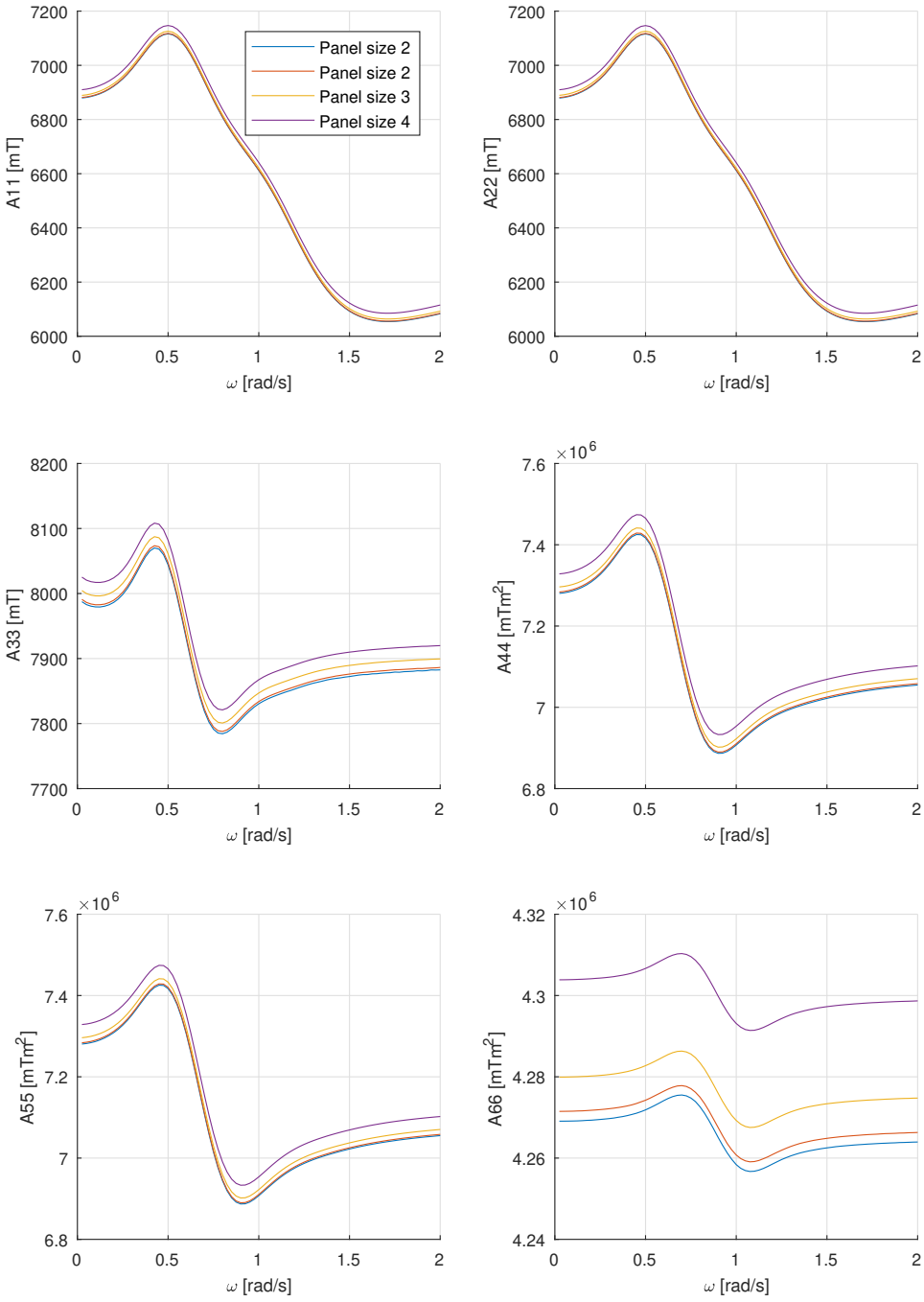


**Figure C.3:** Mesh sensitivity study on the panel size for the Tension-Leg Platform

A mesh sensitivity study is also performed on the hydrodynamic modeling of the vessel. The results for different mesh sizes of the added mass is shown in figure C.4.

Using a mesh with 2867 panels shows the best result. The values for added mass and damping for meshes with a different panel size show similar results at low frequencies, but deviate quickly from the result with 2867 panels due to the presence of an irregular frequency above 2 rad/s. Irregular frequencies occur when WAMIT solves the potential flow around a submerged body through Green's theorem. Irregular frequencies cause one side of the equation following from Green's theorem to be equal to zero. When this happens for a panel, the numerical matrix solver that computes the velocity over the body is not able to find a unique solution to the problem, which causes numerical errors. A finer mesh does not prevent irregular frequencies from occurring, but confines the effect of irregular frequencies to a smaller range around each frequency [34]. Therefore, the mesh with 2867 panels shows the most reliable result.

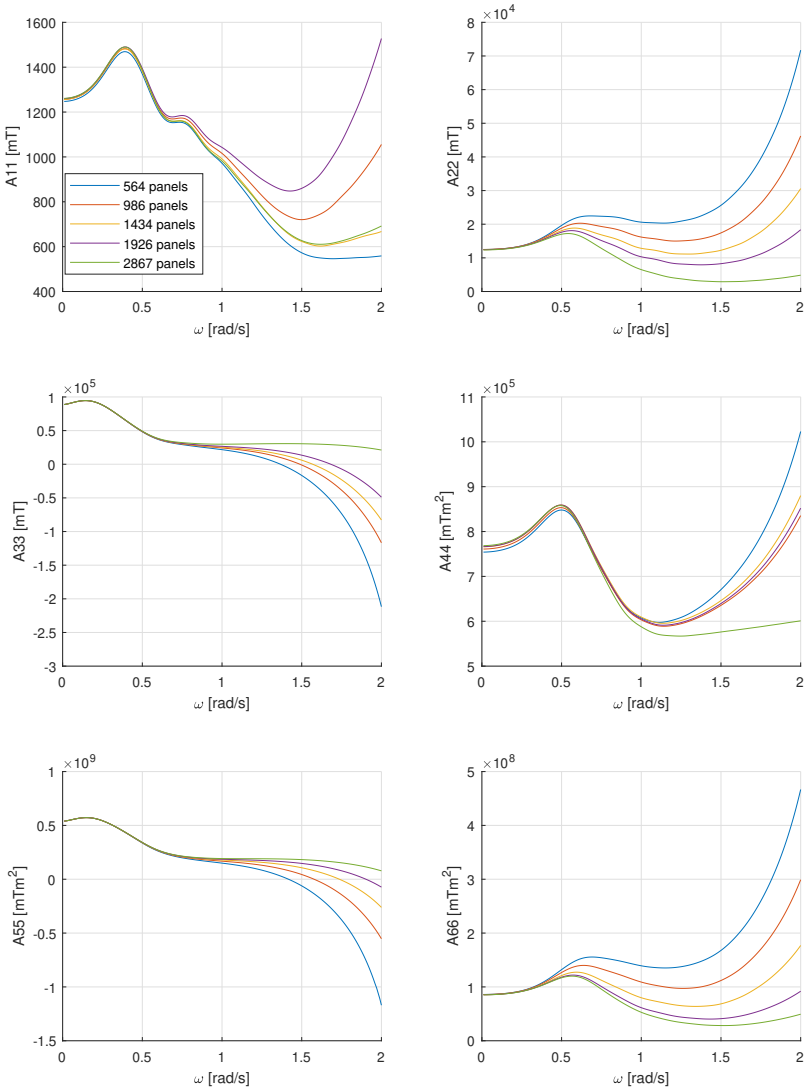


**Figure C.4:** Mesh sensitivity study on the panel size for the added mass of the support vessel

A similar effect is seen in the results for radiation damping, shown in figure C.5.

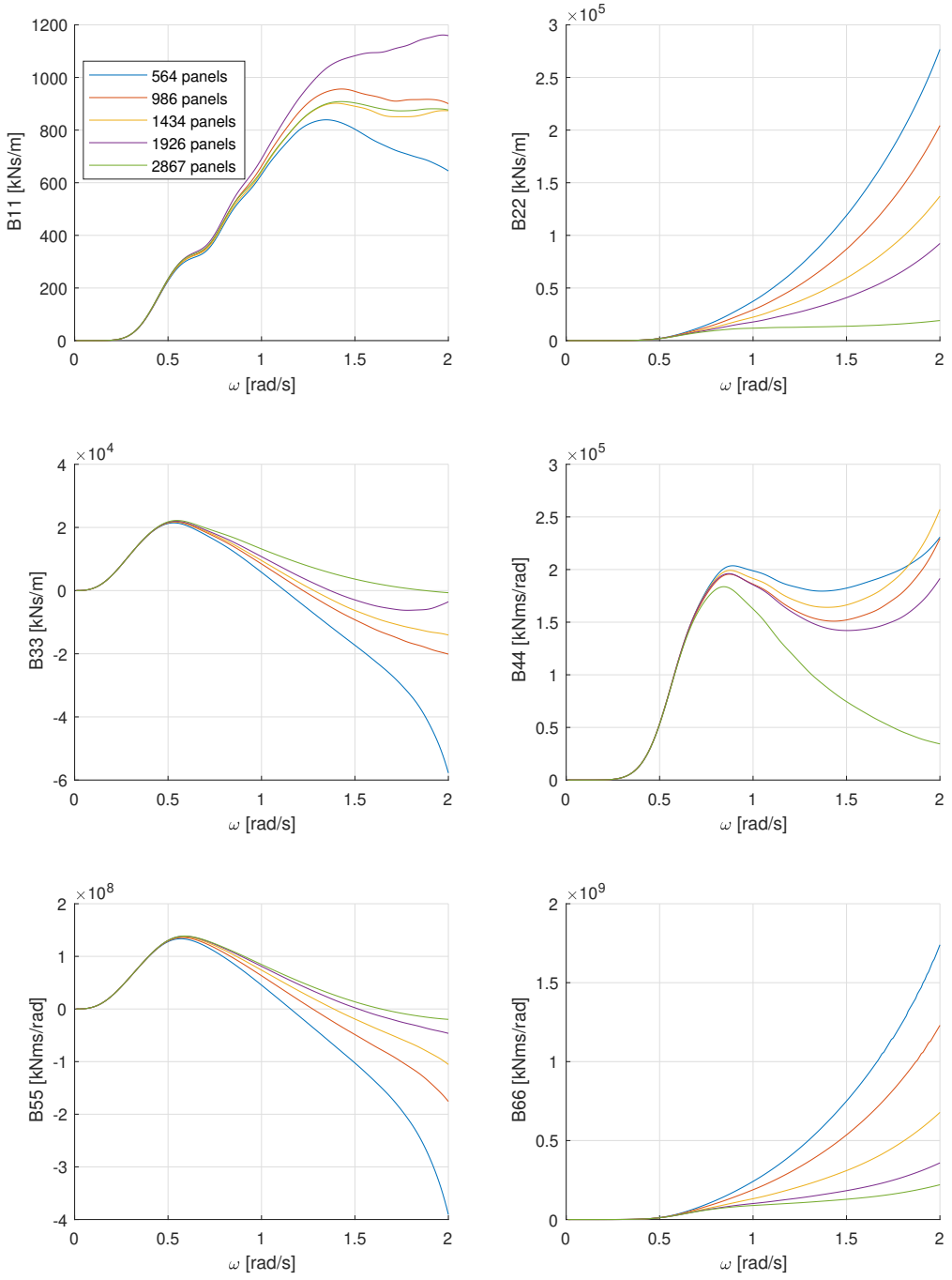


**Figure C.5:** Mesh sensitivity study on the panel size for the radiation damping of the support vessel

## C.3. DP springs

The relevant mass in yaw for calculating the spring stiffness is the moment of inertia of the vessel around its z-axis. The relevant properties are given in table C.1.

**Table C.1:** Mass and added mass properties relevant for the dynamic positioning spring stiffness

| ***Property*** | ***Value*** |
|---|---|
| $M_{11}$ | 31882 mT |
| $M_{22}$ | 31882 mT |
| $M_{66}$ | 6.77e+07 mT*m$^2$ |
| $A_{11}(T = 100)$ | 1261 mT |
| $A_{22}(T = 100)$ | 12356 mT |
| $A_{66}(T = 100)$ | 8.52e+07 mT*m$^2$ |

The spring stiffnesses can be calculated through the equation for the natural frequency. A matrix of the relevant mass and stiffness properties can be set up:

$$\mathbf{C}_{DP} = \begin{bmatrix} C_{11} & 0 & 0 \\ 0 & C_{22} & 0 \\ 0 & 0 & C_{66} \end{bmatrix}, \quad \mathbf{M}_{DP} = \begin{bmatrix} M_{11} & 0 & 0 \\ 0 & M_{22} & 0 \\ 0 & 0 & M_{66} \end{bmatrix}, \quad \mathbf{A}_{DP} = \begin{bmatrix} A_{11} & 0 & 0 \\ 0 & A_{22} & 0 \\ 0 & 0 & A_{66} \end{bmatrix} \tag{C.1}$$

The spring stiffnesses are then calculated as follows:

$$\mathbf{C}_{DP} = \omega_{nat}^2(\mathbf{M}_{DP} + \mathbf{A}_{DP}(\omega_{nat})), \quad \omega_{nat} = \frac{2\pi}{T_{nat}} \tag{C.2}$$

The resulting stiffnesses are given in table C.2:

**Table C.2:** Mass and added mass properties relevant for the dynamic positioning spring stiffness

| ***Property*** | ***Value*** |
|---|---|
| $C_{11}$ | 131 kN/m |
| $C_{22}$ | 175 kN/m |
| $C_{66}$ | 6.04e+05 kNm/rad |

## C.4. Tower damping

The damping in the tower is investigated through its transient response. The tower bottom is modeled as clamped, and the RNA is displaced artificially in order to assess the transient response of the tower bending mode. This is done for the blades modeled as structural elements with structural damping, and for a rigid rotor. The result is shown in figure C.6.

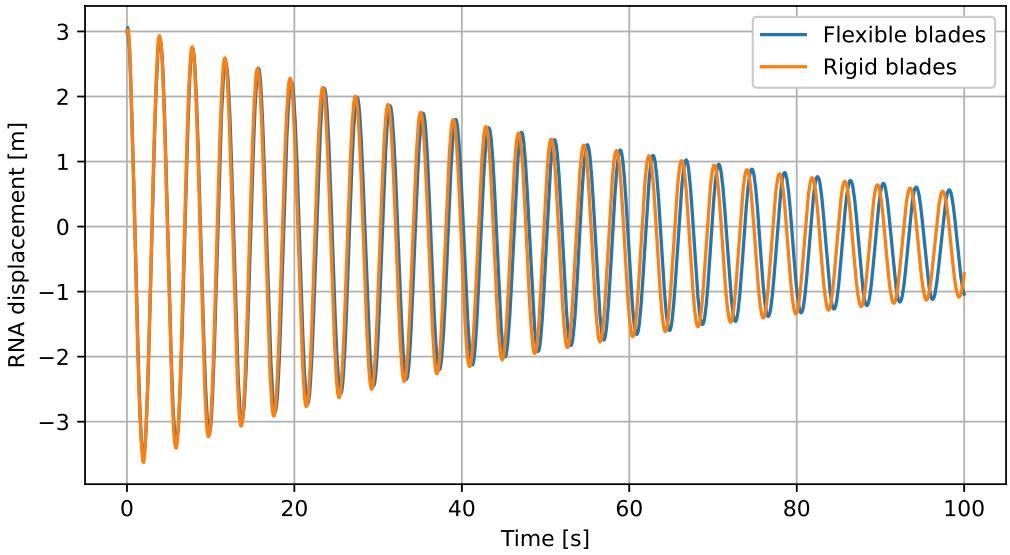


**Figure C.6:** Transient response of the tower bending mode for a flexible and rigid rotor

## C.5. Tendon adjustment for frequency domain software

The response of the RNA can be increase by decreasing the tendon stiffness, and vice versa. This is shown in figure C.7. A suitable tendon stiffness is chosen to match the time domain results with a flexible tower.

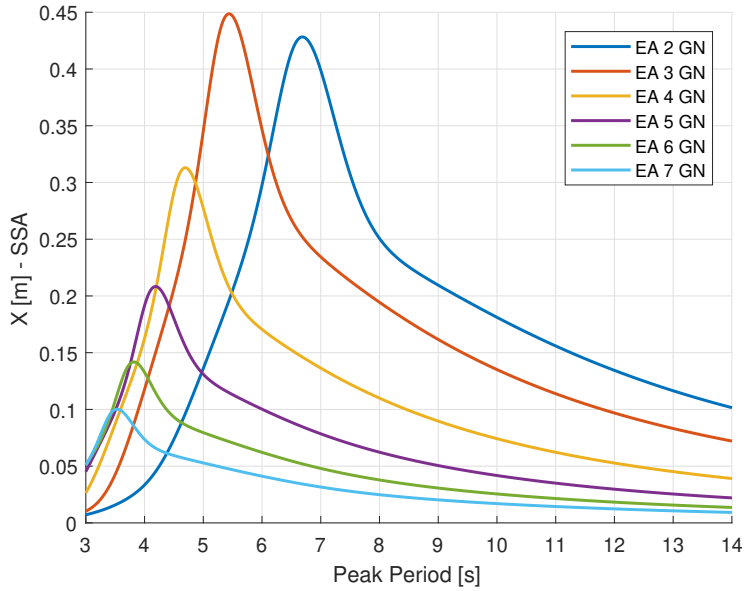


**Figure C.7:** Influence of tendon stiffness on surge response of the RNA of the WTG without the OSCC

The crane tip displacements of the frequency and time domain models are matched, and a tendon stiffness of 4.1 GN is found to give a good agreement between the two models.

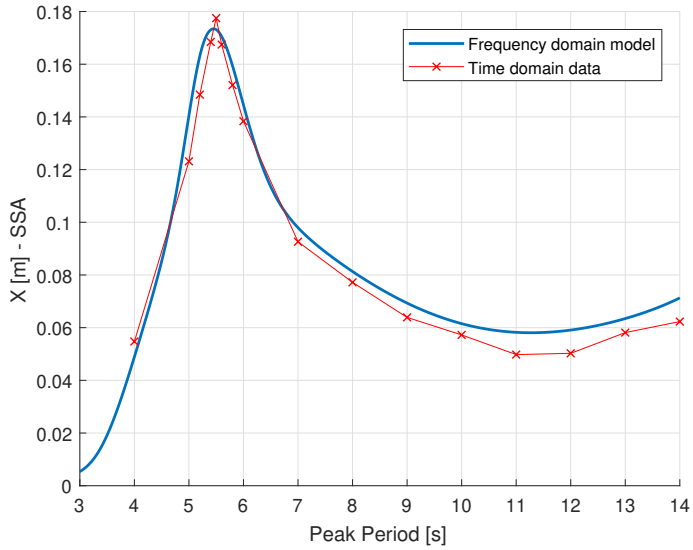


**Figure C.8:** Response of the crane tip of the frequency domain and time domain model with an adjusted tendon stiffness of 4.1 GN in the frequency domain model

## C.6. Line-up tool damping

The results of the sensitivity study on the damping ratio in the line-up tools are shown in figure C.9 and C.10. Different damping values are studied, and the damping ratio for each damping value is computed. A damping ratio of around 1.15 % is used in the models. This corresponds with a damping value of 15 kNm*s/deg for the line-up tool at the root, and 10 kNm*s/deg for the line-up tool at the yoke. As the damping ratio is a function of the stiffness in the corresponding degree of freedom, it follows that different values are found for both line-up tools, as they both have a different stiffness in yaw.

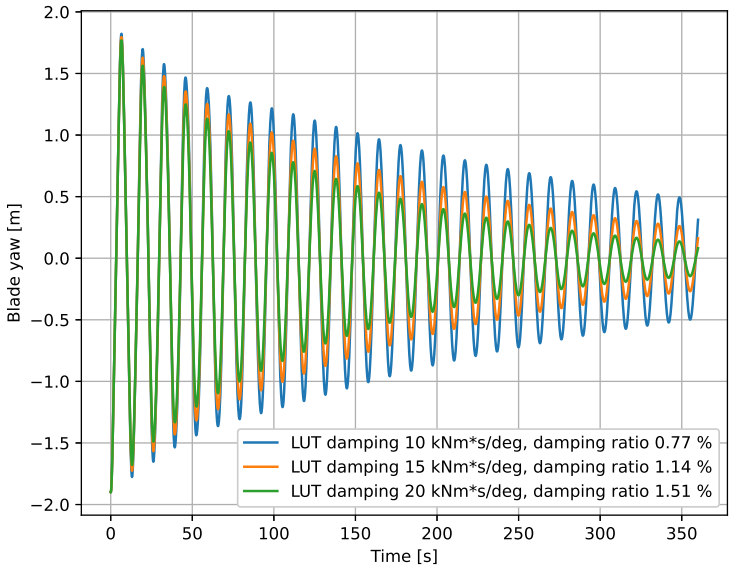


**Figure C.9:** Decay test of the blade with the line-up tool at the root

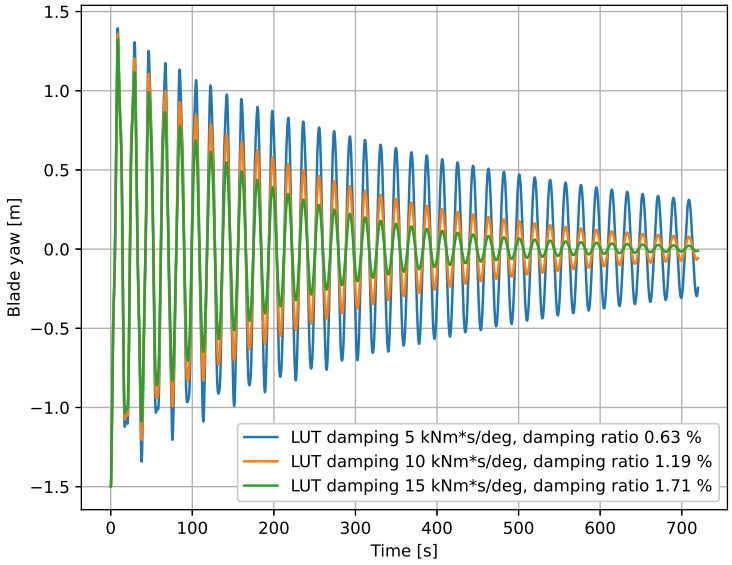


**Figure C.10:** Decay test of the blade with the line-up tool at the yoke

## C.7. Comparison of TLPs with different stiffness characteristics

Figure C.11 shows the significant single amplitude of the response in the RNA of different TLPs under wave loads modeled in time domain with a flexible tower. The TLPs have the same natural frequency in roll and pitch, but a different distribution between tendon stiffness and tower stiffness. The TLP with the highest tower stiffness and therefore highest tower bending natural frequency shows the largest response, as it has the softest tendons.

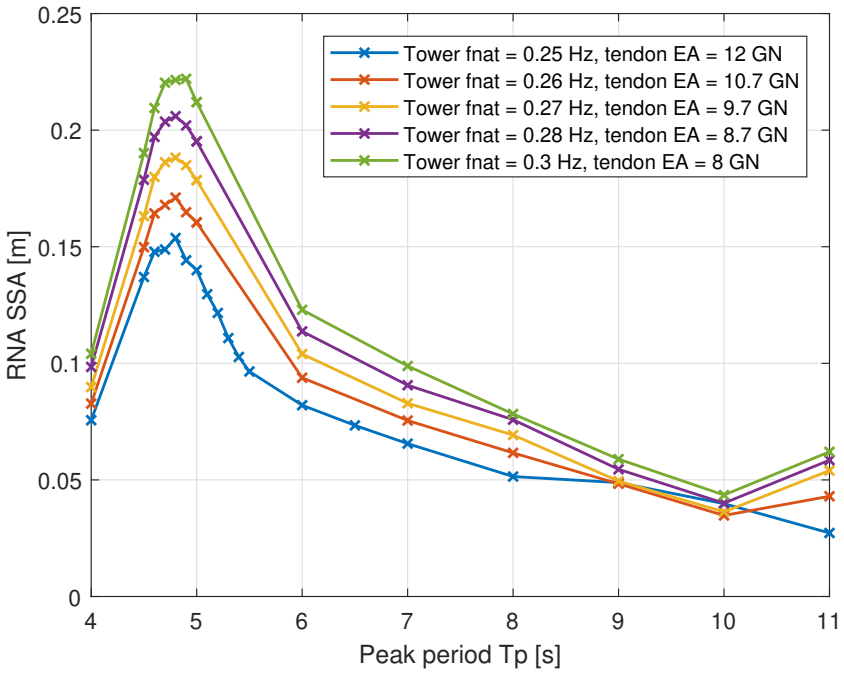


**Figure C.11:** Decay test of the blade with the line-up tool at the yoke

# D

# Additional operability curves

The operability curves that are assessed in section 9.1 are given in this appendix. The operability of the OSCC installation without tugger lines is shown in figure D.1 and D.2.

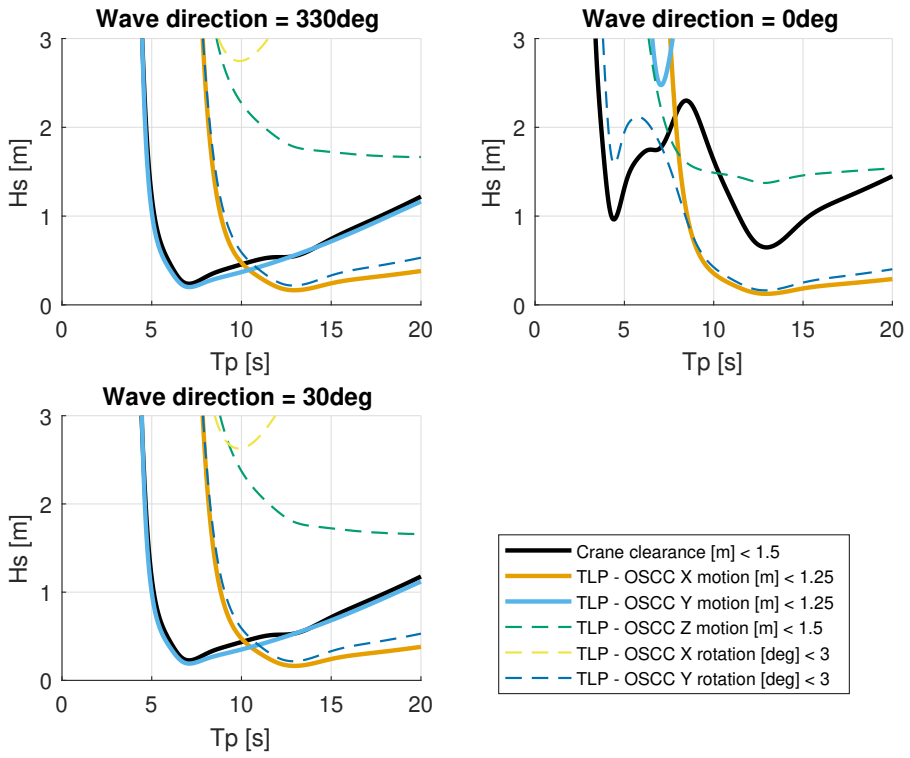


**Figure D.1:** OSCC installation without tugger lines beam seas

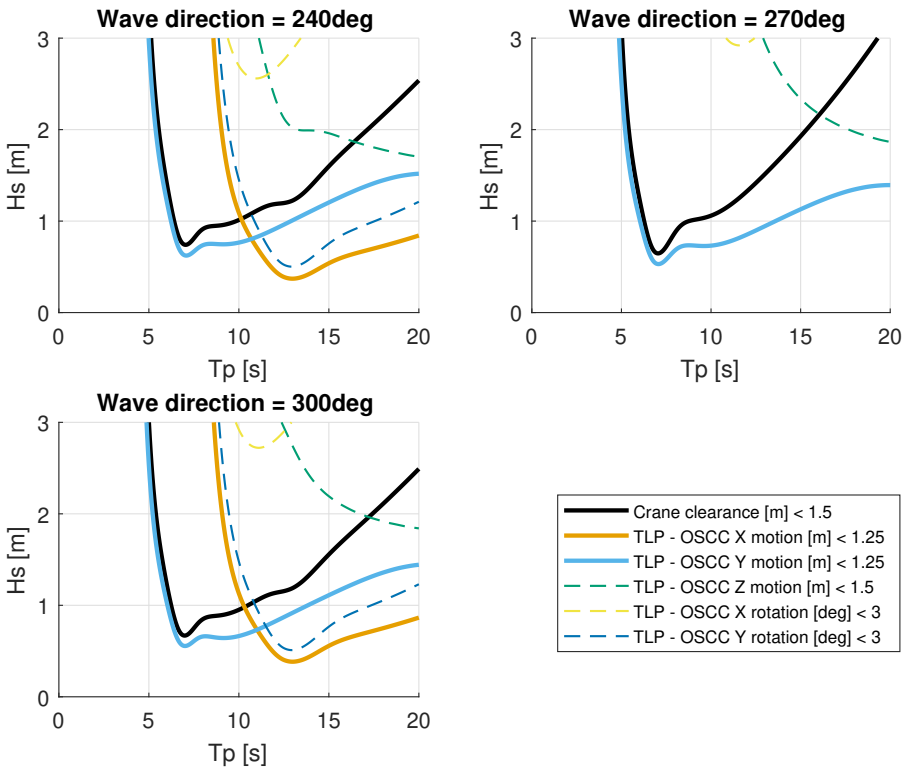


**Figure D.2:** OSCC installation without tugger lines bow seas

The operability of the OSCC installation with tugger line configuration 1 is shown in figure D.3 and D.4.

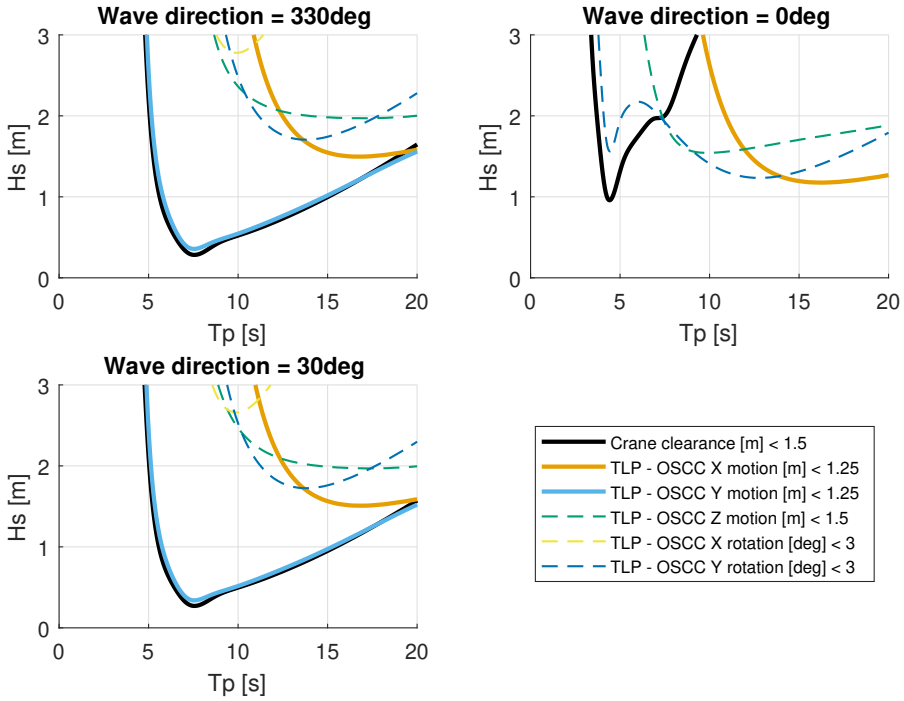


**Figure D.3:** OSCC installation tugger line configuration 1 beam seas

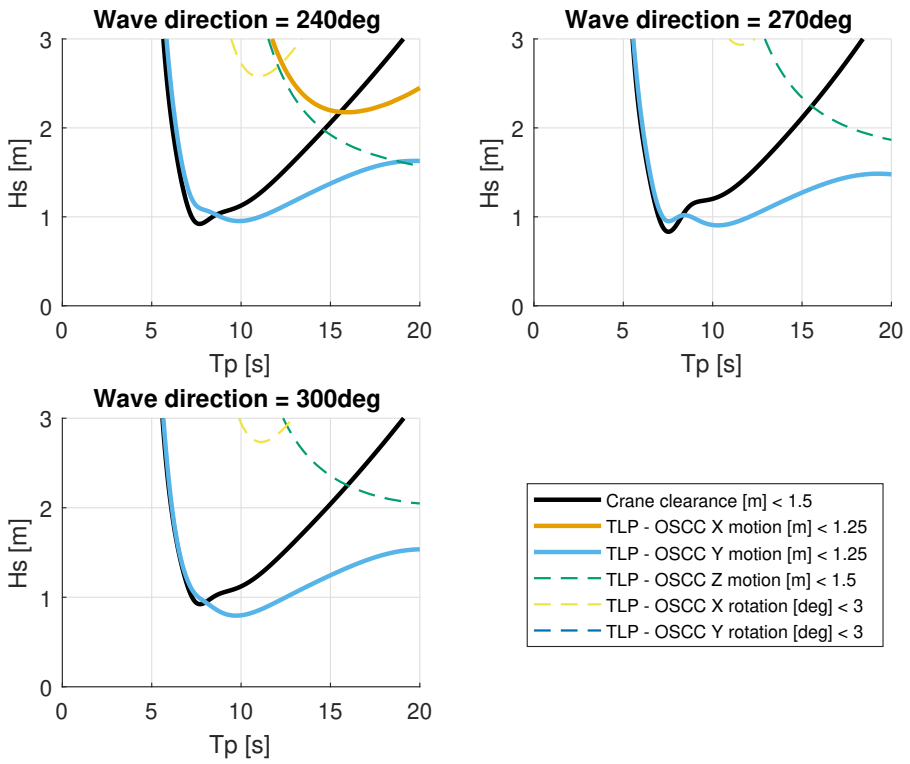


**Figure D.4:** OSCC installation tugger line configuration 1 bow seas

The operability of the OSCC installation with tugger line configuration 2 is shown in figure D.5 and D.6.

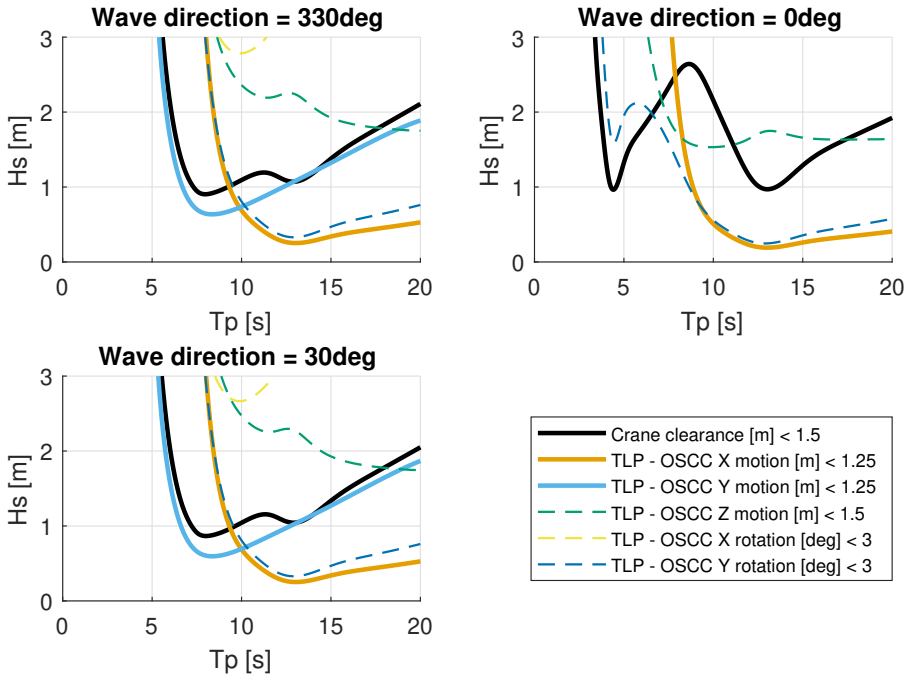


**Figure D.5:** OSCC installation tugger line configuration 2 beam seas

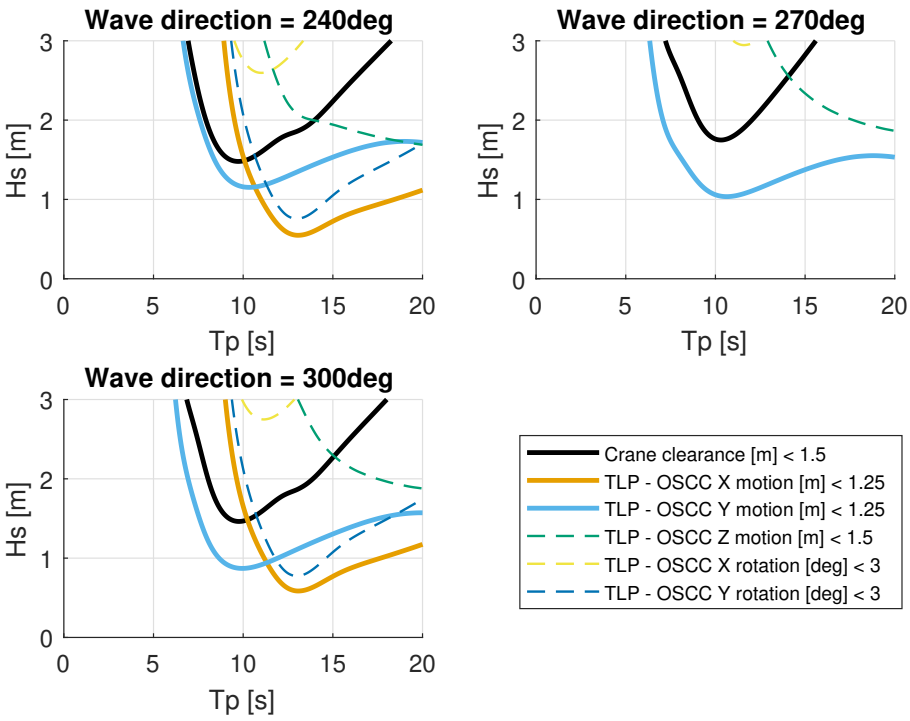


**Figure D.6:** OSCC installation tugger line configuration 2 bow seas